Integration of Geochemical and Isotopic Analyses of Fracture Minerals and Fluids to Assess the Deep Geological Stability at Chalk River Laboratories, Chalk River, Canada

by

Rhys Gwynne

A thesis

presented to the University of Waterloo

in fulfilment of the

thesis requirement for the degree of

Master of Science

in

Earth Sciences

Waterloo, Ontario, Canada, 2019

I hereby declare that I am the sole author of this thesis. This is a true copy of the thesis, including any required final revisions, as accepted by my examiners.

I understand that my thesis may be made electronically available to the public.

Abstract

The crystalline bedrock underlying the Chalk River Laboratories (CRL) at Canadian Nuclear Laboratories (CNL) provides a valuable analogue for potential nuclear waste storage sites. As the main pathways for fluid flow in crystalline rock are facilitated by interconnected fracture networks, it is especially important to study and understand the timeline of fracture formation, the subsequent precipitation and stability of fracture sealing minerals, as well as the glacial, tectonic and geological history of the site as it relates to the local and regional hydrological stability. Previous studies were integrated with new data that was primarily focused on the discrete groundwater sampling of a series of boreholes at the CRL site as well as porewater analyses. Utilizing major ion geochemistry as well as stable isotopic analyses, several trends were noted in order to infer the fluid history at the CRL as well as the theoretical influence of the different possible water types on hydrological and fracture mineral stability. The groundwaters of the CRL were found to be a mixture of mostly meteoric recharge with a smaller glacial meltwater component. A more saline endmember was noted in certain locations thought to originate from mixing with a high conductivity fluid at depth (paleoseawater, rock porewaters, etc.). Meteoric and glacial meltwaters after infiltration from the surface follow typical evolution trends due to mineral dissolution and water-rock interaction progressing from Ca-HCO_3 to Na-HCO_3 to Na-HCO_3-Cl type waters as available minerals are dissolved and longer timescale exchange reactions occur. No evidence of the influence of shield brines or recent hydrothermal waters was noted. Despite the geochemical variability documented there were no significant concerns that could be noted when considering their influence on calcite stability at depth. This supports the findings of previous studies that the crystalline bedrock fracture calcites of the CRL have been stable for more than 250 ka.

Acknowledgements

I would first like to express my sincere gratitude to my thesis advisor Dr. Shaun Frape of the University of Waterloo for his tutelage, support, guidance and friendship throughout this process.

This project would not have been possible without the funding and support of Chalk River Laboratories and Atomic Energy of Canada Limited. My sincere thanks and appreciation to Karen King-Sharp for her assistance and guidance as well as valued input throughout the investigation.

I would also like to think my committee members Dr. Chris Yakymchuk and Dr. Brian Kendall of the University of Waterloo for their valuable contributions and guidance towards the completion of this thesis.

Finally, thank you to my family especially my parents Darryl and Sarah who have been eternally supportive and encouraging throughout my academic career as well as my wife Olivia for her patience and loving support.

Table of Contents

List of Figures

List of Tables

1. **Introduction**

Nuclear power generation is an important source of electricity, especially in a political environment concerned about the effects of anthropogenically driven climate change caused by fossil-fuel derived energy sources (IAEA, 1983). One of the negative side-effects of nuclear power generation is the inevitable production and accumulation of radioactive waste which can remain hazardous for more than 100,000 years (Alley and Alley, 2013) with high level nuclear materials potentially stored in isolation for up to one million years (Frape et al., 1984). As a result, regulatory bodies must investigate and assess potential safe storage sites that will remain undisturbed and hydrologically isolated for these long timescales while ensuring security and limiting access. The International Atomic Energy Agency (IAEA) based in Vienna, Austria is an international regulatory agency that provides several published safety standards associated with radioactive waste management focused mainly on the reduction of the generation of radioactive waste. Included in these safety standards is the IAEA Geological Disposal Facilities for Radioactive Waste Specific Safety Guide No. SSG-14, defining geological disposal as "…the disposal of solid radioactive waste in a disposal facility located underground in a stable geological formation to provide long term containment of the waste and isolation of the waste from the accessible biosphere. Disposal means that there is no intention to retrieve the waste, although such a possibility is not ruled out. Geological disposal is a method for disposing of the more hazardous types of radioactive waste, which pose a significant radiological hazard over long time periods." (IAEA, 2013). The Canadian government currently oversees several radioactive waste facilities and inventories located in 20 different sites at 10 different locations, primarily within Ontario (NWMO, 2018).

Used fuel and radioactive waste can fall into one of several different categories depending on its radioactivity and the approach required to manage it. These are (high-level) nuclear fuel waste, intermediate-level radioactive waste, low-level radioactive waste, and uranium mine and mill waste. By 2050, Canada is anticipating its nuclear waste inventory will be approximately 20,660 m^3 of high-level waste, 67,738 m^3 of intermediate-level waste and 2,499,803 m^3 of low-level nuclear waste based on projected production levels (King-Sharp et al., 2016). The Government of Canada assigned the long-term management of used-nuclear fuel to the Nuclear Waste Management Organization (NWMO, 2018) under the Nuclear Fuel Act of 2002. Going forward NWMO is executing a five-year strategic plan that began in 2018 and will run through 2022 subject to change based on regular assessments. One of the key milestones they are focusing on until 2021 is "to advance preliminary field studies and assessments" based on new findings like those presented in this thesis. Currently NWMO is in Preliminary Assessment: Phase 2 (2015-2022) in which they are expanding their assessments to include field-scale studies (NWMO, 2018). While numerous studies have assessed the suitability of a variety of geologic media, crystalline rock is among a promising subset of candidates for long-term storage of accumulated nuclear waste and has been the focus of extensive investigations to date, focused on geology, hydrology and precipitated fracture minerals, primarily in Canada, Sweden and Finland due to their proximity to the Canadian Shield and Fennoscandian Shield, respectively (Larson and Tullborg, 1984; Gascoyne and Schwarcz, 1985; Fritz et al., 1989; Clauer et al., 1989; Peterman and Wallin, 1999; Blyth et al., 1998; Tullborg, 1989a; Blyth et al., 2000; Bukata, 2000; Blyth et al., 2004; Blyth et al., 2009; Drake et al., 2008; Tullborg et al., 2008; Drake and Tullborg, 2009).

The primary concern when it comes to the long-term storage of nuclear waste in a crystalline bedrock environment is the potential for advection of hazardous waste via fluid flow, through fractures caused by geological stresses after initial formation (Figure 1) (IAEA, 1983). Large fracture networks are usually formed after the crystallization of plutonic rocks, typically during tectonic events. Fluids flowing through this available fracture porosity will deposit minerals through precipitation eventually resulting in the sealing of said fractures (Bottomley et al., 1984). Characterizing existing fractures and the precipitated minerals often contained within them is therefore essential for a comprehensive understanding of the tectonic and hydrogeological history and therefore potential long-term future stability at a crystalline site. The Chalk River Laboratories (CRL) has been a valuable research site for more than 30 years, improving our understanding of the tectonic history of crystalline rock especially through fracture mineral and hydrogeologic investigations (Gadd, 1958; Bottomley et al., 1984; Bottomley, 1987; Bukata, 2000; Blyth et al., 2000; Blyth et al., 2009; Neymark et al., 2013; Peterman et al., 2016; King-Sharp et al., 2016). The CRL is located approximately 200 km northwest of Ottawa, Ontario on the Ottawa River (Figure 2) and is operated by Canadian Nuclear Laboratories, a private sector organization that manages and operates Atomic Energy of Canada Limited's sites under a Government-owned, contractor-operated model (King-Sharp et al., 2016).

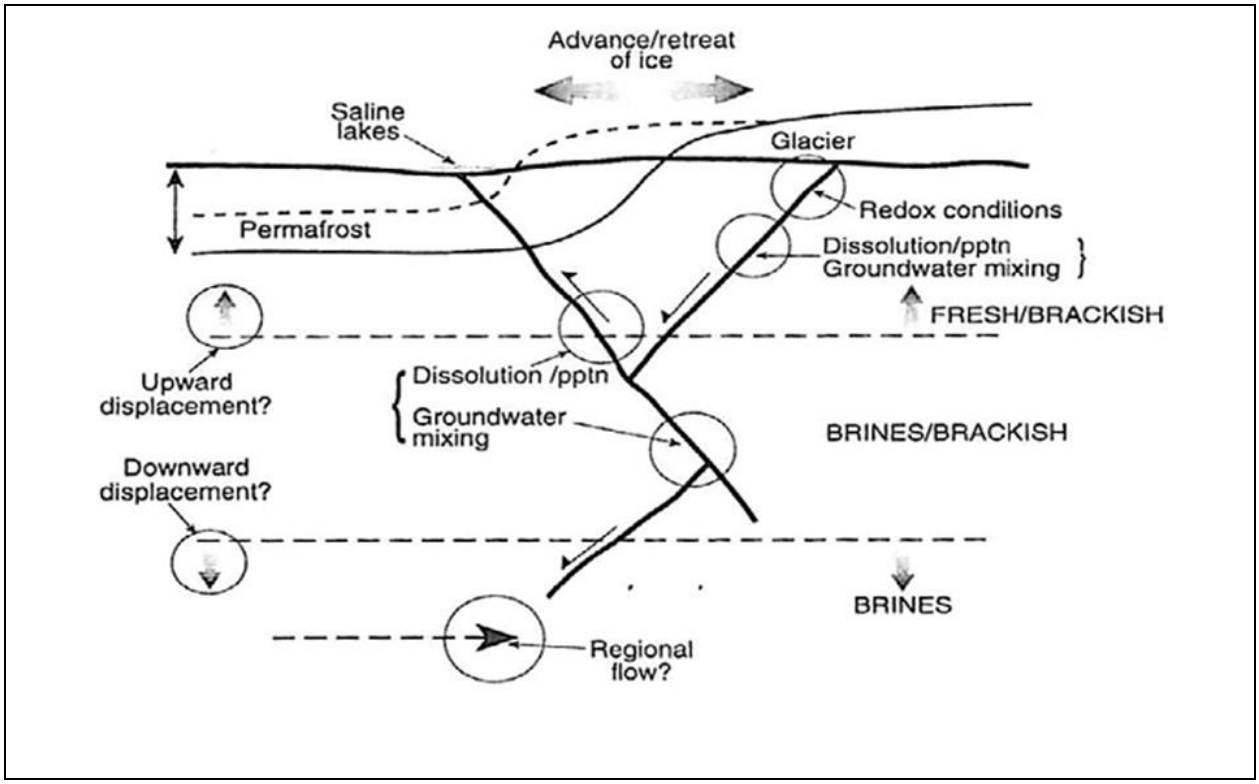

Figure 1. Schematic diagram showing possible fracture flow conduits in crystalline rock (from Smellie and Frape, 1997).

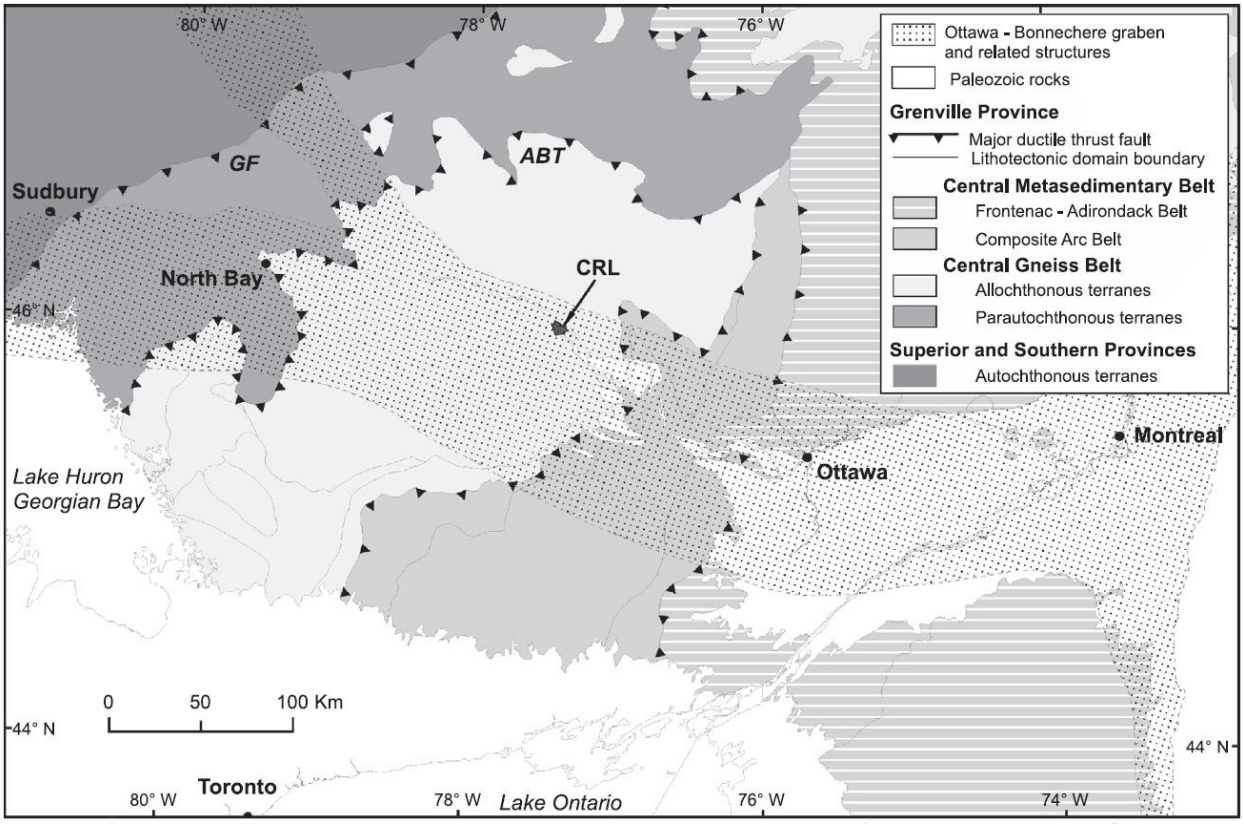

Figure 2. The CRL location in Ontario, Canada showing relevant geology and tectonic divisions (from Neymark et al., 2013).

Over the course of the current investigation at the CRL site, several methods were utilized to investigate and attempt to understand the hydrogeological history of its crystalline bedrock. This study is not being undertaken to precisely locate a theoretical suitable site for a storage facility. Rather, it is intended to add to the accumulated knowledge base focused on assessing the suitability of different geological media for potential nuclear waste storage. The goal of this investigation is to consolidate information and accumulated data and assess the usefulness of several geochemical and isotopic techniques to provide a case-study and framework of useful approaches when assessing analogous crystalline storage sites as a part of the Canadian Government's ongoing strategy. It aims to provide a useful dataset and interpretative approach as an analogue for current and future international nuclear waste disposal investigations in fractured crystalline bedrock. This study was conducted in conjunction with

previous work focused on geological site characterization by Neymark et al. (2013), as well as hydrological studies conducted by Peterman et al. (2016) who focused on physical hydrology, porewater geochemistry and $^{234}U/^{238}U$ studies, as well as King-Sharp et al. (2016) who looked more closely at groundwater geochemistry and fracture mineral studies in conjunction. This investigation was also undertaken in co-operation with Long Tian. Tian (2016) worked with the same boreholes concurrently focusing particularly on geological, mineralogical and petrographic aspects of the fracture mineral history within the investigation. The origins of the investigation lie with Canadian Nuclear Laboratories (CNL) Chalk River Laboratories site initiating a multi-year study from 2005 to 2014 with the focus on investigating crystalline rock feasibility as a storage site for CNL's stock of radioactive non-fuel waste called initially a geological waste management facility (GWMF). Seven new deep boreholes (CRG series) were drilled in the bedrock under the CRL property, six of which are the focus of this investigation (Figure 3) (King-Sharp et al., 2016). The scope of the investigation has evolved from its initial focus on the feasibility of a GWMF to more broadly contribute to the global understanding when it comes to deep crystalline rock sites as potential nuclear waste storage sites. The study presented here centered on understanding the local hydrology and geochemistry, focusing on the relationship between fracture minerals, groundwater and porewaters. The chemical fingerprint measured within a given mineral is limited to a discrete number of sources or a mixture of sources including in this case meteoric waters, shallow low temperature fluids, ascending hydrothermal waters or transportation and recrystallization of older mineral deposits (Bottomley, 1987). When assessing fracture minerals within a fractured bedrock system more specifically, the parent waters can be traced to several distinct sources (Blyth et al. 1998, 2000). In the Chalk River

region, these fluid sources include but are not limited to meteoric, glacial, hydrothermal and magmatic origins (Blyth et al., 2004).

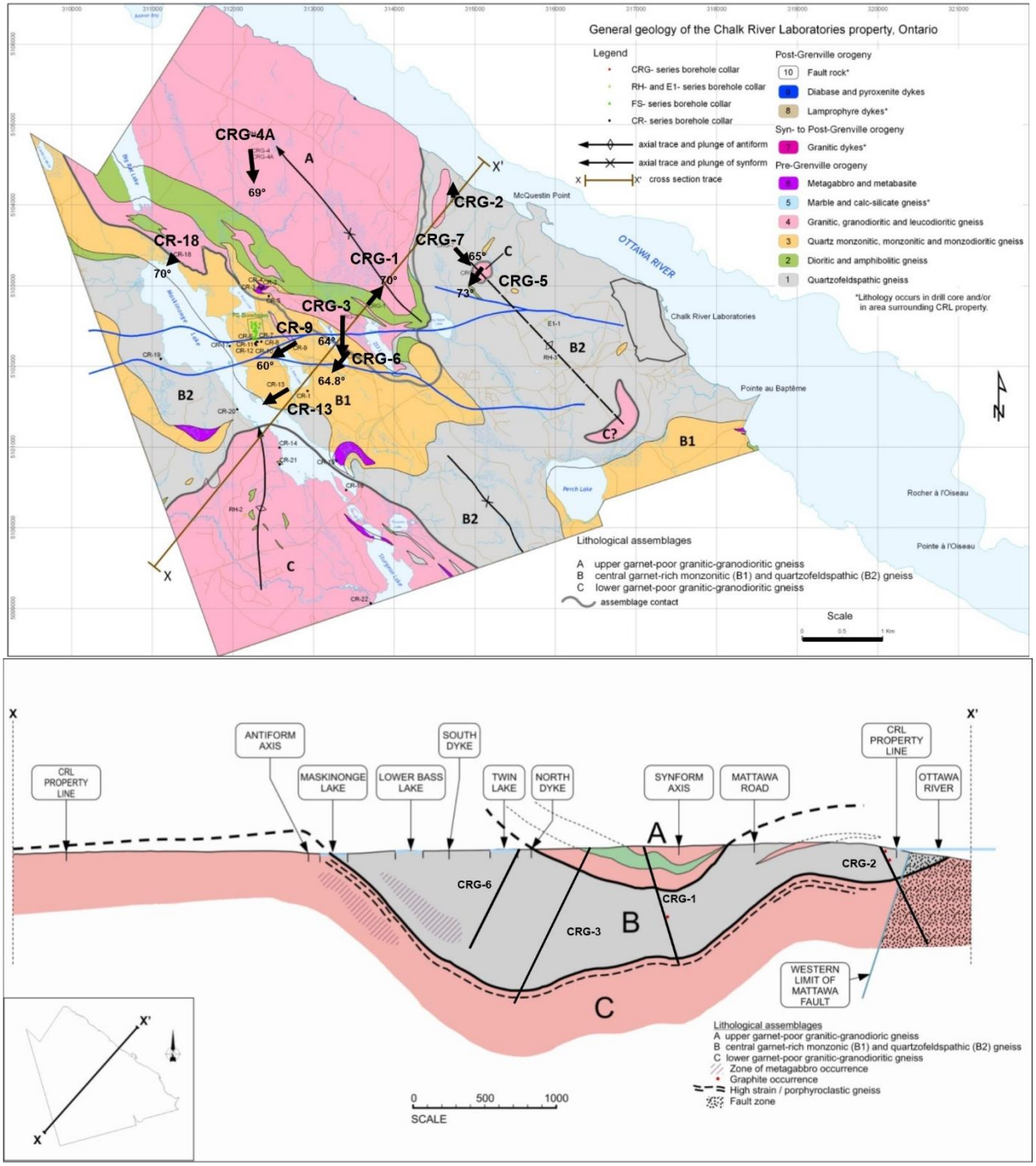

Figure 3. A) Aerial view of the CRL site showing bedrock geology and sampled boreholes showing the direction, magnitude and dip of all studied boreholes; B) A cross section from southwest to northeast across the CRL property showing a selection of boreholes and the synclinal nature of units A, B and C (Neymark et al., 2013) (figure modified from Baumgartner et al., 2012).

1.1 Stable Isotope Geochemistry

The principal tool utilized in this thesis was stable isotope geochemistry. Chemically, the isotopes of these elements remain very similar but will often behave with subtle differences to one another due to their very small mass difference(s) (Hoefs, 2015). In order to quantify the subtle differences in the ratios of the stable isotopes of a given element within a sample, standard materials are used to establish a common baseline reference. The ratio of heavy to light isotopes is compared to the standard value and quantified using delta notation, calculated by equation (1) using oxygen as an example and expressed in terms of permil (‰):

$$\delta^{18}O_{Sample}(‰) = \left(\frac{\left(\frac{^{18}O}{^{16}O}\right)_{Sample}}{\left(\frac{^{18}O}{^{16}O}\right)_{Reference}} - 1 \right) \times 1000 \quad (1)$$

The mass difference between two given isotopes leads to quantifiably different behaviour when it comes to chemical equilibrium and reaction kinetics. This mass discrimination leads to a change in the isotopic delta value in a process described as isotopic fractionation (Clark and Fritz, 1997). The resulting isotopic signature or delta value (δ) can be used in many different applications depending on the environment and potential fractionation factors involved. If isotopic fractionation is observed, a given delta value will change if the heavy or light isotope of a given element is acted upon differently by a given process. Isotopic fractionation is separated into two broad categories: equilibrium fractionation occurs over time typically due to chemical exchange; whereas kinetic fractionation is typically related to one directional processes. Fractionation factors are related to the equilibrium constant “K” where “n” defines the number of atoms exchanged in equation (2):

$$\alpha = K^{\frac{1}{n}} \quad (2)$$

This is typically expressed as $10^3 \ln\alpha$ due to the ease in relating this formulation to the delta value (δ) through the approximation in equation (3):

$$\delta^{18}O_{CO_2} - \delta^{18}O_{CaCo_3} = \Delta_{CO_2-CaCo_3} \approx 10^3 ln\alpha_{CO_2} - 10^3 ln\alpha_{CaCo_3} \quad (3)$$

For C and O isotopes, several fractionation factors need to be considered when it comes to calcite dissolution and precipitation. In terms of the carbon cycle, an initial isotopic fractionation is related to the dissolution of carbon from various sources. Carbon sources in meteoric waters are most often gas (CO_2) and mineral based (Quade, 2014), and the dissolution of both sources are associated with isotopic changes. To account for temperature dependant changes in the $\delta^{13}C$ signature during calcite precipitation for example, several successive reactions must be accounted for depending on the precise set of preconditions. If we begin with gaseous CO_2, the reactions involved include the dissolution of CO_2, the conversion of CO_2 to HCO_3^-, the conversion of HCO_3 to CO_3^{2-}, and finally the precipitation of $CaCO_3$, all of which change the $\delta^{13}C$ signature in a unique way (Bottinga, 1968; Vogel et al., 1970; Deines et al., 1974; Mook et al., 1974). These fractionation factors combine into an overall temperature dependent empirical relationship described by equation (4) (Bottinga, 1968):

$$10^3 \ln \alpha(\delta^{13}C_{CO_2-CaCO_3}) = -2.9880\left(\frac{10^6}{{T_K}^2}\right) + 7.6663\left(\frac{10^3}{T_K}\right) - 2.4612 \quad (4)$$

While equation (4) can quantify the fractionation factor between gaseous CO_2 and calcite, in order to quantify the fractionation factor between dissolved bicarbonate and calcite, a second

temperature dependent empirical relationship must be considered and is shown in equation (5) (O'Neil and Taylor, 1969):

$$10^3 \ln \alpha(\delta^{13}C_{HCO_3-CO_2}) = 9.552\left(\frac{10^3}{T}\right) - 24.09 \quad (5)$$

The combination of these processes in equation (6) can give us the overall isotopic fractionation between dissolved bicarbonate and precipitated calcite.

$$10^3 \ln \alpha(\delta^{13}C_{CO_2-CaCO_3}) + 10^3 \ln \alpha(\delta^{13}C_{HCO_3-CO_2}) = 10^3 \ln \alpha(\delta^{13}C_{HCO_3-CaCO_3}) \quad (6)$$

In the case of $\delta^{18}O$ data interpretation, once again the main factor influencing fractionation factor is a temperature dependence through an inverse relationship (i.e. higher temperature means a lower magnitude of fractionation). Epstein (1953) was the first to empirically characterize this relationship and used this information to generate equation (7) (Epstein, 1953) which allows for the generation of theoretical paleotemperature scales as a geothermometer similar to Figure 4.

$$10^3 \ln \alpha(\delta^{18}O_{CO_2-CaCo_3}) = 2.78\left(\frac{10^6}{{T_K}^2}\right) - 2.89 \quad (7)$$

As a result of this relationship, it is important wherever possible to quantify the temperature of formation for a given calcite using fluid inclusion analysis.

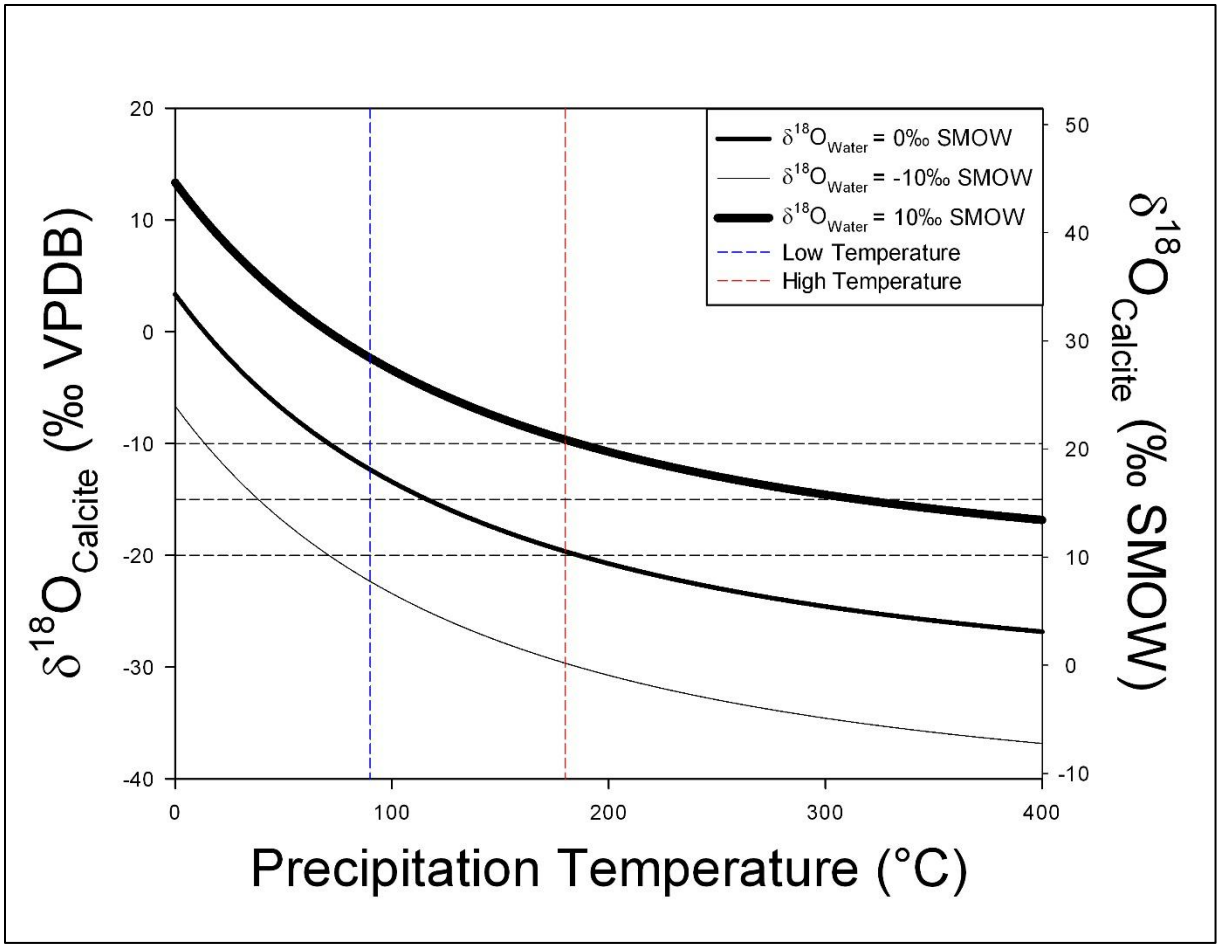

Figure 4. Geothermometry curve generated using equation (7) and displaying the temperature (and therefore fractionation) extremes noted at the CRL site.

1.2 Fluid Inclusion Analysis

Fluid inclusion analysis made up an important part of the investigation and helped the understanding of temperature and salinity conditions during the initial precipitation of fracture minerals at the CRL site (Table 1) (Tian, 2016). Primary fluid inclusions, often 1 to 50 μm in size, are created within the crystal structure of precipitated calcite during formation and can survive intact if the mineral has not undergone extensive post-depositional alteration (Roedder, 1984; Goldstein and Reynolds, 1994). If a fluid inclusion is found to be primary (as in free of alteration after initial deposition, as opposed to secondary or pseudo-secondary inclusions) in an

area free of evidence of post-depositional alteration, several measurements can be made. Within calcite, primary fluid inclusions will contain three phases (solid, liquid and gas) if cooled significantly after precipitation. The temperature of homogenization (T_h) is found by heating the inclusion until all these phases homogenize (Goldstein et al., 2003). This temperature represents the lowest temperature at which the inclusion could have formed within a solid, and therefore that the mineral could have precipitated (Roedder, 1984). This information therefore allows the calculation of the maximum possible $\delta^{18}O$ fractionation during precipitation using equation (7) for any calcite for which $\delta^{18}O$ and T_h is available without the significant error that can be introduced through estimation and assumptions of fluid compositions, especially at lower temperatures (Epstein, 1953) (Figure 4). Any inclusion that formed below ~50°C is considered meta-stable and will typically not form a gas phase bubble. No temperature of formation lower than this temperature can therefore be accurately determined using this method (Blyth et al., 2004). Primary fluid inclusions can also be frozen and reheated to the point of melting to note the temperature of melting (T_m). This temperature is directly related to the salinity of the fluid that originally precipitated the mineral using the following equation (8) from Goldstein and Reynolds (1994), thus contributing additional useful information when it comes to the identification of possible parent fluids:

$$Salinity\ (wt\%)_{NaCl} = 1.78(T_M) - 0.0442(T_M)^2 + 0.000557(T_M)^3 \qquad (8)$$

1.3 Rare Earth Elements

The Rare Earth Elements (REE) are a unique group of fourteen elements that are clustered together on the periodic table from masses 57 (Lanthanum) to 71 (Lutetium). The REE have similar chemical properties and under most conditions all have a trivalent oxidation state (Henderson, 1985). The relative abundance of these elements can be a useful tool when assessing

hydrogeological systems especially when normalized against the relative abundance measured in chondrite meteorites (i.e. chondrite normalized (CN)) (Bau and Möller, 1992). The resulting pattern when plotted can be a useful visual aid when assessing multiple patterns at a site, most simply by noting the slope of the REE normalized abundances plotted in order of atomic mass. Patterns with a negative slope are said to be enriched in Light Rare Earth Elements (LREE) and/or depleted in Heavy Rare Earth Elements (HREE), while the opposite is true of a pattern with a positive slope. While REE abundances and patterns can be a useful fingerprinting tool (Prudêncio et al., 1994), two other useful anomalies are the result of redox reactions/changes altering the oxidation states of Cerium and Europium from the standard REE trivalent (3+) state. Cerium (Ce) can be oxidized from its trivalent (Ce^{3+}) form to Ce^{4+} under suitably oxidizing conditions. Ce^{4+}, due to its charge and smaller atomic radius is more mobile and therefore can be removed from an isolated fluid or precipitate due to its lower solubility relative to Ce^{3+} (Bau and Möller, 1992). In general, when REE patterns are generated from an oxidizing environment and chondrite-normalized, the abundance of cerium will be typically lower than the immediately adjacent praseodymium (Pr) and lanthanum (La), with a value of $\delta Ce<1$ generated from equation (9) (Worrall and Pearson, 2001).

$$\delta \mathrm{Ce} = \frac{\mathrm{Ce}_{CN}}{\sqrt{\mathrm{La}_{CN} \times \mathrm{Pr}_{CN}}} \tag{9}$$

This relative statistical comparison does not however consider the possibility of La and Pr abundances influencing our perceived δCe calculation (i.e. Pr excess exaggerating the perceived δCe depletion). To rule out this possibility, “true” positive or negative Ce anomalies can be approximating taking these factors into account using equations (10) and (11) from Plavansky et al. (2010).

$$\frac{\mathrm{Ce}}{Ce^*_{CN}} = \frac{\mathrm{Ce}_{CN}}{(0.5(Pr_{CN} + La_{CN})} \quad (10)$$

$$\frac{\mathrm{Pr}}{Pr^*_{CN}} = \frac{\mathrm{Pr}_{CN}}{(0.5(Ce_{CN} + Nd_{CN})} \quad (11)$$

The resulting ratios can be compared as in Figure 5 in order to differentiate between true negative Ce anomalies and those that only appear negative due to La excess (Plavansky et al., 2010). Out of the available dataset, only two samples (both calcite) plot in the "true" negative Ce anomaly zone, CRG1 448.6 m and CRG3 24.7 m, implying that the fluids that these fracture calcites precipitated from were reducing.

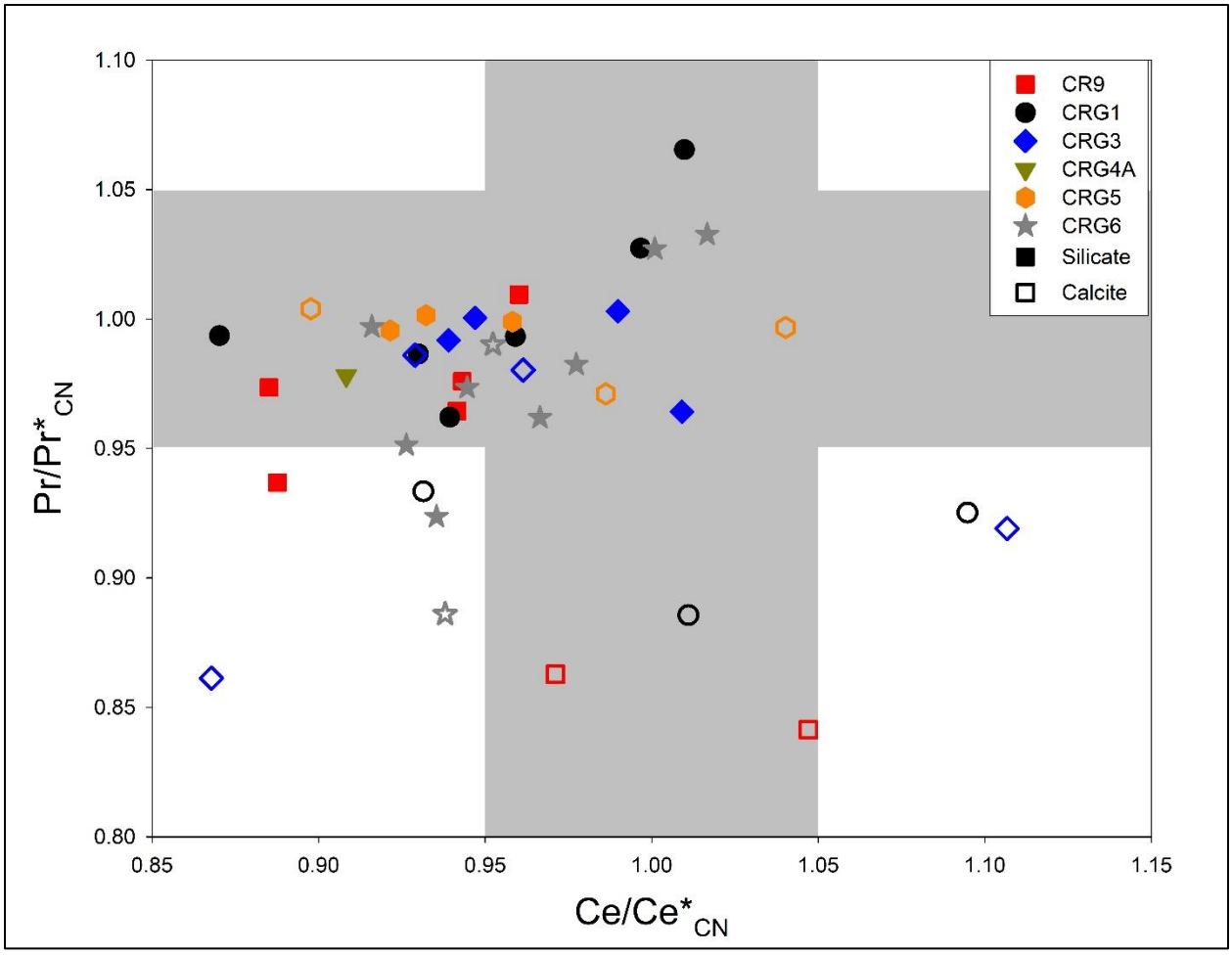

Figure 5. Comparison of Ce_{CN} and Pr_{CN} anomalies for the available CRL silicate and calcite samples to determine true negative Ce anomalies. True negative Ce anomalies are defined in the range of $Ce/Ce^*_{CN} > 1.05$ and $Pr/Pr^*_{CN} < 0.95$ (bottom right) (Plavansky et al., 2010).

Europium similarly can be altered by redox conditions and changed from its trivalent (Eu^{3+}) state. Under reducing conditions, Eu^{3+} is altered to the divalent form Eu^{2+} which can be more easily substituted in place of Ca^{2+} into plagioclase (Bau and Möller, 1992). The europium anomaly can be quantified when comparing its chondrite-normalized abundance to samarium (Sm) and gadolinium (Gd) and described by equation (12) (Henderson, 1985).

$$\delta Eu = \frac{Eu}{\sqrt{Sm \times Gd}} \tag{12}$$

When performing an investigation of REE patterns in both host rock and fracture minerals at the CRL, Tian (2016) was able to make some general inferences:

(1) The patterns of a given fracture calcite is typically similar to the adjacent bedrock.
(2) Almost all mineral samples show enrichment in the LREE, likely due to higher solubility of HREE in the fluid phase
(3) Calcite samples in most instances are enriched in REE relative to adjacent bedrock.

The cerium anomalies noted by Tian (2016) are not significant and difficult to distinguish from the overall LREE enrichment trend, suggesting limited extreme oxidation events on a bulk scale (Bau and Möller, 1992). Europium anomalies, however, are more significant and plentiful, with both positive and negative anomalies occurring in the calcite and adjacent host rock. Enrichment or depletion of Eu is indicative of the presence of Eu^{2+} during rock and mineral formation. As Eu^{2+} can be readily substituted for Ca^{2+}, in environments in which Eu^{2+} is readily available such as reducing environments or those with high temperatures and or pressures (Bau and Möller, 1992), Eu will substitute particularly readily into plagioclase. As a result, positive europium anomalies are typically indicative of the presence of plagioclase within a given rock mass whereas negative europium anomalies can be present in fluids that have precipitated plagioclase. Fluids and their resulting mineral precipitates that have interacted with a given rock mass will typically be enriched in these REE patterns due to water-rock interaction and can be useful fingerprints in heterogeneous bedrock geology (Habermann et al., 1996). A selection of chondrite normalized REE values for CRL host rock as well as carbonates are listed in Table 8.

1.4 Objective

The objective of this investigation is to combine interpretations of available chemical, hydrological and fluid inclusion datasets in conjunction with statistical techniques to provide a comprehensive geochemical and isotopic investigation for potential future nuclear waste storage sites with this study providing new data most prominently from groundwater geochemical and isotopic analyses. The unique and well-studied bedrock geology below the CRL property provided an excellent opportunity to combine several investigative techniques accumulated over several decades to make predictions about long term site stability that are relevant on a global scale (Tullborg, 1989a; Bottomley and Veizer, 1992; Frape et al., 1992; Blyth et al., 2004, 2009; Drake et al., 2008, 2017; Wallin and Peterman, 2014). Studies thus far have shown that the crystalline bedrock at Chalk River is similar in terms of mineralogy, density, porosity of water content to other Canadian Shield sites as well as Fennoscandian Shield sites also under investigation by Sweden and Norway for potential long-term nuclear waste storage, thus illustrating the value of the CRL as a useful wealth of relevant information (Peterman et al., 2016).

1.5 Site Description

The Chalk River Laboratory (CRL) site is located on the Ottawa river near the Ontario-Quebec border about 150 km straight line distance northwest of Ottawa or 180 km northwest via road (Figure 2). Generally, the area has a low topography and geological outcrops are high grade metamorphic crystalline rock typical of this part of the Canadian Shield. The landscape has been shaped most significantly by erosional forces and multiple glacial advances and retreats and is dotted with several lakes and rivers (King-Sharp et al., 2016). This region has a semi-continental climate with extremes in both heat and cold in the summers and winters with daily temperature

averages ranging from –19°C in January to 26°C in July (Environment Canada, 2018). The total expected precipitation annually is 800 mm with 600 mm as rain and 200 mm as snow. This budget exceeds evaporation rates of approximately 500 mm/a with recharge rates thought to be between 0.6 to 31 mm/a depending on local subsurface conditions (King-Sharp et al., 2016). There is limited topographic variability at the site with a maximum elevation difference of 60 m. Hydraulic heads indicate flow toward the Ottawa River or towards several lakes in the area (Bottomley et al., 1992; Peterman et al., 2016). At the CRL site, all but the shallowest of waters are contained within fractured gneissic crystalline rock. As a result, groundwater chemical migration would be restricted to advective flow and diffusion within the fracture porosity in the rock mass (Blyth et al., 2009). Models developed for other deep crystalline flow systems in the Canadian shield show similarities to corresponding shallow flow regimes demonstrating the influence of local terrain at the surface level on deeper groundwater flow (Sykes et al., 2009; Peterman et al., 2016). The Mattawa Fault Zone cuts across the northeast of the site following the Ottawa River Valley as a part of the Ottawa-Bonnechere Graben (Figure 2) (Neymark et al., 2013). There is a topographic high between the Ottawa River and Maskinonge Lake as well as a lowland running parallel to both water bodies that was a former drainage channel of the river and causes groundwater to flow to the west and east of this elevated area (King-Sharp et al., 2016). In its recent history (<15,000 a) the CRL area was subject to glaciation through most of the "Wisconsin Stage" of the Quaternary ice age. The Quaternary stratigraphy in the area as a result is highly heterogeneous, containing soil, peat, gravel, sand, silt and clay in glaciomarine and fluvial-aeolian sequences (Catto et al., 1982). This recent glaciation was postulated to have involved a glacial advance followed by a retreat and the creation of a large proglacial lake open to the Atlantic Ocean referred to as the Champlain Sea (Gadd, 1958). The CRL site specifically

is thought to have been inundated by a late incursion of the Champlain sea, possibly only during the end of its existence (11,300 to 11,100 a), resulting in the deposition of marine sand, silt and clay (Catto et al., 1981).

1.6 Bedrock Geology

The Chalk River Laboratory (CRL) property is located within the Grenville Province on the northwest edge of the Central Metasedimentary Belt (CMB) as well as within the Central Gneiss Belt (CGB) (Figure 2) (Ketchum and Davidson, 2000; Neymark et al., 2013). On a smaller scale, CRL is near the northern boundary of the East-West Ottawa-Bonnechere (O-B) Graben south of the Mattawa Fault (Figure 2) (Easton, 1986). Topographically, the O-B graben stretches out in a 55 km wide low from Montreal to Ottawa, bound by the Petawawa Fault to the south and the Mattawa Fault to the north (Rimando and Benn, 2005). The O-B Graben combines with the Saguenay Graben to the east to form the St. Lawrence rift system. The zone of faulting in the O-B Graben trends WNW with major tectonic events typically due to aborted crustal rifting during the Paleozoic and Mesozoic related to collision events in the Appalachian (Kamo et al., 1995). The bedrock underlying the CRL is Proterozoic in age (1.74-1.45 Ga) and has undergone several deformation events including high grade metamorphism and ductile deformation. Three main periods of faulting are noted with the oldest likely associated with the closing of the Proto-Atlantic during the Paleozoic; a second stage associated with the opening of the Atlantic and the appearance of Cretaceous carbonatite dykes during the Mesozoic; and most recently associated with post-Cretaceous stresses in Eastern North America (Rimando and Benn, 2005). The tectonic history of the region is important to understand in order to predict future stability and potential seismic events. The CRL site is located adjacent to the Mattawa Fault Zone. Locally a syncline and anticline run from NE to SW (Figure 3) (Neymark et al., 2013;

King-Sharp et al., 2016). The area has undergone several orogenic periods of note. Two especially significant events to local geology are the Grenville Orogeny (1.1-0.98 Ga) and the Appalachian orogenies (540-250 Ma) which caused faulting in the Chalk River crystalline bedrock and allowed for hydrothermal activity to occur as a result of subsidence (Kumarapeli, 1985). Multiple dyke intrusions in the area caused additional fracturing and potential conduits for fluid advection along their margins or promoted the cycling of hydrothermal activity (Caringan et al., 1997).

At a local geological scale, the CRL site can be divided into three similar but separate assemblages. Figure 5 shows the three lithologic assemblages as well as the borehole locations used. All boreholes investigated as a part of this study except CR-9 and CR-13 were a part of the "CRG" series boreholes drilled in 2005-2014 as a part of the Canadian Nuclear Laboratory's (CNL's) geological waste management facility (GWMF) feasibility study at Chalk River Laboratories (CRL) (King-Sharp et al., 2016). CR-9 and CR-13 are two of the "CR" series boreholes originating in the late 1970s and early 1980s as a part of the Canadian Nuclear Fuel Waste Management Program's preliminary investigations (Bottomley et al., 1984; Bottomley, 1987; Bottomley and Veizer, 1992). Nearest the surface, assemblage A is a garnet-poor gneiss, the outcrops of which are generally restricted to the north of the CRL property (Figure 3). This hornblende-biotite quartz-feldspar gneiss has a granitic-dioritic composition (Neymark et al., 2013). Below assemblage A is assemblage B which outcrops on the majority of the CRL property (Figure 3) and makes up the majority of available core (Figure 6). Assemblage B is a garnet-rich gneiss made up of biotite-hornblende monzonitic gneiss in addition to garnet-biotite quartz-feldspar gneiss (Neymark et al., 2013). Finally, the lowest assemblage, assemblage C which outcrops at the southern tip of the CRL (Figure 6), is a garnet-poor gneiss composed of

migmatitic magnetite-biotite granitic or granodioritic gneiss (Neymark et al., 2013). The most common fracture-filling material is calcite. Pegmatitic granites and diabase intrusions occur as well as low temperature fracture-filling minerals like chlorite, iron oxide bearing minerals, and clays (Bottomley, 1987).

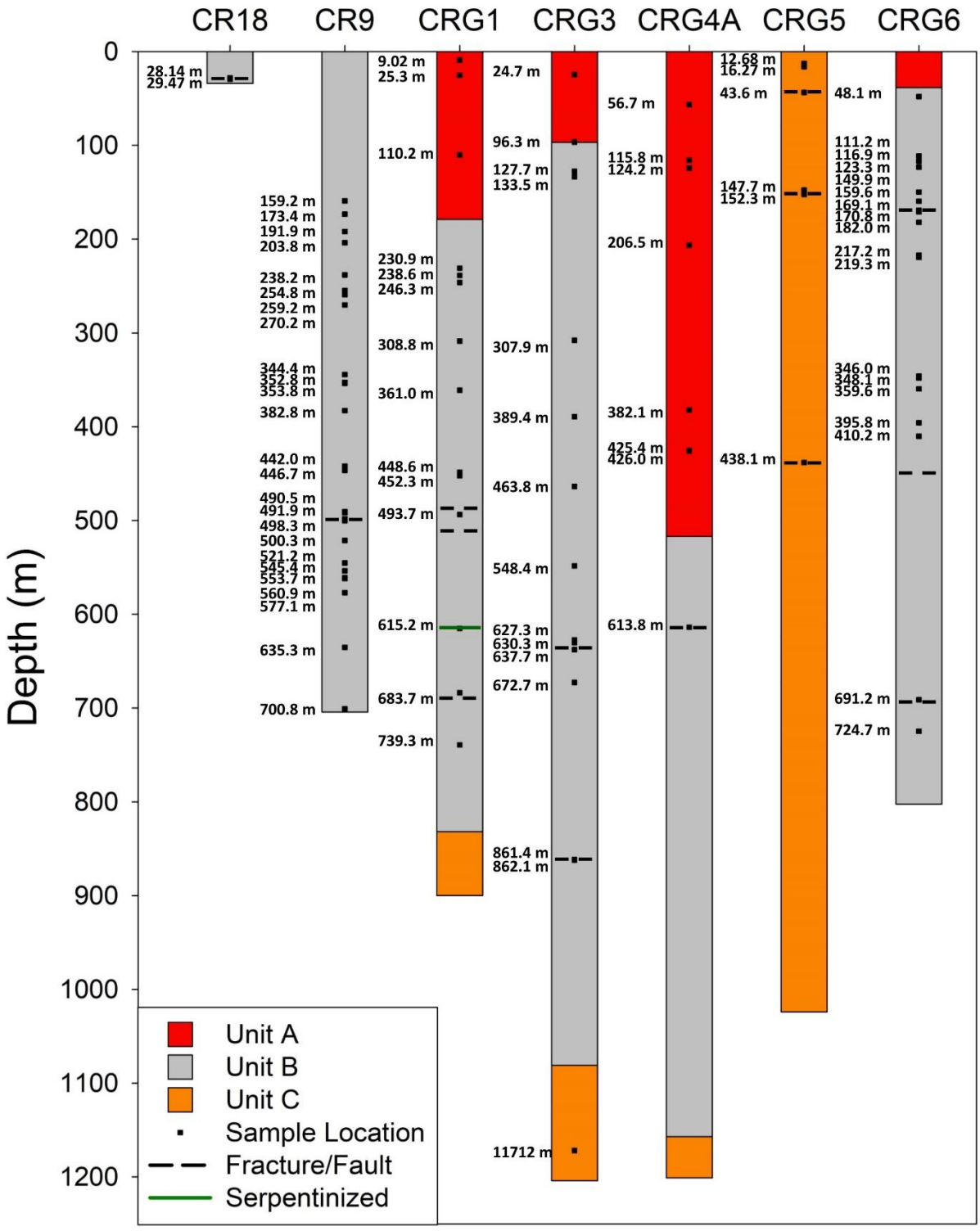

Figure 6. A selection of the boreholes studied at the CRL showing local geological classifications and notable features as well as the fracture mineral sample locations from Tian (2016) (from Tian, 2016).

2. **Methodology**

Calcite ($CaCO_3$) can be readily digested into gaseous carbon dioxide (CO_2) using acid in order to quantify the $\delta^{13}C$ and $\delta^{18}O$ within the mineral via Gas Chromatography Continuous Flow Mass Spectrometry (GC-CF-IRMS). Stable isotope analysis of calcite is a widely used tool for investigating calcite formation in crystalline rocks (Bottomley and Veizer, 1992; Blyth et al., 1998, 2004, 2009; Wallin and Peterman, 2009; Sandström and Tullborg, 2009). Samples were prepared and analyzed at the University of Waterloo Environmental Isotope Lab (UW-EIL), using a consistent methodology and calibrating all results using international standards. About 0.1 mg of calcite material was weighed and placed into a septum vial then flushed with helium to remove any interfering atmospheric gasses. Subsequently, 0.1 mL of phosphoric acid was added to the sample through an airtight septum, and all available carbon and oxygen was digested and converted to CO_2 at 90 ˚C for 1 hour. The gas produced was then sampled and separated chromatographically using a Gilson autosampler and 500 µL sample loop and the stable isotopes were quantified using a Micromass Isoprime Continuous Flow Isotope Ratio Mass Spectrometer to a precision of approximately ±0.2‰ for both $\delta^{13}C$ and $\delta^{18}O$ (Swart et al., 1991).

For chlorine stable isotope analysis to proceed, several chemical treatments had to be applied for purification and conversion purposes. A volume of groundwater or porewater typically amounting to 1-10 mg total chloride was acidified to a pH of ~2. All available chloride was then precipitated as silver chloride and converted to methyl chloride (CH_3Cl) for analysis after reacting with methyl iodide (CH_3I) for 48 hours at 100 ˚C in a sealed reaction vessel. The $\delta^{37}Cl$ signature was measured using gas chromatography continuous flow mass spectrometry (GC-CF-IRMS). The methyl chloride samples were diluted with helium, mixed with methyl iodide, and then were injected into an Agilent 7890B gas chromatograph using a CTC PAL

headspace autosampler. The injected volume was chromatographically separated using a 60 m Agilent J&W DB-5MS column and all unwanted compounds (CH_3I, CH_3Br, and He) were diverted to waste. The pure aliquot of CH_3Cl was instead redirected to a GV Instruments Isoprime CF-IRMS where the sample was ionized and mass fractions 52 and 50 are quantified (corresponding to ^{37}Cl and ^{35}Cl respectively). Each sample is analyzed against a reference gas and several internationally calibrated standards in order to quantify the $\delta^{37}Cl$ value in ‰ vs standard mean ocean chlorine (SMOC) (Equation (13)). The analytical technique produces an external precision of ±0.1‰ for samples as small as 0.3μmol (Shouakar-Stash et al., 2005b).

$$\delta^{37}Cl_{Sample}(‰) = \left(\frac{\left(\frac{^{37}Cl}{^{35}Cl}\right)_{Sample}}{\left(\frac{^{37}Cl}{^{35}Cl}\right)_{Reference}} - 1 \right) \times 1000 \quad (13)$$

For strontium isotope ratio measurements ($^{87}Sr/^{86}Sr$) for both aqueous and mineral forms, purification of strontium is achieved via exchange with a strontium specific resin (Eichrom Sr Resin SR-B100-S) after dilution/digestion using ultrapure MilliQ water mixed with Omnitrace ultrapure nitric acid. The collected aqueous strontium is then trapped, purified and eluted using Milli-Q ultrapure water and dried before being loaded onto degassed, high purity rhenium filaments. These filaments are loaded into a ThermoFinnigan Triton thermal ionization mass spectrometer (TIMS) where the filament is heated under vacuum and the sample is ionized. Mass fractions corresponding to ^{85}Rb (to correct for ^{87}Rb interference), ^{86}Sr, ^{87}Sr, and ^{88}Sr are collected in order to quantify the $^{87}Sr/^{86}Sr$ for a given sample. Samples are analyzed alongside NIST-SRM-987, an internationally calibrated strontium standard to ensure accuracy. Precision reported as standard error is typically less than ±0.00002 for samples as small as 5 ug.

Some major ion geochemistry, stable isotope ($\delta^{18}O$, $\delta^{2}H$, $\delta^{13}C_{DIC}$, $\delta^{37}Cl$, $\delta^{81}Br$, and $^{87}Sr/^{86}Sr$) and radioisotope data (^{3}H and ^{14}C) for groundwater as well as some precipitation and surface waters were provided by Chalk River Laboratories (CRL). The remaining geochemistry data as well as bulk Rare Earth Element (REE) analyses were performed commercially by Activation Laboratories Ltd. utilizing lithium metaborate/tetraborate fusion ICP and trace element ICP/MS by a Perkin Elmer Sciex ELAN 6000, 6100 or 9000 ICP/MS. Three blanks and five control samples were analyzed per group and duplicates were analyzed every 15 samples. The instrument is recalibrated every 40 samples (Activation Laboratories Ltd., 2016). A limited selection of calcite samples were analysed for REE in the Metal Isotope Geochemistry Laboratory at the University of Waterloo utilizing laser ablation inductively coupled mass spectrometry (ICP-MS). Samples were loaded onto pucks and analyzed using an Analyte G2 excimer laser ablation system coupled with an Agilent 8800 triple quadrupole ICP-MS. Samples were ablated for 30 seconds resulting in ~40 µm of sample from a spot size of 110 µm. The standards used for calibration were NIST 610 and 612 to match the calcite composition (Ongaro, 2018). Nine additional calcites were analyzed for REE by Tian (2016) at the Analytical Laboratory Beijing Research Institute of Uranium Geology (ALBRIUG). These samples were petrographically identified and digested in hydrofluoric and nitric acid then analyzed by ICP-MS for chemical composition and REE (0.01% detection limit).

Several boreholes were selected for crush and leach analysis in order to assess the geochemical signatures of trapped porewaters within the crystalline rock-mass. A length of available host rock core material (typically 500-1000 g) is pulverized and screened down to a fine rock flour. This flour is combined with Milli-Q ultrapure water in a 1:1 rock to water ratio by weight and oscillated at ~120 RPM for 24 hours. This slurry is then left to settle for 24 hours

before the available water is decanted and filtered to 0.45 micron for analysis. The resulting water samples could then be analyzed for geochemistry as well as stable isotopes without any additional special treatment (Waber and Smellie, 2008).

3. Results

Fracture mineral samples from 158 discrete locations in 7 different boreholes were analyzed for $\delta^{13}C$ and $\delta^{18}O$, predominantly in calcite, along with a selection that were analyzed for $^{87}Sr/^{86}Sr$ as a part of the MSc thesis undertaken by Long Tian (Table 1) (Tian, 2016). Major ion geochemistry for boreholes CR-9 and CR-13 from older geochemical studies (Bottomley et al., 1984; Bottomley, 1987; Bottomley and Veizer, 1992) are shown in Table 2. These results were compared with extensive new geochemical and isotopic analyses performed on local groundwaters pumped from isolated intervals within 5 key boreholes: CR-9, CRG-1, CRG-3, CRG-4A and CRG-6. Table 3 lists the major ion geochemistry for these CRG series boreholes. $^{87}Sr/^{86}Sr$ analyses were performed along with stable isotopic analyses including $\delta^{18}O$, $\delta^{2}H$, $\delta^{13}C$, $\delta^{37}Cl$ and $\delta^{81}Br$ on groundwaters and from the CR boreholes (Table 4) as well as $\delta^{18}O$, $\delta^{2}H$, $\delta^{13}C$, $\delta^{37}Cl$ and $\delta^{81}Br$ on groundwaters from the CRG boreholes (Table 5). A selection of $^{87}Sr/^{86}Sr$ and $\delta^{37}Cl$ results for porewaters leached via crush and leach extraction are included in Table 7 (Waber and Smellie, 2008).

3.1 Fracture Mineralogy, Stable Isotopes and Rare Earth Elements

The main fracture networks that exist in the bedrock of Chalk River Laboratories (CRL) were predominantly formed during several periods of increased tectonic activity (Kumarapeli, 1985). The Grenville Orogeny (1.1-0.98 Ga) for example caused significant sedimentation and faulting events in the Ottawa-Bonnechere (O-B) Graben (Neymark et al., 2013). This orogeny likely also induced hydrothermal cycling as subsidence occurred and flow paths were formed in

newly created fracture networks (Kumarapeli, 1985). As soon as interconnected fractures were formed, they would be likely conduits for fluid flow and available groundwater and hydrothermal fluids began advecting through these pathways. The evolution of these fluids over time resulted in the precipitation and/or alteration of minerals, often sealing the fractures as a result (Wallin and Peterman, 2016). Fracture-infilling minerals vary from chlorite and calcite, which are most abundant, to quartz, clays and serpentine (Bottomley, 1987). Although the existence of these minerals will significantly reduce the permeability of a fracture, the possibility of fault reactivation and additional fluid events could result in remobilization of soluble mineral phases such as calcite and later stage precipitation and alteration events. According to Tian (2016), there are six different dominant fracture-filling minerals found in the boreholes investigated parallel to this study: chlorite, quartz, fine-grained crystalline calcite, coarse-grained crystalline calcite, fibrous calcite, and dolomite (Tian, 2016).

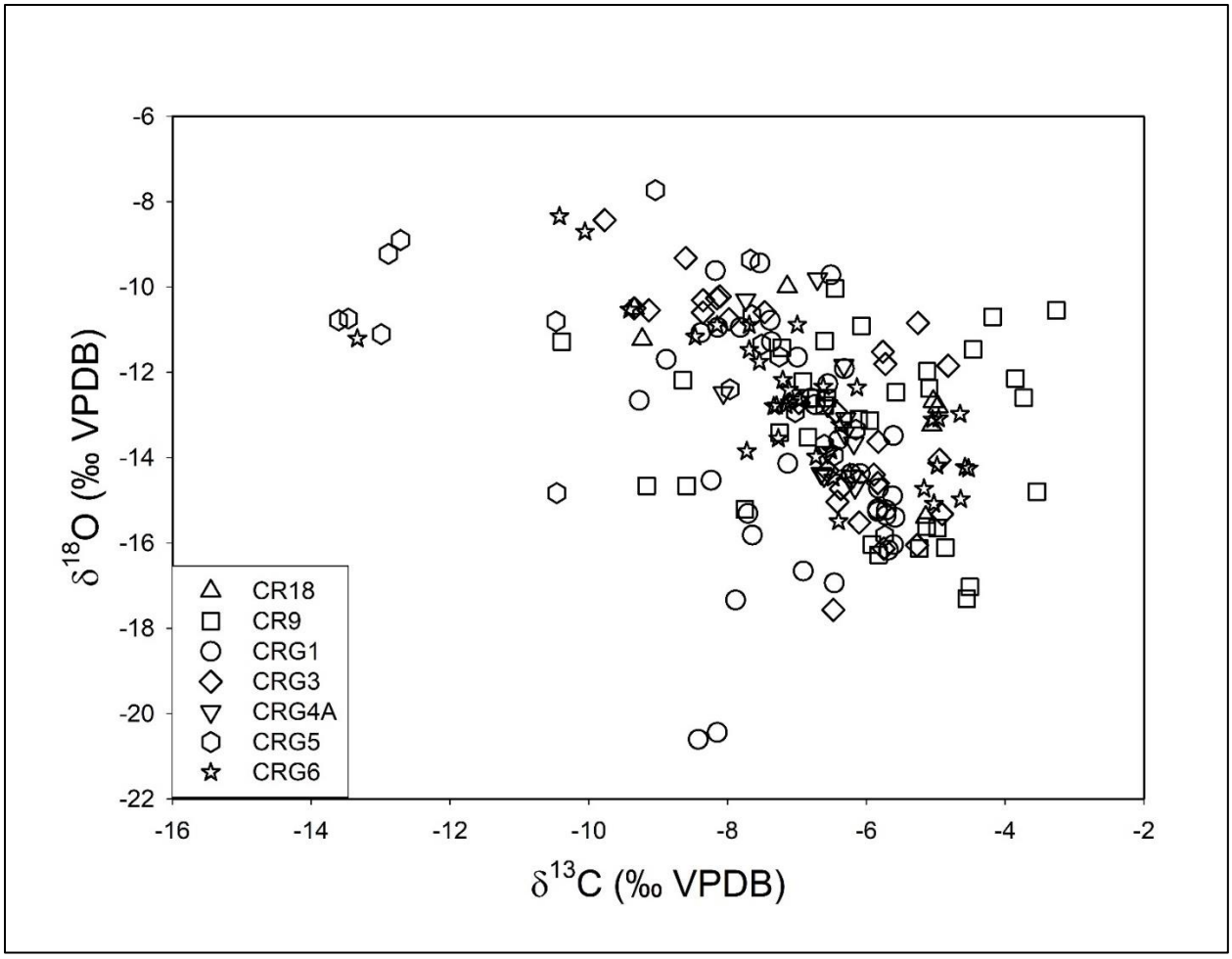

Figure 7. A survey of calcite $\delta^{13}C$ and $\delta^{18}O$ values measured in fracture minerals from the CRL (from Tian, 2016).

The results of $\delta^{13}C$ and $\delta^{18}O$ from over 150 fracture calcites sampled by Tian (2016) and Bottomley and Veizer (1992) are provided in Table 1 and Figure 7. These samples were collected from 6 of the 8 boreholes and were analyzed during the parallel investigation by Tian (2016) (CR-9, CRG-1, CRG-3, CRG-4A, CRG-5 and CRG-6) and supplemental $\delta^{13}C$ and $\delta^{18}O$ data was taken from Bottomley and Veizer (1992) for borehole CR-9. $\delta^{18}O$ results across the CRL varied from -21 to -8‰ VPDB (+10 to +23‰ VSMOW) and $\delta^{13}C$ varied from -14 to -3‰ VPDB. This is relative to a global range of -50 to +30‰ VPDB for $\delta^{13}C$ and -30 to 0‰ VPDB (0 to +30‰ VSMOW) for $\delta^{18}O$ (Blyth et al., 2009), placing the dataset from the CRL well

within the extremes of fracture mineral carbonate isotope values when compared to a global survey (Figure 8).

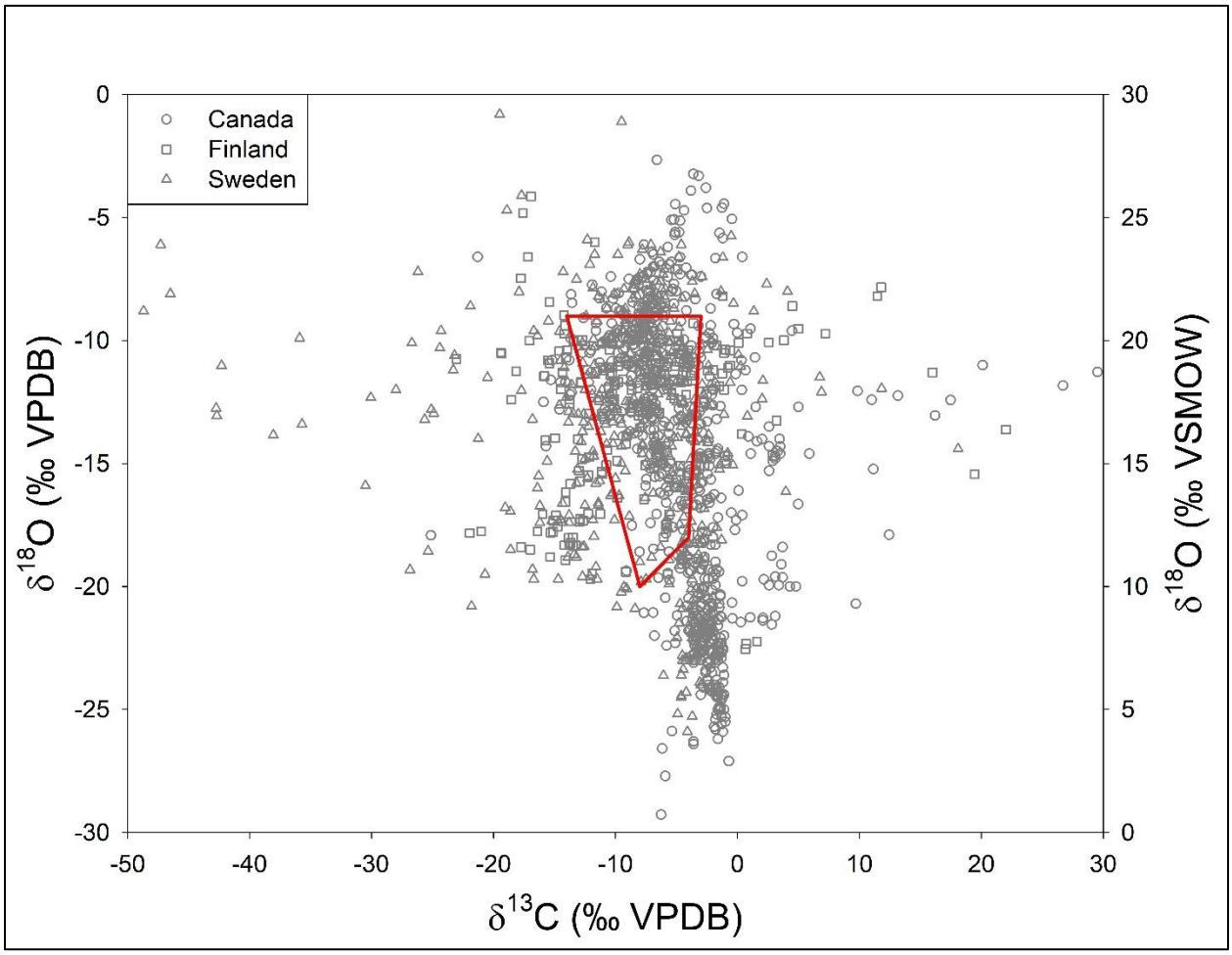

Figure 8. A comparison of the stable isotopic composition found in the CRL carbonates (red) against carbonates from similar geological settings in Canada, Finland and Sweden (Blyth et al., 2009).

Rare Earth Element analyses were performed on a selection of silicates, fracture minerals and leachable minerals from boreholes at the Chalk River Laboratory (CRL) site (Table 8) all of which originate from the investigation of Tian (2016). While the scraping required to remove vein calcites and other minerals can sometimes be contaminated with small amounts of host rock material, five samples were determined to be high enough purity based on lithium metaborate/tetraborate fusion ICP and trace element ICP/MS compositional analysis to be trusted

as truly representative of the calcite, which when combined with the calcite REE samples previously analyzed in China, brought the total number of viable fracture mineral REE results to 14 (Table 8) (Tian, 2016). While a gentle acid digestion of the calcite samples is somewhat selective for carbonate materials, the non-selective destructive nature of lithium metaborate/tetraborate fusion ICP makes the purity of the samples selected for this type of analysis very important (Activation Laboratories Ltd., 2016). An available tool to assist in the interpretation and rule out the possibility of contamination is laser ablation ICP-MS. Laser ablation ICP-MS utilizes much smaller sample sizes and can ablate the sample directly from calcites mounted onto pucks. This allows not only for higher precision in terms of specific locations on the calcite vein, but also the ability to track the changes in REE signatures across a given fracture and its often many layered precipitation generations. Utilizing this technology, Ongaro (2018) was able to perform several measurements from REE fracture calcite samples, focusing on two principal objectives: comparison to the bulk "solution analysis" results, and special comparisons across several transects. The comparison of small-scale samples to bulk solution series data was largely successful with minor discrepancies explainable due to scale differences and heterogeneity. Significant differences where they did occur were likely caused by host rock silicate contamination during sampling for the bulk solution series data (Ongaro, 2018). The sample selected for transect analysis was CR9-553.7m due to apparent zoning visible in the calcite crystals as a result of cumulative precipitation events, and three separate transects were performed for a total of 28 discrete REE analyses. The transects did not show significant variability overall in the REE analyses but some interesting trends were notable (Figure 9) (Ongaro, 2018).

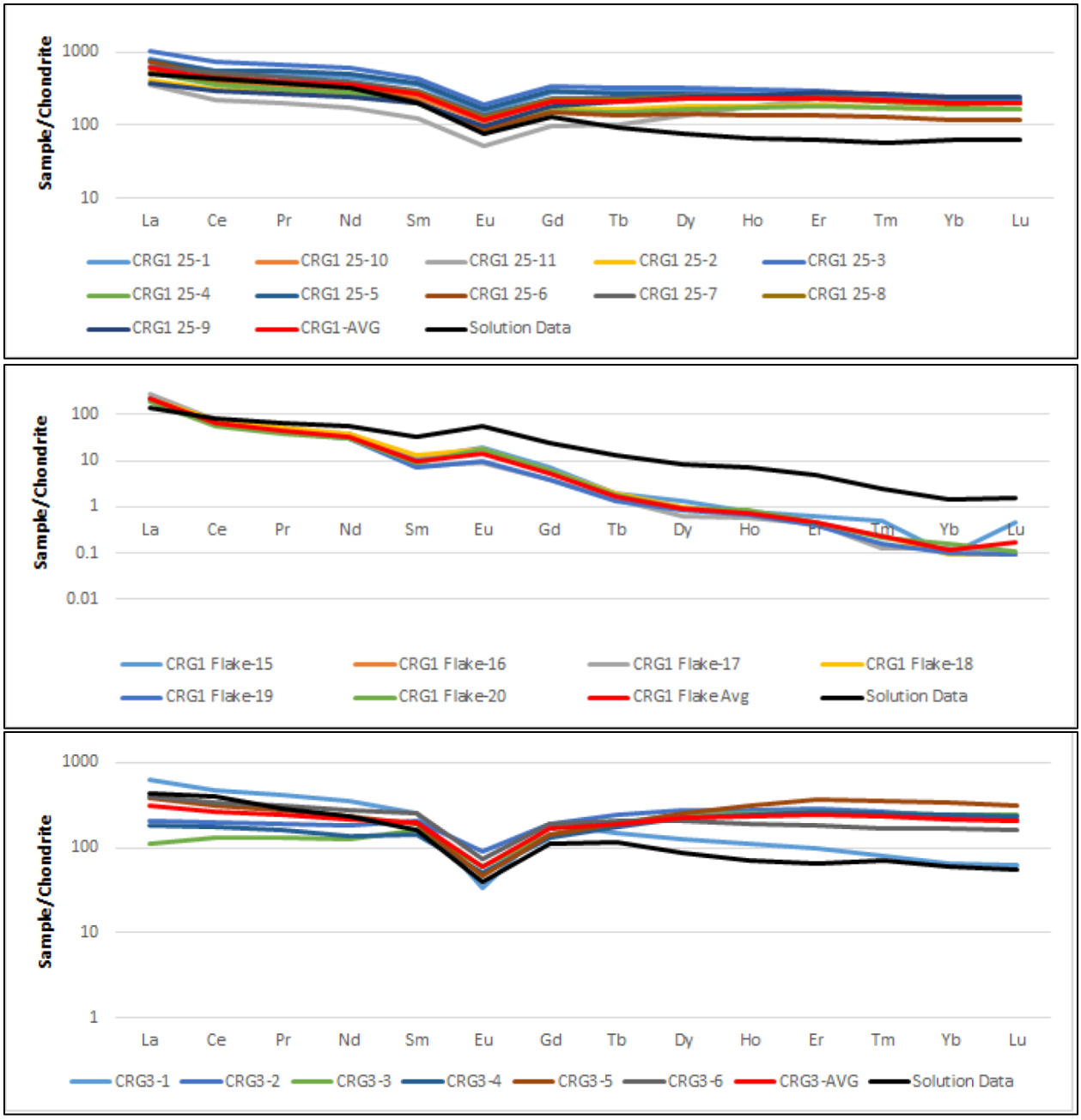

Figure 9. Chondrite-normalized rare earth element transect data generated by Ongaro (2018) for sampled calcite vein transects from CRG-1 25.3 m, CRG-1 615.2 m and CRG-3 24.7 m.

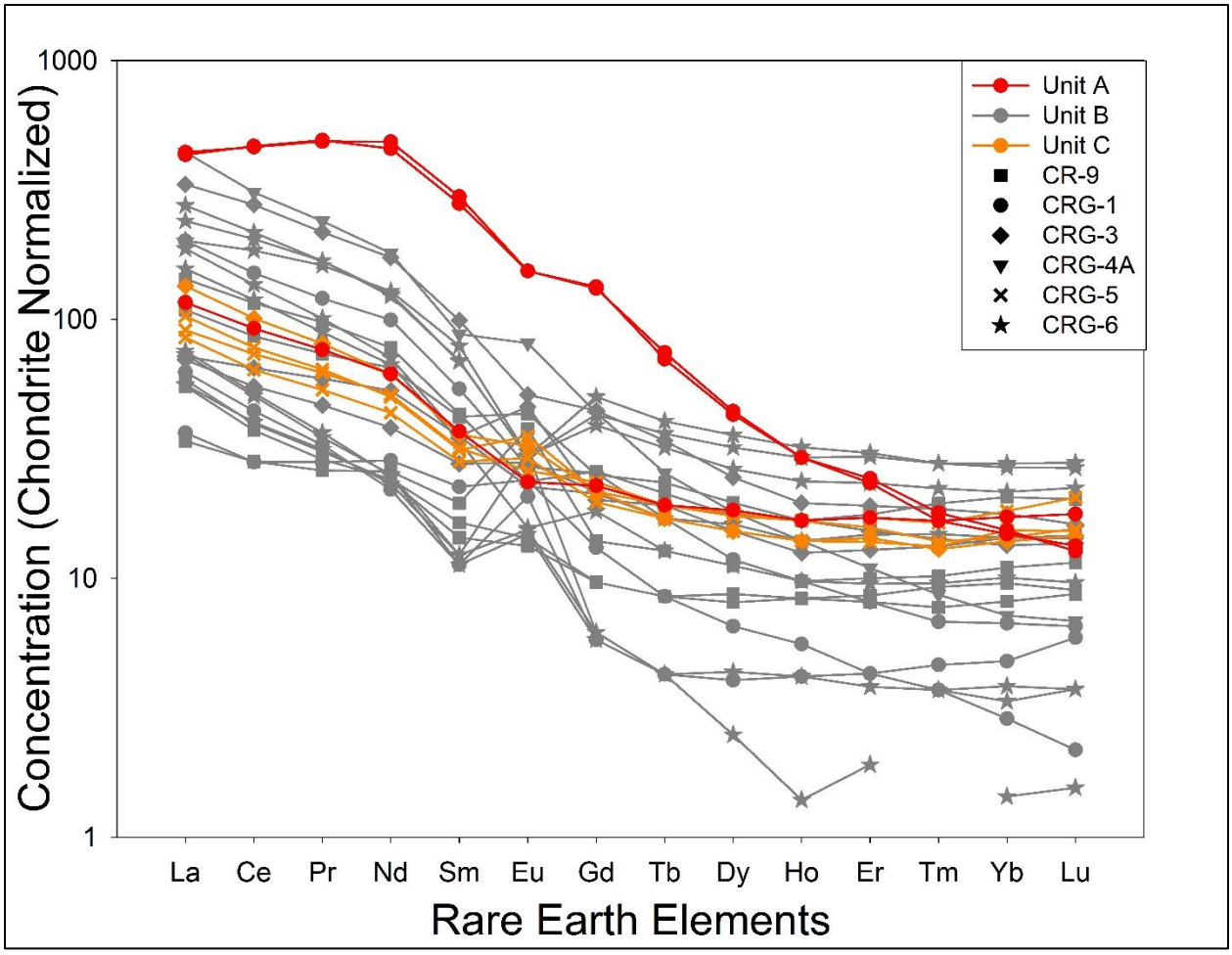

Figure 10. Chondrite-normalized REE results in silicate samples from boreholes in the CRL.

The largest database of bulk REE analyses available for this study were performed on host rock silicates in order to assess the influence of water-rock interaction on fracture fluid chemistry (Table 8). A limited number of silicate REE results are available for Unit A (Figure 10), which is described as a garnet-poor hornblende-biotite quartz-feldspar gneiss (Neymark et al., 2013), and is limited to CRG-1. The Unit A silicates contain among the highest concentrations of REE, are significantly enriched in LREE and have uniform REE patterns with a slightly negative δEu anomaly of 0.8. Unit C, described as a garnet-poor gneiss and more specifically migmatitic magnetite-biotite granitic or granodioritic gneiss (Neymark et al., 2013), also has limited data. In this case, samples originate mostly from CRG-5 with one deep sample

from CRG-3. The REE patterns observed at these locations were all very similar (Figure 10) with the most significant differences occurring in the observed δEu anomaly which varied from negative at 0.7 to positive at 1.4, suggesting possible differences in plagioclase content. The largest and therefore most variable dataset comes from Unit B, described as a garnet-rich gneiss containing biotite-hornblende monzonitic gneiss as well as garnet-biotite quartz-feldspar gneiss. This unit, which dominates the boreholes studied during this investigation, spans almost the entirety of the CRL property.

3.2 Groundwater Geochemistry

In order to assess site stability further, a large groundwater database collected by Chalk River Laboratories (CRL) researchers (Table 3, Table 5) was assessed and compared to the fracture mineral data compiled by Tian (2016). Additional analyses of the stable isotopes of chloride, bromide and strontium isotopes were performed on many of these samples (Table 4, Table 5). The combined results of groundwater chemical and isotopic analyses from all sources are presented in this section borehole by borehole at the CRL site (Figure 3). Average values of pH, major and significant ion concentrations, as well as $\delta^{37}Cl$ and $^{87}Sr/^{86}Sr$ measured in groundwater are listed for the five principal boreholes for this study (Table 6), clearly showing the influence of higher conductivity waters on CR-9 and CRG-1. Rock pore waters extracted using a crush and leach technique modified from Waber and Smellie (2008) were studied for comparison to the groundwaters at the site (Peterman et al., 2016) (Table 7). Overall there were general trends noted in some of the boreholes and some major similarities and differences that can be noted. CR-9 and CRG-1 contain higher salinity Na-Cl waters at depth that are not present in other boreholes except possibly CRG-6 and CR-13 (Figure 11). The boreholes that displayed the least chemical variability at depth were CRG-3 and CRG-2, both firmly Na-HCO_3 water

types (Figure 11). CRG-6, CR-13 and CRG-4A were the most varied in terms of geochemical classifications and include waters that share similar geochemical signatures with the other borehole groups.

3.2.1 CR-9

Borehole CR-9 is the westernmost and oldest of the boreholes studied during this investigation (Figure 3). Geologically, the dominant rock unit along the length of the borehole is made up entirely of unit B as defined by Neymark et al. (2013) (Figure 6). Drilled during the late 1980s, it was the subject of several early studies to assess the potential stability of the CRL bedrock and to understand the fracture minerals present (Bottomley, 1987; Bottomley and Veizer, 1992). The borehole was reopened, rehabilitated, and pumped in September 2009 utilizing 12 discrete packer intervals to pump and sample groundwater down to a depth along the borehole of 704.3 m. Notably, all major ions increase below this zone except for bicarbonate (HCO_3^-). The shallowest available sample (0-76 m) can be categorized as a Ca-HCO_3 type, chemically like surface and shallow meteoric recharge waters found in the area (Figure 11). Deeper intervals above the fracture zone described at ~500 m are classified as Na-HCO_3 type (Figure 11), while the more saline samples from packered intervals at depths below the fracture zone are chloride dominated Na-Cl type waters. Chemically, waters measured above a fracture zone at ~500 m depth along the borehole are fresh (conductivities 213-1277 µS/cm); while those measured below the fracture zone are brackish to saline (3100-4300 µS/cm) (Figure 12). Isotopically, the measured $\delta^{37}Cl$ in groundwater showed very little variability (-0.10 to +0.07 ‰ vs SMOC) with all results falling within the expected analytical precision (±0.1‰) of seawater (0‰ SMOC) (Figure 12). $^{87}Sr/^{86}Sr$ values measured in the waters from packer intervals were slightly more radiogenic than the $^{87}Sr/^{86}Sr$ measured in associated fracture calcites with a general trend to more

radiogenic values with depth (from 0.709046 at 0-76 m depth along the borehole to 0.709802 at 640-704 m depth along the borehole with a spike at ~300 m depth) (Figure 12). There is a strong correlation between the $^{87}Sr/^{86}Sr$ measured in the groundwater and $^{87}Sr/^{86}Sr$ measured in rock porewaters collected via crush and leach of core material (Figure 12). $\delta^{18}O$ and $\delta^{2}H$ showed limited variability (-11.02 to -12.66‰ VSMOW and -79 to -89‰ VSMOW, respectively) with no discernible trends with depth (Figure 12). When compared to the local meteoric water line (Figure 13), the lack of significant variability is apparent. Interestingly, more than any other borehole, CR9 water stable isotope data plot above the meteoric water line. This could be the result of several possible influences including, but not limited to, processes described as impacting many Canadian Shield saline fluid sites such as the hydration of silicates (Fritz and Frape, 1987; IAEA, 1983). As compared to values found in fracture carbonates, the $\delta^{13}C$ of DIC cluster into two distinct groups, separated by the previously noted fracture zone. $\delta^{13}C$ in the more dilute shallow waters (above ~500 m depth along the borehole) is more enriched and varies from -14.9 to -17.2‰ VPDB while the waters below that zone are more saline and depleted, ranging from -24.8 to -20.2‰ VPDB (Figure 12).

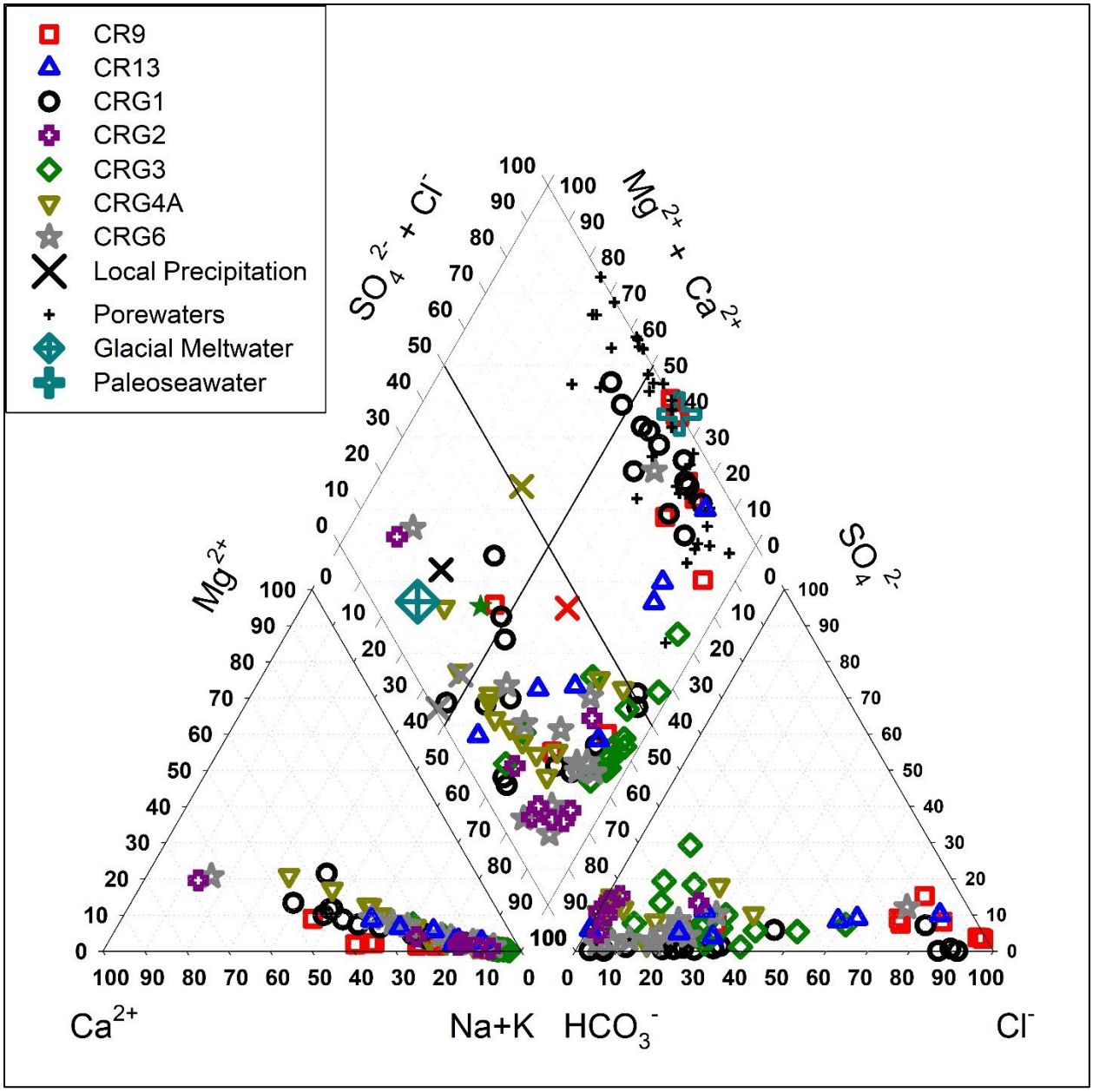

Figure 11. Piper plot comparing the major ion geochemistry of the sampled borehole groundwaters as well as a selection of porewaters (Peterman et al., 2016), out diffusion waters and theoretical end members.

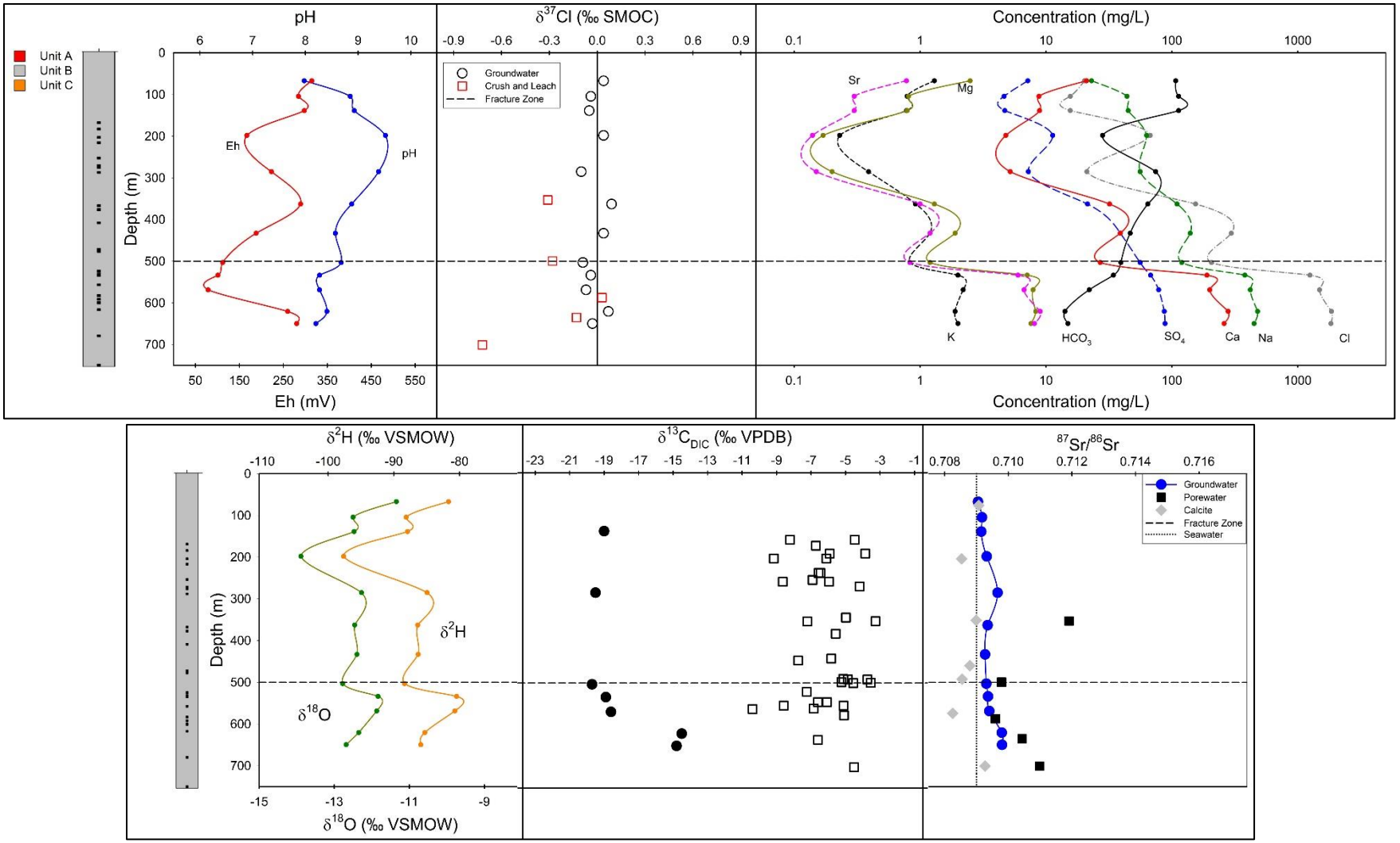

Figure 12. Geochemical and isotopic parameters (Eh, pH, δ^{37}Cl, major ion geochemistry, δ^{18}O, δ^{2}H, $\delta^{13}C_{DIC}$ (black circles), $\delta^{13}C_{CALCITE}$ (open black squares) and $^{87}Sr/^{86}Sr$) measured from the packer intervals in borehole CR-9 plotted versus depth along the borehole. Geology as well as fracture sample locations are included (solid black squares). Also shown as a dashed horizontal line is the major fracture zone at 500 m.

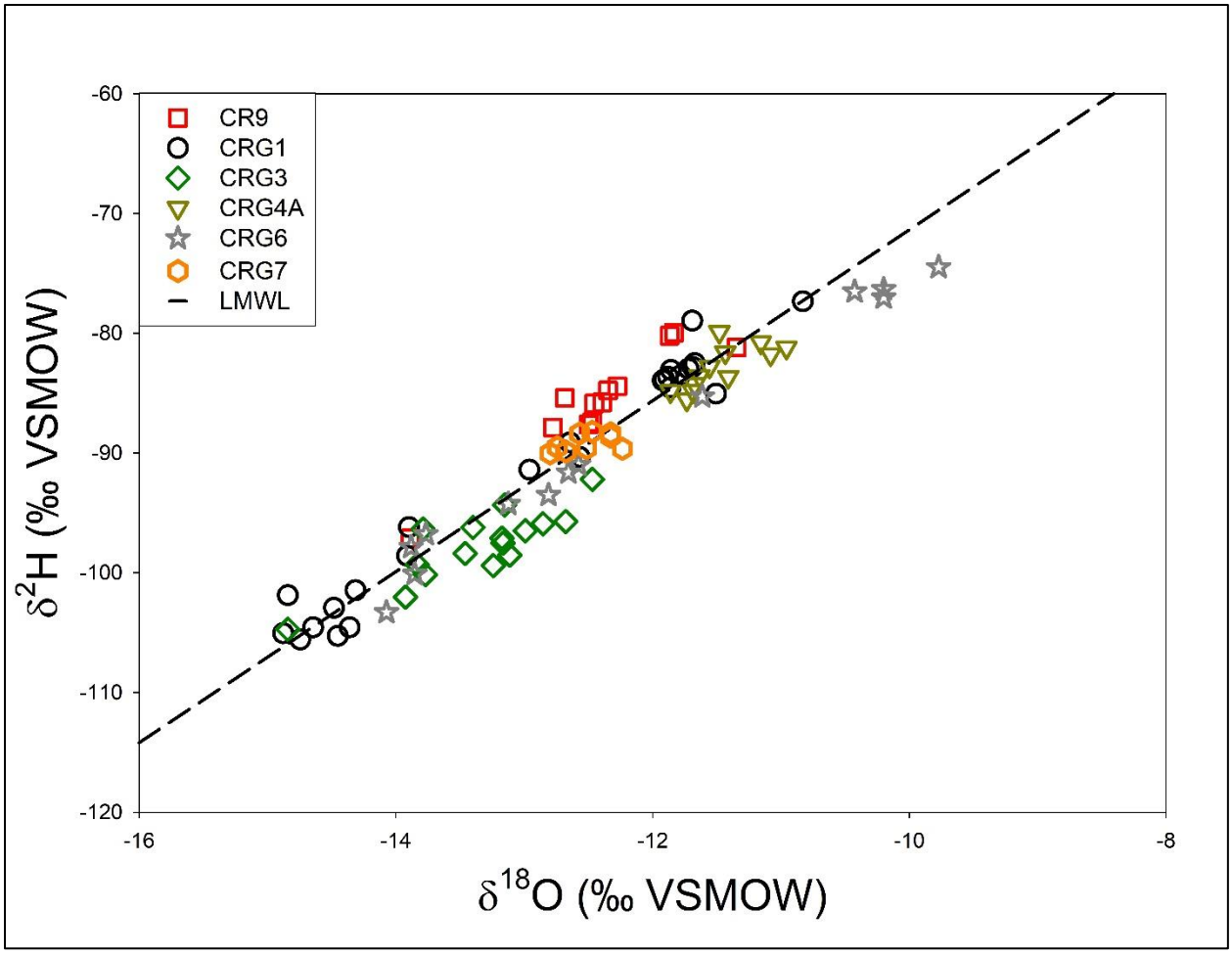

Figure 13. $\delta^{18}O$ and $\delta^{2}H$ values of groundwaters sampled from the CRL boreholes in this study compared to the local meteoric waterline.

3.2.2 CRG-1

The CRG-1 borehole located in the northeastern portion of the study area (Figure 3) was drilled as part of Chalk River Laboratory's (CRL) investigation into the feasibility of a geological waste management facility (GWMF) (King-Sharp et al., 2016). Geologically, CRG-1 contains examples of all three locally defined units (Figure 14) and also contains several easily identifiable faults and alteration zones (Figure 6). Groundwater geochemistry from CRG-1 is the most variable of all the boreholes included in this study. The borehole was pumped from 21 discrete packer intervals up to a depth along the borehole of 899.86 m in May 2011 (Figure 14).

However, intervals 13, 15, 16, 17, 19, and 20 (Figure 14) were not productive enough to purge the appropriate water volume for a sample. The borehole was re-sampled in 2016 for all missing intervals except interval 21 (Table 3). All groundwaters from above 431 m along the borehole were relatively dilute (<1000 µS/cm), however, below this depth intervals were significantly more variable in geochemical composition as seen in multiple parameters plotted on Figure 14. This is possibly due to infiltration of fluids from a zone of fracturing noted at ~450 m along the borehole. At a packer interval of 432-460 m there is a significant and sharp increase in the concentration of dissolved species (Figure 14). From 461 m to 593 m, groundwaters become more dilute like the composition observed in shallower waters. Below 594 m, there is another spike in concentrations (Figure 14). An additional zone of alteration occurs at ~613 m along the borehole associated with serpentinization and potentially localized hydrothermal processes. Most CRG-1 intervals (especially the intervals with higher conductivity) are Na-Cl type waters very similar to seawater composition and locally measured rock porewater compositions (Peterman et al., 2016) (Figure 11). The shallow waters of CRG-1 are classified as Ca-HCO_3 type fluids and have a similar chemistry to the local meteoric recharge waters and surface lakes. Many of the groundwaters from deeper intervals are most likely mixtures of fresh and saline fluids and would be classified as Ca-Na-HCO_3-Cl waters (Figure 11). Isotopically, groundwaters from the intervals sampled in CRG-1 show significant variability in measured $\delta^{37}Cl$ isotopic values compared to the 0.17‰ of variability noted in CR-9 (Figure 14). $\delta^{37}Cl$ values varied from -0.54‰ SMOC at a depth of 286-319 m along the borehole to +0.70‰ SMOC at a depth of 594 to 637 m along the borehole (Figure 14) (corresponding to the zone of shearing and alteration associated with serpentinization). For the four intervals in which corresponding rock porewater $\delta^{37}Cl$ values were measured, three measured values are significantly more depleted than the

associated groundwater ($\Delta^{37}Cl_{GROUNDWATETR\text{-}POREWATER}$=0.3‰ to 0.8‰) (Figure 14). The fourth interval (594-637 m) showed very similar $\delta^{37}Cl$ for both groundwater and porewater samples. The $^{87}Sr/^{86}Sr$ measured in groundwaters from the packer intervals of CRG-1 were more radiogenic than the corresponding fracture calcites and an overall trend toward more radiogenic values can be observed with depth from 0.70919 at interval 70-119 m along the borehole to 0.71123 at interval 824-900 m along the borehole. Generally, the $^{87}Sr/^{86}Sr$ observed in the groundwaters are less radiogenic than corresponding porewater measurements, except for interval 594-637 m (serpentinized zone) in which both the measured groundwater and porewater values are very similar, much like the relationship seen for $\delta^{37}Cl$. $\delta^{18}O$ and $\delta^{2}H$ in the groundwater packer intervals showed an interesting relationship with depth. With the exceptions of intervals 1 and 2 (corresponding to 0-119 m), $\delta^{18}O$ and $\delta^{2}H$ values are slightly more depleted in intervals 3-12 (121-460 m) than intervals 13-21 (461-900 m). When compared to the local meteoric water line, these measured isotopic values seem to cluster in two distinct zones, a colder climate group of fluids with values approximately -15‰ and -105‰ VSMOW for $\delta^{18}O$ and $\delta^{2}H$, respectively, and a warmer climate zone of approximately -11‰ and -80‰ VSMOW for $\delta^{18}O$ and $\delta^{2}H$, respectively (Figure 13). The water isotopes do not show significant evidence of evaporation, but two values plot with deuterium excess like data collected from CR9. Dividing these two groups is a zone containing a major planar fracture feature from 447.2-448.7 m (Figure 14). Limited available $\delta^{13}C$ data from DIC show significant variability with depth (-18.9‰ to -13.8‰ VPDB) although there are no discernable trends.

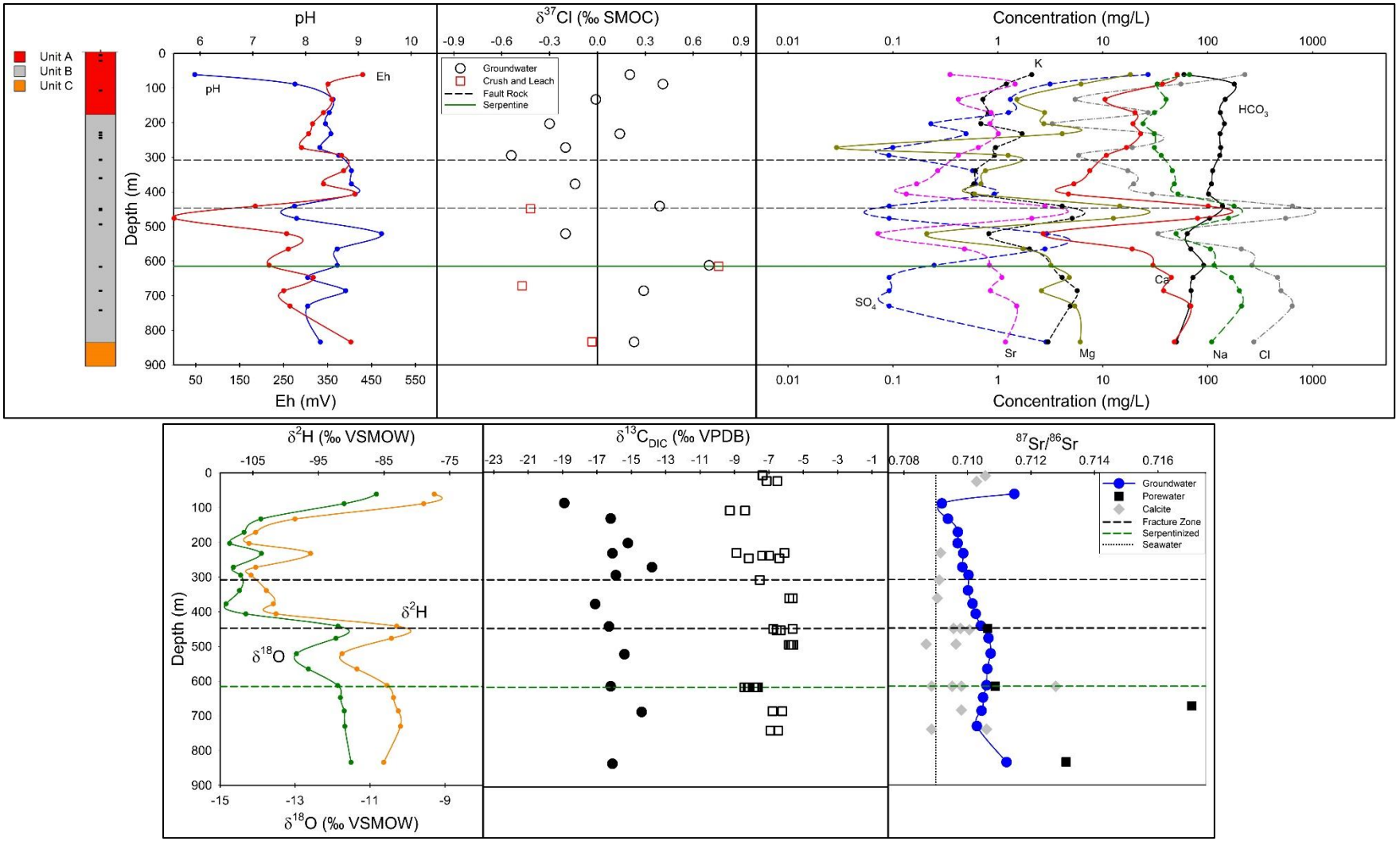

Figure 14. Geochemical and isotopic parameters (Eh, pH, δ^{37}Cl, major ion geochemistry, δ^{18}O, δ^{2}H, $\delta^{13}C_{DIC}$ (black circles), $\delta^{13}C_{CALCITE}$ (open black squares) and $^{87}Sr/^{86}Sr$) measured from the packer intervals in borehole CRG-1 plotted versus depth along the borehole. Geology as well as fracture sample locations are included (solid black squares). Also shown as a dashed horizontal line is the fracture zones at 300 m and 450 m and a green line that represents an area of serpentinization at 600 m along the borehole.

3.2.3 CRG-3

The CRG-3 borehole has the most consistent groundwater geochemistry along its length in this study. It was drilled as a part of CRL's GWMF feasibility study between 2005 and 2014 (King-Sharp, 2016) in the central portion of the CRL research site, ~500 m north of CRG-6 and 500 m southwest of CRG-1 (Figure 3). CRG-3 was the longest borehole available to this study, reaching a length of more than 1200 m and spanning all three geological units (Figure 6, Figure 15). For groundwater geochemical and isotopic analysis, the CRG-3 borehole was instrumented with Westbay packers and pumped in May of 2012 for 17 different intervals down to a depth along the borehole of 1204 m (Figure 15), although interval 17 (1063-1204 m) was not productive enough to sample (Table 3). Measured conductivities are very uniform and stable throughout the borehole intervals with a range from 235.4 to 342 µS/cm, well within the range of fresh water. The only ion that shows some slight changes in trend from the others is chloride with a small spike observed at interval 8 (416-492 m), enough to shift the waters collected from interval 8 and interval 9 (493-542 m) from Na-Ca-HCO_3 and Na-HCO_3 type waters to a Na-Cl type (Figure 11). Isotopically, the $\delta^{37}Cl$ values measured from available packer intervals in CRG-3 did not show any significant variability (Figure 15). The groundwaters sampled varied from -0.35‰ to -0.17‰ SMOC, slightly more depleted than seawater (0‰ SMOC). $^{87}Sr/^{86}Sr$ measured in the groundwaters sampled from CRG-3 showed very little change below 74 m depth along the borehole, although a slight trend towards more radiogenic values can be observed with depth (Figure 15). Available crush and leach and calcite samples analyzed for $^{87}Sr/^{86}Sr$ plotted consistently with the groundwater values, with all available $^{87}Sr/^{86}Sr$ data (groundwater, porewaters, fracture calcites) measured between 0.70940 and 0.71073 (Figure 15). $\delta^{18}O$ and $\delta^{2}H$ were measured at all intervals and had a range of -12.5‰ to -14.8 and -92‰ to -105‰ VSMOW,

respectively. When compared to the local meteoric water line, the CRG-3 data plots in a group that is slightly depleted versus what would be expected for local meteoric recharge (Figure 13). This depletion could be related to several processes, likely limited to either slight evaporation or possibly exchange reactions with local rock minerals, or more likely mixtures with a more depleted colder source. Available $\delta^{13}C$ data from dissolved inorganic carbon (DIC) were like other groundwaters in the area and did not vary greatly (-17.1‰ to -14.7‰ VPDB).

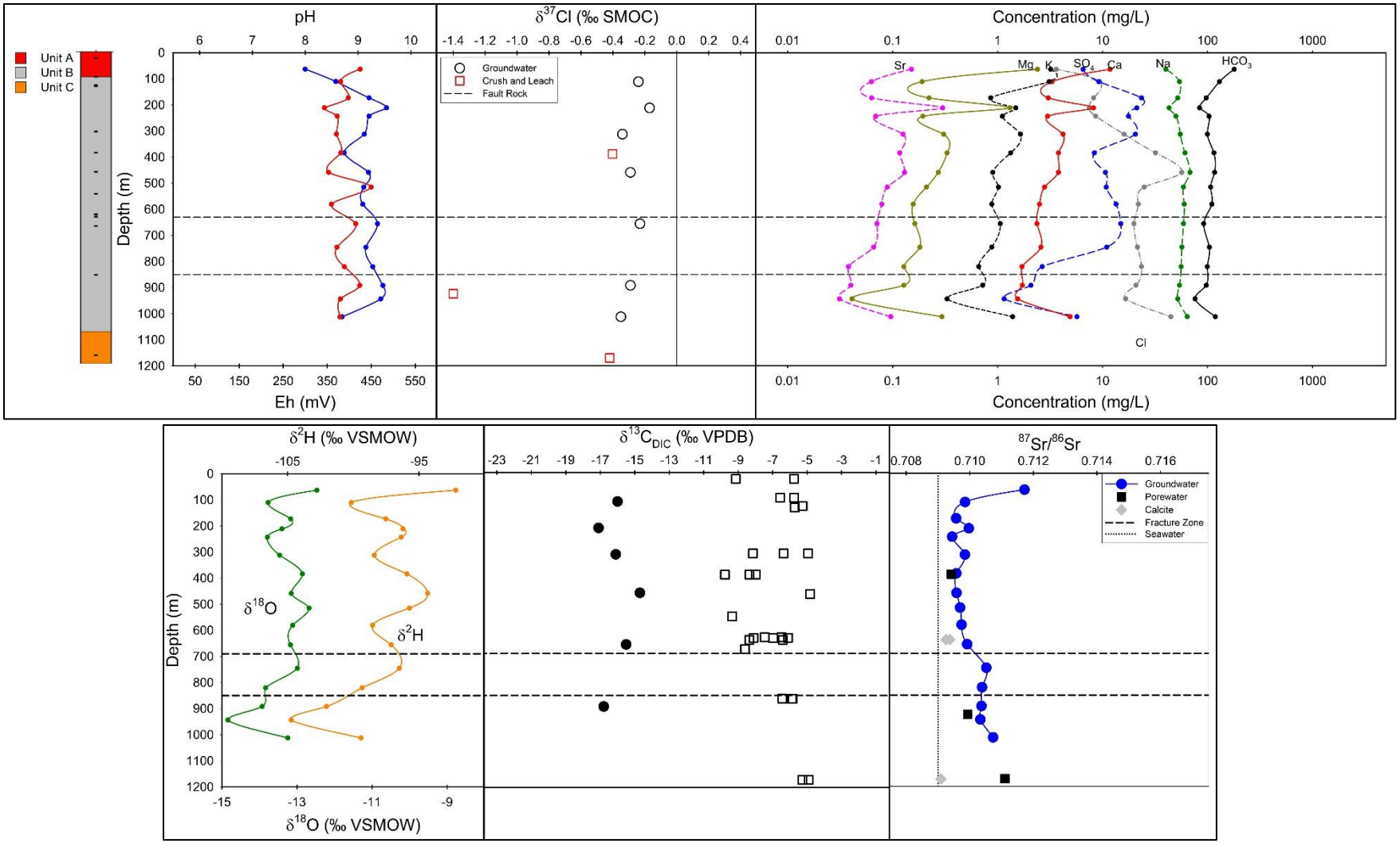

Figure 15. Geochemical and isotopic parameters (Eh, pH, $\delta^{37}Cl$, major ion geochemistry, $\delta^{18}O$, $\delta^{2}H$, $\delta^{13}C_{DIC}$ (black circles), $\delta^{13}C_{CALCITE}$ (open black squares) and $^{87}Sr/^{86}Sr$) measured from the packer intervals in borehole CRG-3 plotted versus depth along the borehole. Geology as well as fracture sample locations are included (solid black squares). Also shown as a dashed horizontal line is the fracture zones at 700 m and 850 m.

3.2.4 CRG-6

Approximately 500 m south of CRG-3, the CRG-6 borehole was drilled as a part of the CRL's GWMF feasibility project from 2005-2014. CRG-6 is located near the middle of the CRL property but represents the southernmost borehole studied during this investigation (Figure 3). Geologically, CRG-6 is dominated by Unit B with only a small shallow section (~-0-40 m) being made up of Unit A (Figure 6). For the collection of groundwater samples, CRG-6 had Westbay casing and packers installed in May of 2013 in 15 distinct intervals to a depth of 800 m along the borehole (Figure 16). Thirteen of the fifteen intervals produced enough water to sample except for Interval 13 and 15 (663-700 m and 752-800 m respectively). The results for CRG-6 plotted on Figure 16 show a variety of geochemical and isotopic trends with depth along the length of the borehole but in terms of salinity, all samples are fresh and within a conductivity range of 229 to 420 µS/cm. There are several faults associated with the granitic to granodioritic gneiss typical of unit B (Neymark et al., 2013), but only one of the three faults at ~440 m appears to have an impact on groundwater geochemistry. The intrusive diabase dyke in CRG-6 extends from 440 to 480 m; it is suspected that a "fault" leakage occurs at the bottom of the dyke influencing interval 10 geochemistry from 481 to 530 m. There is a slight increase in all major ions except for SO_4^{2-} and HCO_3^- which both decrease slightly relative to other intervals. This can also be observed on Figure 11 as the CRG-6 samples that plot as a Na-Cl type water, unlike the majority of waters that can be classified as Na-Ca-HCO_3. As is typical of the groundwater in the CRL boreholes, the near surface interval in CRG-6 (0-69 m) can be considered a Ca-HCO_3 type water similar to meteoric waters sampled in the area (Figure 11). $\delta^{37}Cl$ values measured from several intervals in CRG6 showed significantly more variability than was observed in CRG-3 and CR-9, although no obvious trends could be noted (Figure 16). The $\delta^{37}Cl$ of aqueous chloride varied from -0.72‰

SMOC at interval 3 (106-139 m) to +0.06‰ SMOC at interval 8 (393-439 m) (Table 5). The $^{87}Sr/^{86}Sr$ measured for dissolved strontium in CRG-6 groundwaters showed a similar pattern to those observed elsewhere. The familiar hook pattern moving towards more radiogenic values at depth can be seen, likely a result of waters with longer residence times in association with leachable minerals having a more radiogenic $^{87}Sr/^{86}Sr$ signature (Figure 16). Much like CRG-3, a minor amount of variability can be observed in $^{87}Sr/^{86}Sr$ (Figure 16). Porewaters measured from CRG-6 had significantly more radiogenic $^{87}Sr/^{86}Sr$ than groundwaters, except for the fracture zone at 440 m. Here, porewater and groundwater $^{87}Sr/^{86}Sr$ values are in close agreement. Groundwater $\delta^{18}O$ and $\delta^{2}H$ was measured for all available intervals and some variability was observed with values ranging from -14.1‰ and -104‰ VSMOW, respectively, at interval 3 (106-139 m) to -9.8‰ and -74‰ VSMOW, respectively, at interval 1 (0-69 m). Samples that are shallower than interval 8 (393-439 m, roughly corresponding to the noted fracture area) except for interval 1 were more depleted in groundwater $\delta^{18}O$ and $\delta^{2}H$ (-14.1‰ to -12.7‰ VSMOW and -104‰ to 92‰ VSMOW respectively) than the deeper intervals (-13.1‰ to -10.2‰ VSMOW and -94‰ to -76‰ VSMOW respectively) although a negative trend can be observed in the intervals at depth (Figure 16) (Table 5). When compared to the local meteoric water line, the wide range in data relative to the other boreholes is apparent (Figure 13). The majority of CRG-6 water isotopes plot below the water line like CRG-3. $\delta^{13}C$ data from DIC was measured for several intervals with some variability observed (-22.2‰ to -15.1‰ VPDB).

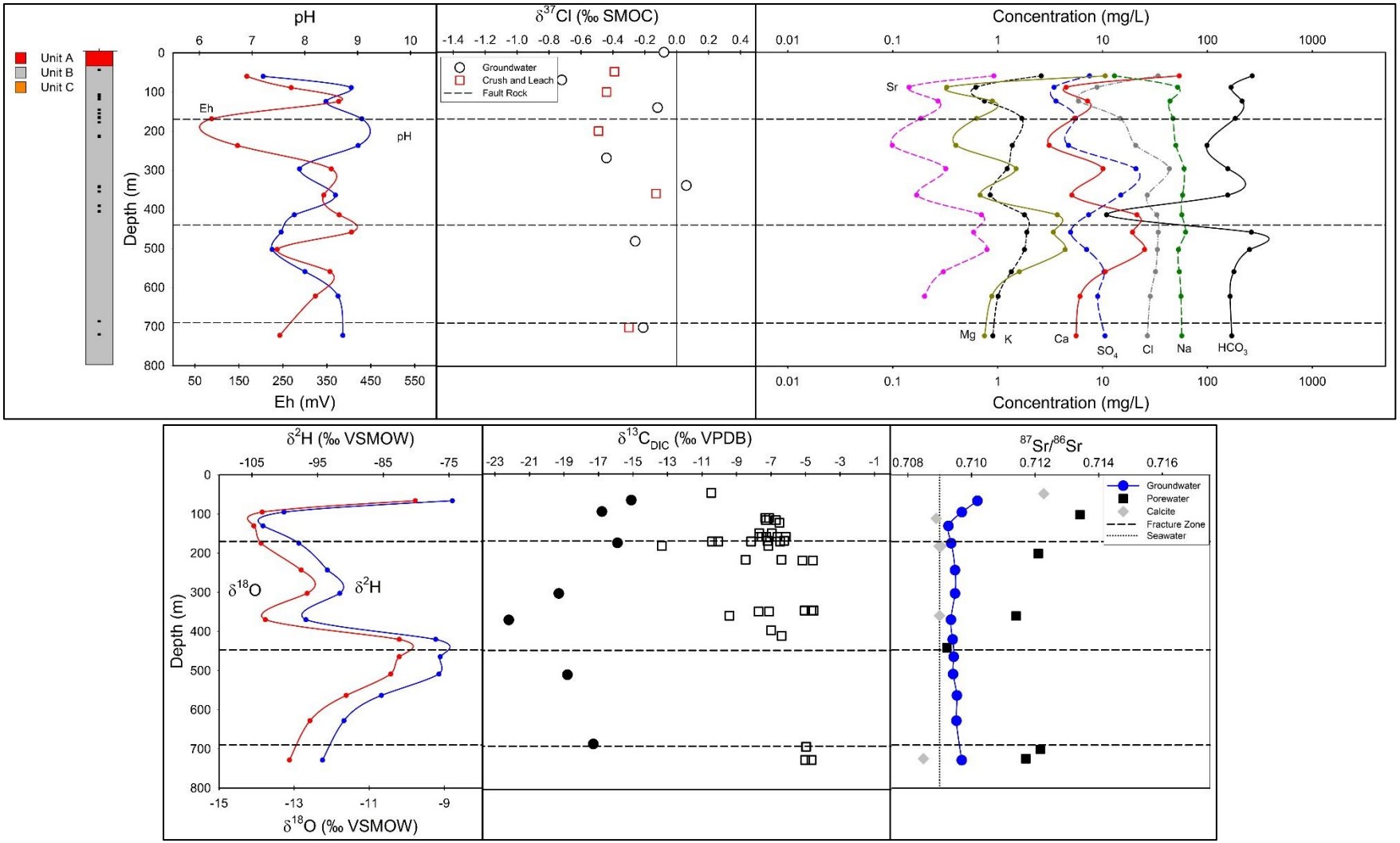

Figure 16. Geochemical and isotopic parameters (Eh, pH, $\delta^{37}Cl$, major ion geochemistry, $\delta^{18}O$, $\delta^{2}H$, $\delta^{13}C_{DIC}$ (black circles), $\delta^{13}C_{CALCITE}$ (open black squares) and $^{87}Sr/^{86}Sr$) measured from the packer intervals in borehole CRG-6 plotted versus depth along the borehole. Geology as well as fracture sample locations are included (solid black squares). Also shown as a dashed horizontal line is the higher conductivity/fracture zones at 170 m, 450 m and 700 m.

3.2.5 CRG-4A

CRG-4A was another borehole included in the series of CRG boreholes drilled from 2005-2014 as a part of CRL's GMWF feasibility study (King-Sharp et al., 2016). It is located in the northern section of the CRL property and representing the northernmost borehole studied in this investigation (Figure 3). CRG-4A contains the largest section of core from Unit A available to this investigation and is otherwise made up of rock from Unit B with a small section of Unit C near the bottom of the borehole (~1150 m) (Figure 6). CRG-4A had Westbay packers installed and was first sampled in August of 2011 from 12 distinct intervals from 0 to 870 m depth along the borehole (Figure 17). Limited isotopic data exists for CRG-4A, but it was sampled for both geochemistry and the stable isotopes of groundwater ($\delta^{18}O$ and $\delta^{2}H$). Conductivities measured in CRG-4A were extremely consistent for intervals 1-8 (0-577 m) with all samples classified as fresh and varying from 200 to 215 µS/cm. Below interval 8, a slight increasing trend can be noted with depth up to a maximum conductivity measured in interval 12 (101.6 µS/cm between 810-870 m). Geochemically, intervals 1 and 2 (0-78 m and 80-143 m, respectively) plot similarly to meteoric waters sampled from the area, much like other shallow waters observed in the CRL site and can be classified as a Ca-HCO_3 type water (Figure 11). Intervals 3 to 10 evolve from Ca-Na-HCO_3 groundwaters to Na-HCO_3 groundwaters with depth before changing towards a Na-Cl type water (although still having a large component of Ca-Na-HCO_3 type water) due to a relative increase in chloride concentrations with depth, possibly related to small lamprophyre dykes (King-Sharp et al., 2016) (Figure 17, Figure 11). All intervals were analyzed for water isotopes in CRG-4A with a limited variability in results observed relative to groundwaters sampled from other boreholes at the CRL. $\delta^{18}O$ and $\delta^{2}H$ varied from -11.9‰ to -11.0‰ VSMOW and -85‰ to -80‰ VSMOW, respectively. When plotted relative to the local meteoric water line, CRG-4A

samples plot in a tight grouping near what would be expected from local recharge waters (Figure 13). Available $\delta^{13}C$ data from DIC was limited in quantity but varied from -20.3‰ to -14.2‰ VPDB with an apparent depletion trend with depth (Figure 17).

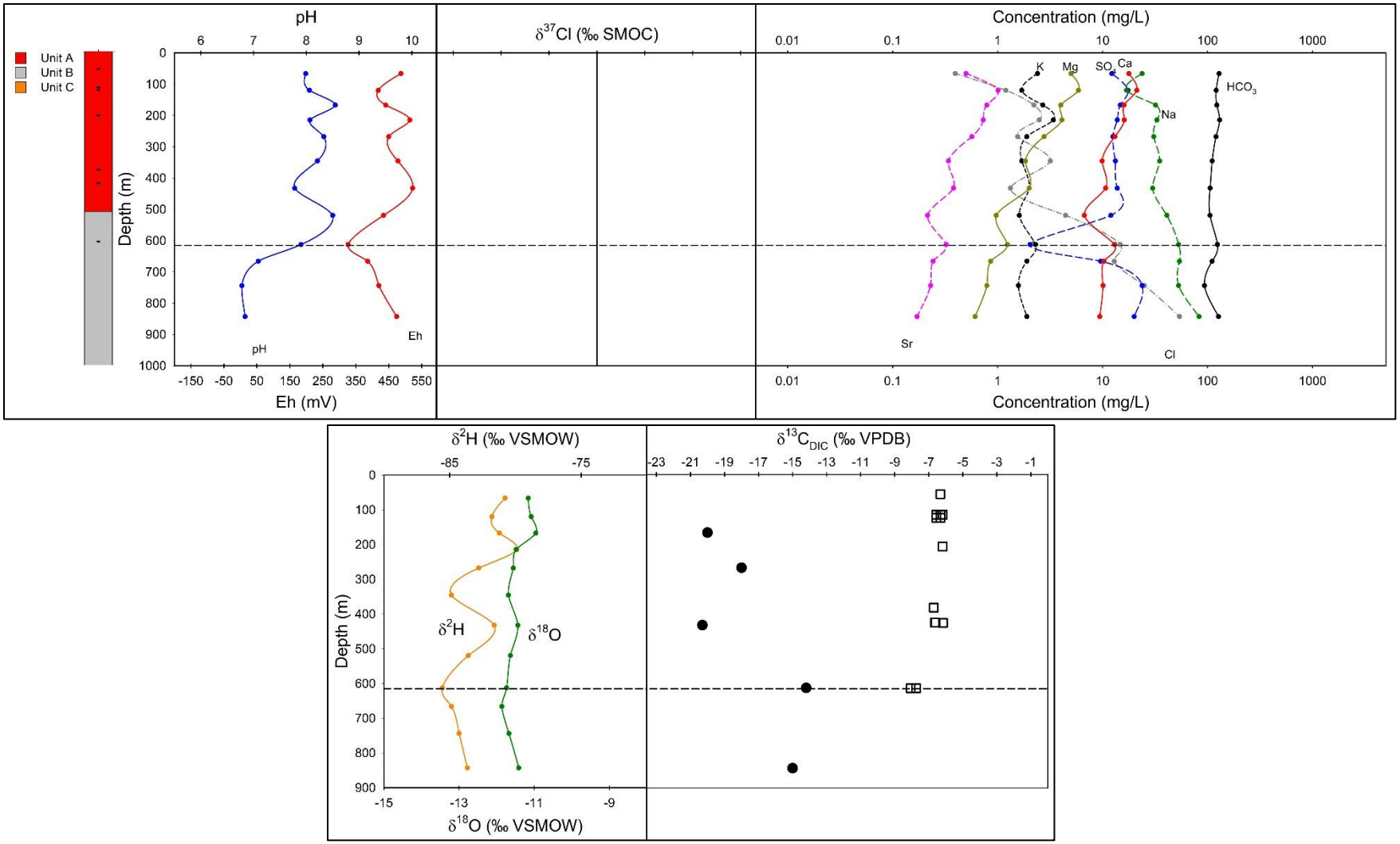

Figure 17. Geochemical and isotopic parameters (Eh, pH, major ion geochemistry, $\delta^{18}O$, $\delta^{2}H$, $\delta^{13}C_{DIC}$ (black circles) and $\delta^{13}C_{CALCITE}$ (open black squares)) measured from the packer intervals in borehole CRG-4A plotted versus depth along the borehole. Geology as well as fracture sample locations are included (black squares). Also shown as a dashed horizontal line is the fracture zone at 600 m.

3.2.6 Additional and Previously Studied Boreholes

CRG-5 was the eastern most borehole drilled in the CRG series and was used for fracture mineral analysis (Figure 3). CRG-5 was sampled in 2011 as a part of the CRL GWMF feasibility study (King-Sharp et al., 2016) and while fracture mineral samples could be sampled, unfortunately leaky packers rendered all available groundwater data unusable. In order to provide a 6th location for comparison at the CRL, this study used the data available in Bottomley et al. (1984) from borehole CR-13 for groundwater geochemical comparisons. CR-13 is located adjacent to Lower Bass Lake (Figure 18) and represents the southern most borehole utilized in the study. CR-13 was initially drilled as a part of the early investigations by the Canadian Nuclear Fuel Waste Management Program (King-Sharp et al., 2016). The study was one of the earlier investigations utilizing packers, and 7 successful intervals were sampled down to a depth of 576 m along the borehole (Bottomley et al., 1984). Major ion concentrations were relatively consistent with depth with the notable exception of chloride which increases in concentration from 200-400 m along the borehole (Figure 18). Most samples from CR-13 are classified as mixed Ca-Na-HCO_3 waters except for three intervals that are classified as a Na-Cl type water due to comparatively high chloride concentrations (Figure 12).

A limited amount of groundwater packer data was available to this study from borehole CRG-2, located in the northeastern section of the CRL property straddling the Ottawa River and Mattawa Fault Zone (Figure 3). CRG-2 was geochemically consistent with depth following an initial drop in concentration from 50-150 m (Figure 19) but is drilled to only 300 m. The geochemical data that is available is similar to local meteoric waters in the shallowest intervals but quickly evolves into a Na-HCO_3 type water with depth (Figure 11).

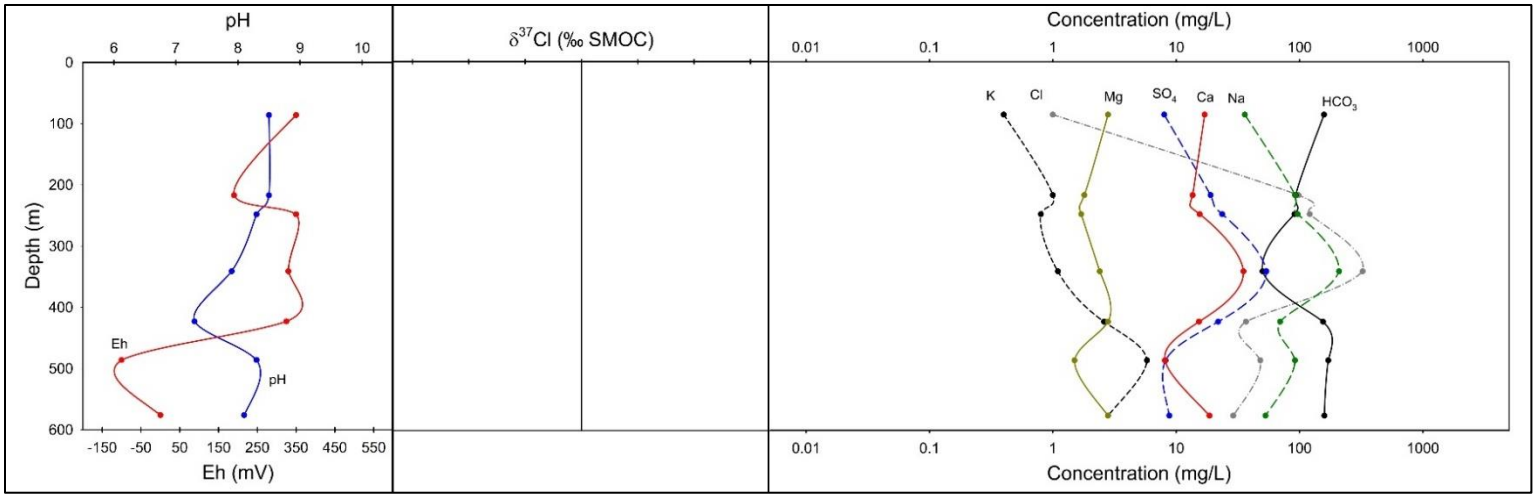

Figure 18. pH and major ion geochemistry measured from the packer intervals in borehole CR-13 plotted versus depth along the borehole.

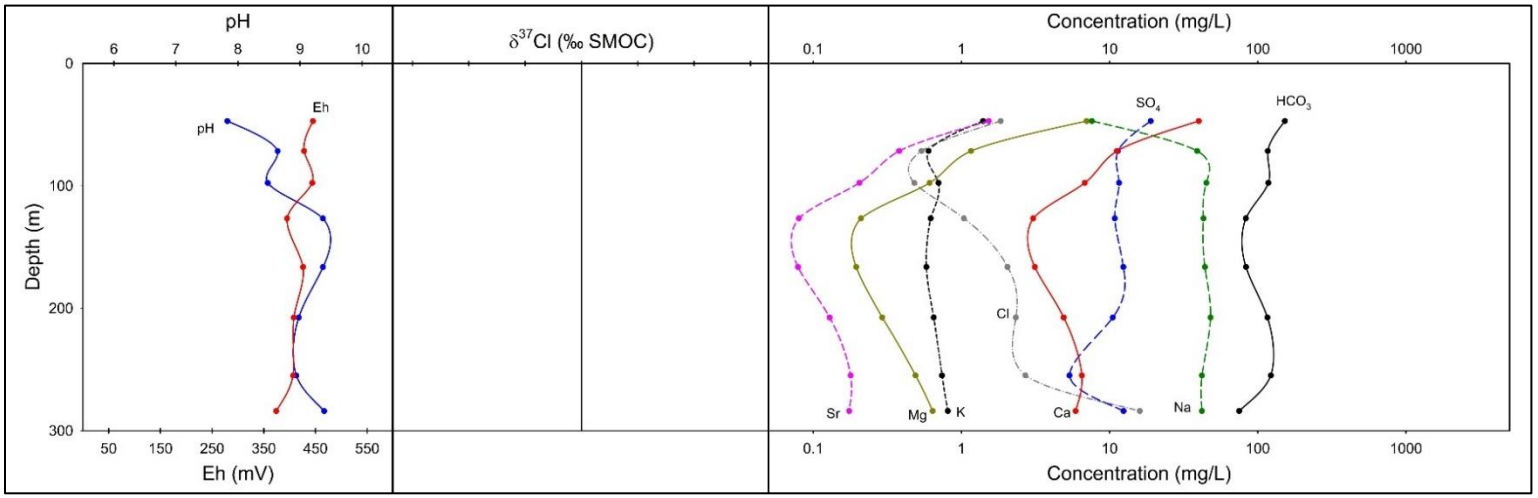

Figure 19. pH and major ion geochemistry measured from the packer intervals in borehole CRG-2 plotted versus depth along the borehole.

4. Discussion

4.1 Formation Fluids and Initial Mineral Precipitation

Prior to investigating the historical, modern and theoretical future fluids and their implication to the CRL site stability, it is important to consider the fracture minerals as they currently exist and their theoretical fluids of origin. This aspect of the investigation was the principal focus of Tian (2016) who sought to date the relative ages of emplacement of the available fracture sealing calcites and theorize a potential origin based on the tectonic and geological history of the region (Tian, 2016).

The $\delta^{18}O$ and $\delta^{13}C$ of carbonates can be directly linked to the isotopic signature of the parent fluids that precipitated them, provided that the required parameters are available in order to account for fractionation factors during mineral formation (Bottinga, 1968; Epstein, 1953). The fractionation of O isotopes during the formation of calcite is extremely temperature dependent and therefore it is important to know the temperature of formation in order to back-calculate the signature of the formation fluid. For this information fluid inclusion measurements were made in addition to a larger dataset measured by Tian (2016). Tian (2016) documented several typical temperatures of formations found across the entirety of the CRL site. The dominant temperatures measured were between 70 and 110 ˚C with some differences in salinity noted between the various petrographically identified crystalline and fibrous calcites (low salinity) contrasting with calcites identified as metasomatic, vuggy, or fibrous as well as dolomite minerals, all of which occurred in a similar temperature range (70 to 110 ˚C) but had higher salinity. A small group of higher temperature crystalline calcites were noted in both CRG-1 and CRG-4A with temperatures ranging between 160 and 200 ˚C (Table 1) (Tian, 2016). This information in conjunction with a wealth of available calcite isotopic data makes back-

calculations to the theoretical formation fluids feasible from 95 distinct homogenization temperature measurements. Equations (5), (6) and (7) were used to calculate the theoretical $\delta^{18}O$ and $\delta^{13}C$ values of parent fluids and these are displayed on Figure 20. These parent fluid values were compared to theoretical fluids of origin described by Carignan et al. (1997) (Figure 20) (Tian, 2016). Figure 20 illustrates that most of the calculations fall within the same isotopic range as what is described by Carignan et al. (1997) as the Saguenay Graben (SG) fluids. Although not immediately adjacent, the Saguenay Graben is regionally relevant, of similar age and geology. The SG Graben is located approximately 550 km northeast of Chalk River, combining with the O-B Graben to the west to form the St. Lawrence rift system (Ketchum and Davidson, 2000). It was concluded that the vein minerals, particularly the carbonates present at the SG site were hydrothermal in nature, possibly a mixture between downward percolating meteoric waters heated and combined with deeper higher temperature waters of the Canadian Shield. These fluids, although not confirmed through fluid inclusion measurements, were estimated to have a mean temperature of 120 ˚C during mineral. This temperature was derived from measurements in the Rossie veins in New York State, USA which were shown to have similar paragenesis and textures precipitation (Ayuso et al., 1987; Carignan et al., 1997). A similar history of fracture mineral deposition is plausible to have occurred at the CRL site and this is supported by the petrographic findings in Tian (2016) where it was theorized that the majority of the calcites sampled from the CRL site were likely of Paleozoic age (544 to 245 Ma) and precipitated from a mixture of ancient meteoric waters with upward moving hydrothermal fluids having elevated temperatures (Tian, 2016). The assessed old age of the fracture calcites at the CRL implies long term historical stability for >200 Ma. These findings contrast somewhat with the findings of Neymark et al. (2013) from the site using $^{234}U/^{238}U$ activity ratios (AR)

measurements in calcites, which yielded an excess ^{234}U age range of 593 to 1515 ka (Neymark et al., 2013). While these measurements do not rule out an emplacement age of >200 Ma, it does suggest that at least partial fracture flow has occurred within the sampled fractures in the last 1.5 Ma, assuming that the minerals initial $^{234}U/^{238}U$ AR was equal to modern groundwater (Neymark et al,. 2013). This study will endeavour to build on these findings and look more closely at the groundwater hydrology and geochemistry of the site in order to assess how current and theoretical future groundwaters could impact the stability of existing fracture minerals and the implications for site stability.

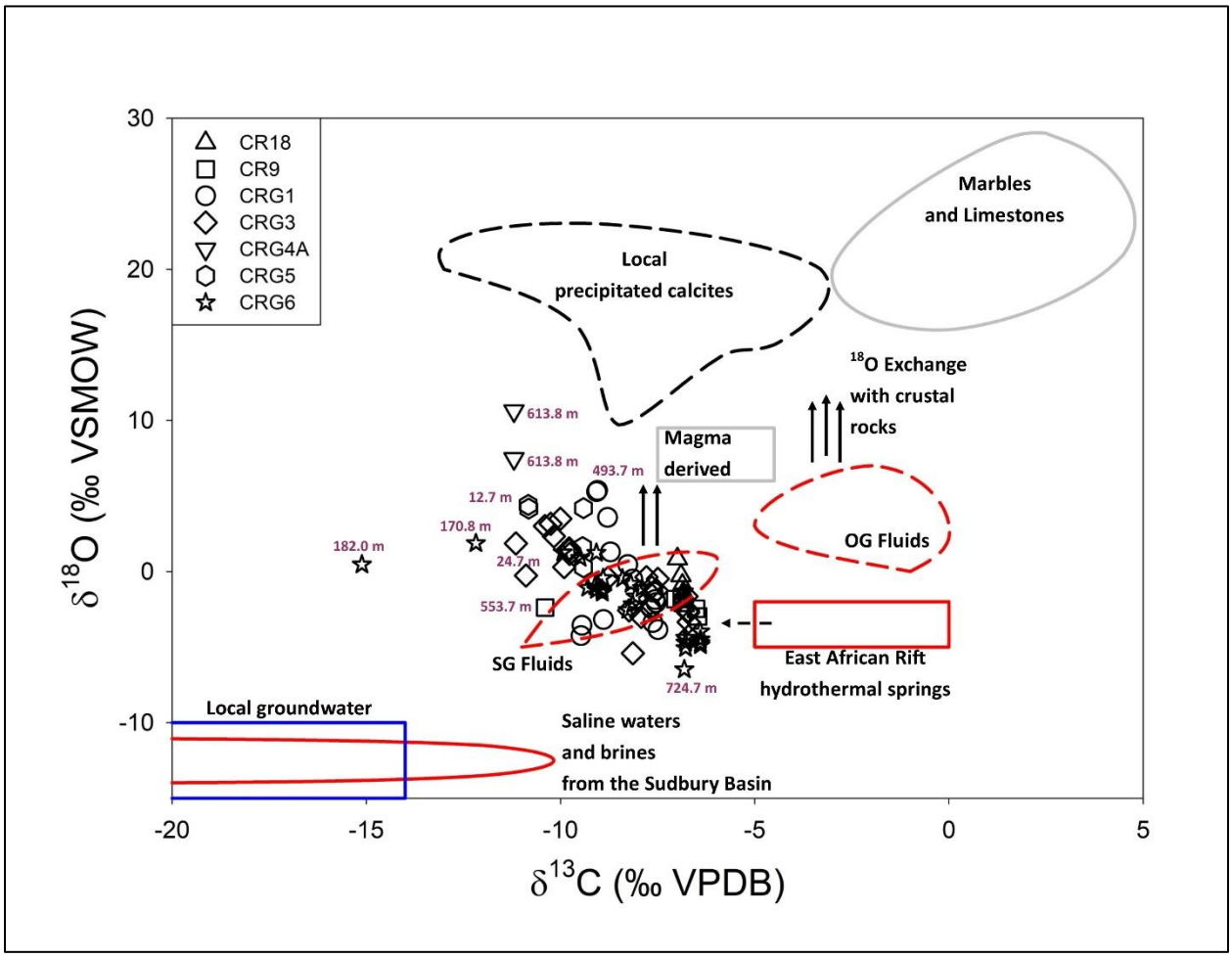

Figure 20. Calculated $\delta^{18}O$ and $\delta^{13}C$ for the formation fluids of available calcites at the CRL. These values are compared to the theoretical isotopic abundance suggested by Carignan et al.

(1997) for formation fluids in the St. Lawrence Rift System. Includes theoretical abundance ranges for waters from the Saguenay (SG) and Ottawa (OG) grabens (from Tian, 2016).

4.2 Geochemical Classification of Local Groundwaters

Major ion geochemistry of groundwater can be applied towards interpretation of the original parent waters and later potential evolution and interaction of precipitated fracture minerals and rock porewaters to more fully understand the fluid history, mixing scenarios and potential future stability of a crystalline bedrock nuclear waste storage site (Kaija et al., 2000). Distinct water sources will often contain unique proportions of dissolved species and mixing trends can be evident when comparing compositions in this manner. The proportions of the major ions in Westbay groundwater intervals from select boreholes at the Chalk River Laboratories (CRL) are visually represented and interpreted using a Piper Plot (Figure 21), which illustrates changes and aids in understanding distinct fluid end-member sources. When plotted on a Piper Plot, the groundwaters sampled from the CRL can be separated and classified into four somewhat distinct geochemical groups in this investigation (Figure 21).

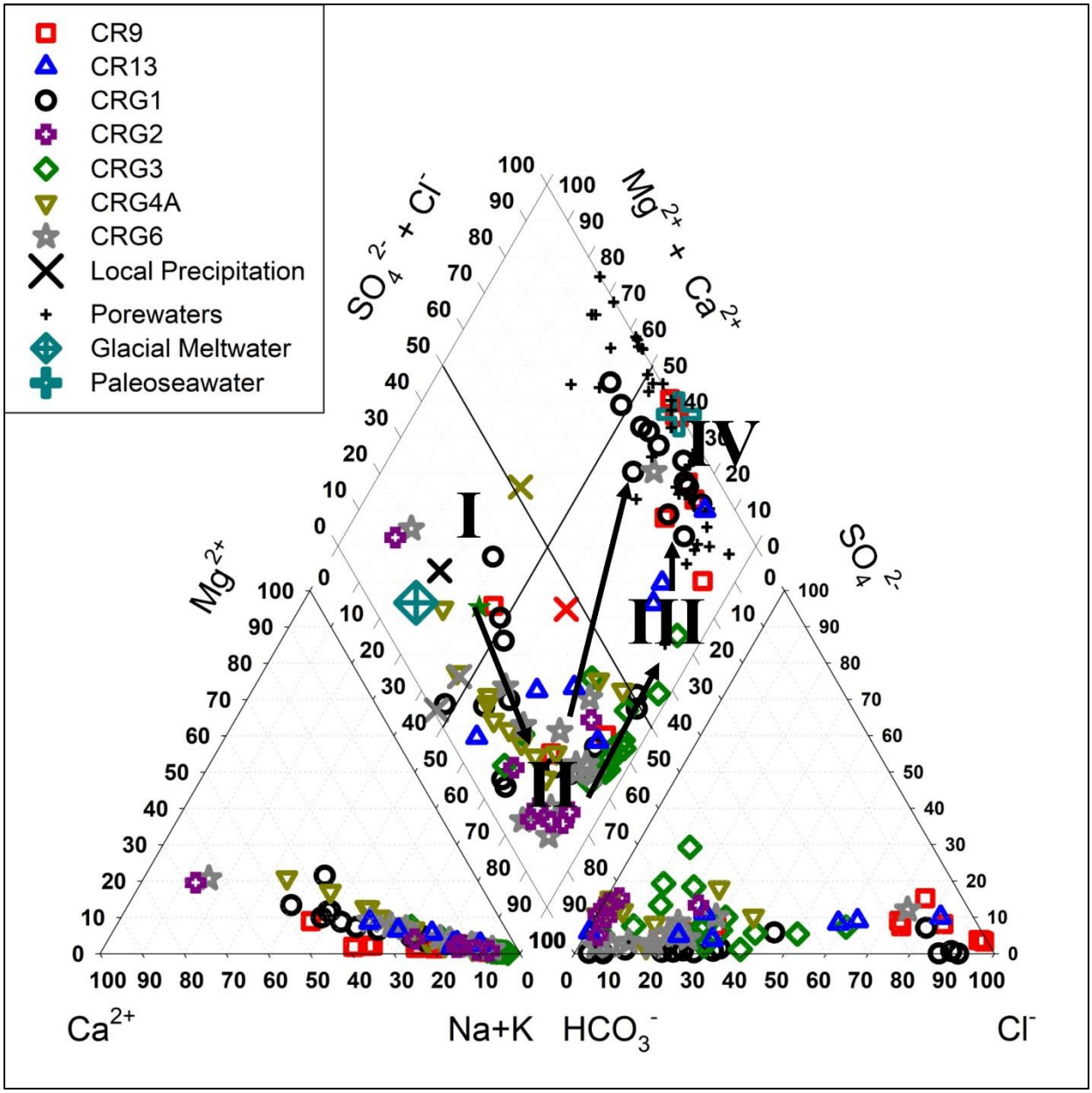

Figure 21. Piper plot comparing the major ion geochemistry of the sampled borehole groundwaters as well as a selection of porewaters (Peterman et al., 2016) and theoretical end members. Groundwater types and potential evolution pathways identified in this study are included.

Group I waters (Figure 21) are classified as Ca-HCO_3 and are present in the groundwaters from all boreholes except for CR-9 and CR-13 (Figure 21). Relative to other waters sampled at the CRL site, Group I waters are higher in calcium and magnesium than sodium and potassium and high in bicarbonate. The chemical composition of Group I waters is likely driven by

leaching/dissolution of easily weathered surface materials by meteoric waters during infiltration. Dilute meteoric waters containing dissolved atmospheric gasses such as O_2 and CO_2 have a high capacity to interact with minerals including carbonate material (providing a proportion of the HCO_3 in solution) and have the potential to impact fracture mineral stability. Dissolved strontium $^{87}Sr/^{86}Sr$ measured in Group I groundwater tends to be relatively radiogenic and possibly reflective of rapid leaching of more radiogenic minerals (i.e. mafic minerals, clays, micas) in the more easily weathered soil materials and shallow rocks compared to less weatherable minerals like feldspar and quartz. Group I waters closely resemble geochemically and isotopically both meteoric precipitation and surface waters in the area suggesting a recent origin and evolution from these sources (Figure 21).

Group II groundwaters in comparison are found deeper and are likely older than Group I waters according to tritium analyses performed for this investigation (Table 5). Geochemically they are more sodium dominated and classified as Na-HCO_3 type waters (Figure 21). A well documented flow system in Palmottu, Finland showed a similar geochemical evolutionary pathway from Ca-HCO_3 to Na-HCO_3 due to calcium-sodium exchange during water-rock interaction (Frape et al., 2014). The $^{87}Sr/^{86}Sr$ of Group II groundwaters is less radiogenic than the Group I waters her Ca-rich silicates (McNutt, 2000) when compared to more radiogenic $^{87}Sr/^{86}Sr$ values found in more easily weatherable K-rich minerals such as potassium feldspar and biotite found in the soil and more surficial rocks (Clow et al., 1997). Most fractures at the site are sealed by precipitated minerals, but evidence of vuggy calcites and open fractures was found at depths below 100 m along the borehole in CRG-1, CRG-5, and CRG-6. These open fractures create pathways at depth and may import surface waters to depth, resulting in a higher degree of water-rock interaction with dominant host silicate rocks and dissolution of fracture filling materials.

Group III waters exist along a trend towards the chloride/sulphate end member on the Piper Plot (Figure 21). This trend is likely due to long-term leaching of chloride (most common) or sulphate/sulphide (CRG-3, some intervals) dominant source through water-rock interaction or a mixing scenario with a higher concentration chloride-dominated water. Group III waters are classified as Na-HCO_3-Cl type and contain more chloride than the group II waters (Figure 21). A very similar evolutionary trend was also observed at the Palmottu, Finland field site as deeper waters increased in SO_4^{2-} and Cl^- proportionally due to water-rock interaction, calcite precipitation and mineral weathering (Figure 22A) (Frape et al., 2014). Often the samples in this group are the deepest samples and as a result (due to a typical trend of more radiogenic values with depth), $^{87}Sr/^{86}Sr$ tends to be more radiogenic in Group III groundwaters). The longer residence times and high rock to water ratios typical of crystalline rocks associated with these samples allows for the possibility of longer timescale exchange reactions via water-rock interaction, and helps explain the overall trend towards more radiogenic groundwater $^{87}Sr/^{86}Sr$ values with depth despite no accompanying trends in host-rock geology (McNutt et al., 1990).

Group IV type waters are very distinct geochemically from both group I and II waters as they are dominated by chloride. They can be classified as Na-Cl type waters and can be found in almost every one of the deeper boreholes in this study (Figure 21). The chemical difference between these waters and the other groundwaters found at the site make them of interest to this study as they relate to their effect and long-term impact on the stability of fracture minerals at the site. While the meteoric water nature of Group I waters and some of the Group II waters and the influence of carbonate and silicate minerals on the shallow Group I and II waters are relatively apparent, the evolution of the deeper groundwaters towards either Group III or Group IV classification appears to be more complicated. Group IV waters closely resemble both a

theoretical seawater signature as well as measured rock porewaters both of which are typically highly saline fluids (Blyth et al., 2004). As a result, a mixing scenario with one of these highly saline fluid types could cause the evolution seen towards the Group IV end member type waters (Figure 21). Unfortunately, the similar chemical composition of both a theoretical paleoseawater (assuming a similar contribution to modern seawater), as well as a mixing scenario with mobilized highly saline porewaters make these two hypotheses difficult to differentiate using geochemical means alone (Figure 21). Therefore, a brief review of the types and evolution of highly saline fluids in crystalline rock environments is useful currently.

The Palmottu Natural Analogue Project in Palmottu, Finland noted a similar evolution of groundwater geochemistry with depth for groundwaters sampled from fractured crystalline bedrock, and the complete findings of this investigation are summarized in Kaija et al. (2000). A conceptual model generated from the project is shown in Figure 22A that includes possible processes effecting isotopic signatures and geochemical classification that are relevant and similar in evolution with depth to the CRL site (Frape et al., 2014). A comparison can also be made to the data collected at the Palmottu site when assessing the carbon cycle as it relates to dissolved inorganic carbon (DIC) $\delta^{13}C$ and ^{14}C measurements (Kaija et al., 2000). The data displayed on Figure 22B illustrates the influence of carbonate dissolution especially concerning the evolving shallower Na-HCO_3 and Ca-HCO_3 type waters at Palmottu (Figure 22B). A similar assessment of the inorganic carbon cycle at the CRL was performed as a result of the packer intervals at various depths in boreholes CR-9, CRG-1, CRG-3 and CRG-4A (Figure 23). In general, groundwaters trend to older (lower in ^{14}C values) with depth and in some cases more enriched in $\delta^{13}C$ with depth (Figure 23). The trend towards older waters with depth is compatible with the hypothesis that the origin of most of the groundwaters found at the CRL is meteoric or

glacial meltwaters that infiltrated from the surface (King-Sharp et al., 2016). The only example of Group I water (Ca-HCO_3) available in the dataset is at ~120 m depth along the borehole in CRG-1. This sample showed a younger or higher percentage of modern carbon (PMC) than other groundwaters sampled deeper in the borehole (Figure 23). As samples transition from Group I to Group II (Na-HCO_3) and Group III (Na-HCO_3-Cl) in CRG-1 they have lower PMC values (older) and are more enriched in $\delta^{13}C$. The enrichment in ^{13}C evolving parallel to the decreasing PMC could be what would be expected due to carbonate dissolution of ancient fracture calcites, although these values are more depleted than would be expected due to carbonate dissolution alone. Group II and III waters are the oldest sampled according to measured ^{14}C values. Interesting excursions from the typical range of carbon isotopic values (10 to 20 PMC, -15 to -18‰ vs VPDB for ^{14}C and $\delta^{13}C$, respectively) are noted in CR-9 and CRG-4A. In CR-9 there are two distinct clusters of values separated by a fault in the borehole at ~500 m depth (Figure 23). The shallow group are Group II type waters, low salinity and PMC values are possibly influenced by calcite dissolution (0 PMC carbon sink) based on their carbon isotopic composition. The deeper group are more saline and classified as a Group IV (Na-Cl) type water, but interestingly have a more modern (~60 PMC) value than their shallower counterparts (~40 PMC). The absence of tritium in these deep waters (<0.8 TU) as compared to a trace amount measured in the shallower samples (0.8-2 TU) suggests that it is possible that the groundwater radiocarbon sampled from the deeper intervals could have absorbed some modern atmospheric CO_2 during pumping depending on CO_2 saturation levels in groundwater before pumping. The lower pH noted in these samples (<8) relative to the shallower groundwaters (8.2-9) could support this hypothesis. In CRG-4A, a trend towards more enriched $\delta^{13}C$ values is observed with depth. This trend may be related to calcite dissolution associated with a lamprophyre (ultra-

potassic) dyke noted at depth although 87Sr/86Sr analyses are not available for this borehole to support this influence.

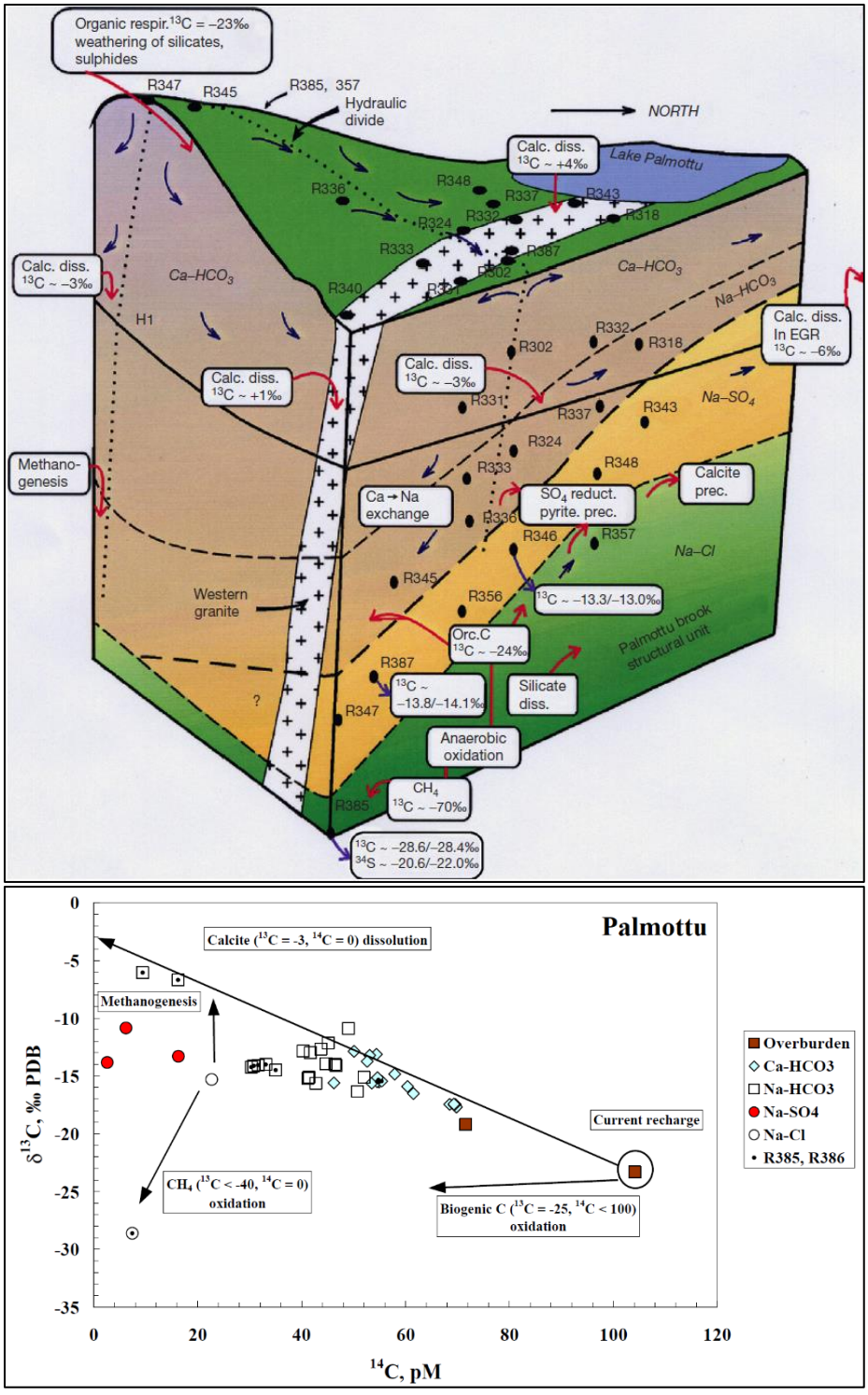

Figure 22. (A) A diagram displaying the evolution of groundwater at Palmottu, Finland showing possible processes affecting isotopic signatures and geochemical classifications as well as (B) A comparison of the carbon isotopes ($\delta^{13}C$ and ^{14}C) measured in packered groundwater samples at the Palmottu Natural Analogue Project (from Kaija et al., 2000).

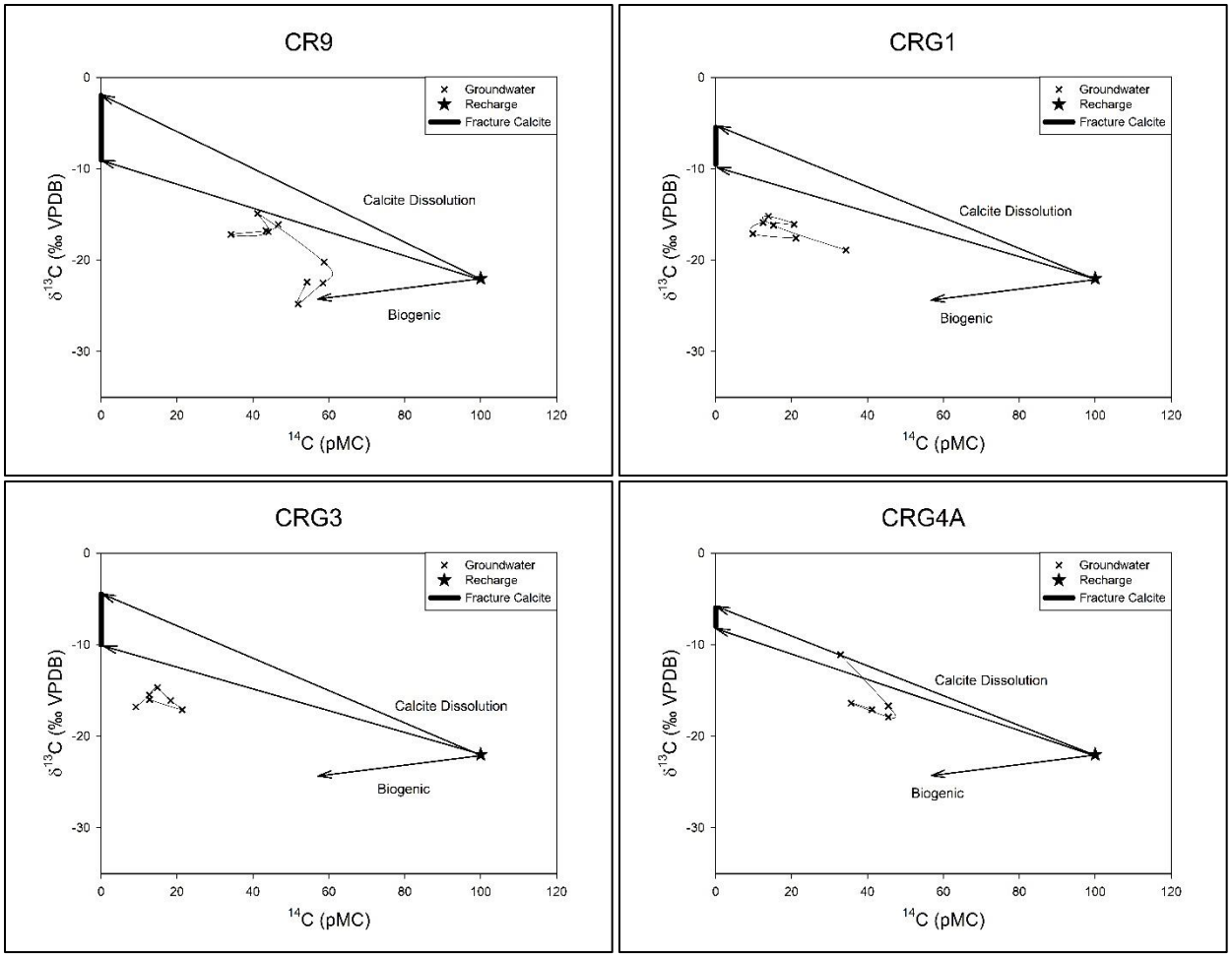

Figure 23. A comparison of the carbon isotopes ($\delta^{13}C$ and ^{14}C) measured in packered groundwater samples at Chalk River Laboratories. Included are evolution trends for possible old carbon sinks from Kaija et al. (2000).

4.3 Deep Fluids and Shield Brines

When studying deep crystalline rock environments, a potential endmember and source of chemical contamination is shield brines and formation waters (Frape et al., 2014). Generally, in both sedimentary and crystalline environments, there is an increasing trend in total dissolved solids (TDS) with depth. This is due to several factors including fluid density, evapotranspiration, weathering, mineral dissolution and water-rock interaction (Peterman et al., 2016). These deep fluids as a result can carry unique geochemical signatures and TDS loads of more than 100 g/L (Frape et al., 2014). Shield brines and formation waters are a potential

concern to the long-term stability of a theoretical nuclear waste storage facility due to their high concentration and potential for corrosion (Gascoyne et al., 1995) so they must be considered and quantified if possible. When surveying the deep waters sampled elsewhere in the Canadian Shield, the deep bedrock waters at the CRL site are comparatively dilute (King-Sharp et al., 2016) suggesting that the influence of high salinity deep fluids on present day groundwater at the depths studied is not significant. Long (2016) suggested that at times during the Paleozoic upward migrating higher temperature fluids mixed with colder, shallower meteoric waters and were the source of most fracture filling minerals at the site. These deeper fluids would have likely made up a proportion of the upwelling hydrothermal fluids during fracture sealing calcite precipitation, helping explain the presence of several highly saline primary fluid inclusions found in the calcites (Tian, 2016). Stable isotope ratios, specifically those of $\delta^{37}Cl$, $\delta^{18}O$ and $\delta^{2}H$ can be another indicator of the presence of deep shield fluids in groundwaters (Stotler et al., 2010). At the CRL site, groundwater packer intervals were sampled for measurement of all three isotope systems in CR-9, CRG-1, CRG-3, and CRG-6 as well as $\delta^{18}O$ and $\delta^{2}H$ for CRG-4A (Figure 12, Figure 13, Figure 14, Figure 15, Figure 16, Figure 17). Where available, $\delta^{37}Cl$ does not display conclusive evidence of the presence or absence of shield brines. Increases in conductivity could also be explained by several other possibilities including palaeowater and porewater diffusion and migration into open fractures. $\delta^{18}O$ and $\delta^{2}H$ where available also does not show evidence of the deviations above the local meteoric waterline expected in deep saline fluids. These typical deviations to more enriched $\delta^{2}H$ values in deep brines are caused by several processes, most significantly hydration of silicates, H_2S exchange and methanogenesis (Frape and Fritz, 1981). Most measured water isotopes fall along or below the meteoric waterline (Figure 13). It can be noted that the Palmottu site in Finland referred to earlier has a very similar geochemical and

isotopic evolutionary history to the Chalk River site and the presence of typical deep crystalline fluids could not be proven at the site (Frape et al., 2014).

4.4 Water-Rock Interaction and Porewater Diffusion

Meteoric fluid infiltration and advection through fracture networks in crystalline rocks with high rock to water ratios combined with potential long-term residence times of low TDS meteoric waters indicates that water-rock interaction is a possible influence on groundwater geochemical evolution (Blyth et al., 2009) (Figure 1). A useful tool for assessing the contributions of water-rock interaction to groundwater geochemistry is $^{87}Sr/^{86}Sr$ (McNutt et al., 1991). A notable trend in the $^{87}Sr/^{86}Sr$ values measured in for the dissolved groundwater Sr at almost all locations was a "hook" trend with depth (Figure 12, Figure 14, Figure 15, Figure 16) with more radiogenic values near the surface likely related to the preferential initial weathering of more radiogenic $^{87}Sr/^{86}Sr$ from K- and Rb-rich mineral phases such as biotite and potassium feldspar initially (Franklyn et al., 1991), followed by a drop towards less radiogenic values at deeper depths as additional dissolution of Ca- and Sr-rich plagioclase minerals occurs. Finally a gradual progression toward more radiogenic values occurs at depth in much older fluids where longer residence times allow more time for exchange with radiogenic host rock minerals (Figure 12, Figure 14, Figure 15, Figure 16). A strong candidate for the more radiogenic end member that is driving this evolution is the mineralogy of the host rock through water-rock interaction. In general, silicate rocks, especially those containing a significant K-feldspar component will measure at more radiogenic $^{87}Sr/^{86}Sr$ values due to the decay or Rb that has been substituted into the lattice (McNutt, 2000). This ^{87}Rb after deposition decays to ^{87}Sr over extremely long but geologically relevant timescales ($t_{½}=4.9\times10^{10}$ a), increasing the relative $^{87}Sr/^{86}Sr$ signature in the process (Capo et al., 1998). Whole rock $^{87}Sr/^{86}Sr$ values are available for borehole CR-9

specifically as a part of the investigation by Bottomley and Veizer (1992). This study found that the host rock material that would be available to leach into local groundwaters had an $^{87}Sr/^{86}Sr$ value ranging from 0.71085 to 0.72121 with variability depending on the age and chemical composition of local host rock and no obvious trend with depth (Bottomley and Veizer, 1992). These values are more radiogenic than those measured in the majority of groundwaters and calcites sampled at the CRL (Figure 12, Figure 14, Figure 15, Figure 16) and may help explain the trend towards more radiogenic aqueous $^{87}Sr/^{86}Sr$ values with depth as in general deeper waters are older and have more time to leach strontium and equilibrate with the rock (King-Sharpe et al., 2016).

A possible host-rock derived source of potential geochemistry is grain boundary porewaters. Grain boundary porewaters are waters that become trapped in the dead end-pore space that occurs between grains (Frape et al., 1984). While under normal conditions these fluids and salts are trapped in the low permeability pore space in the bedrock matrix, fracture events and other geological stresses can mobilize them into fracture networks. While not necessarily making up a large relative volume, these waters can have a disproportionate effect on the overall fluid chemistry when mixing as they are typically highly concentrated (Nordstrom et al., 1989), however leaching experiments have demonstrated that fluid inclusions are a more significant source of salinity than grain-boundary salts (Peters, 1986). Porewaters extracted via centrifugation at the Chalk River Laboratory (CRL) site were analyzed for dissolved ions and strontium isotopes and contained 15 times higher concentrations of ions than the associated groundwaters, allowing the $^{87}Sr/^{86}Sr$ in the porewaters (if different) to shift the bulk $^{87}Sr/^{86}Sr$ measured in adjacent groundwaters (Peterman et al., 2016). Crush and leach analyses performed at the University of Waterloo were useful when interpreting the influence of host rock

mineralogy and porewater contributions on groundwater evolution. Crush and leach analysis involves pulverising available rock samples into a fine rock flour which is then leached using ultra-pure water (Waber and Smellie, 2008). This technique does not discriminate between ion contributions from leachable minerals, grain boundary salts/porewaters and fluid inclusions, but it does provide a useful analogue for historical tectonic events which could have mobilized these rock matrix components (Waber and Smellie, 2008). The available $^{87}Sr/^{86}Sr$ from crush and leach analyses are plotted alongside fracture groundwater and calcite values (Figure 12, Figure 14, Figure 15, Figure 16). These values help explain the deviations in many cases of the $^{87}Sr/^{86}Sr$ groundwater profiles from the general trend to more radiogenic values with depth noted in all available boreholes. In particular, an increase in aqueous $^{87}Sr/^{86}Sr$ at 300 m in CR-9 (Figure 12), a sharp increase in $^{87}Sr/^{86}Sr$ at 800 m in CRG-1 (Figure 14), and two less radiogenic excursions in $^{87}Sr/^{86}Sr$ values at 400 m and 900 m in CRG-3 (Figure 15) are possibly attributable to diffusional inputs from porewater infiltration from the rock matrix.

Some interesting insights into the influence of water-rock interaction on the fluids that precipitated the fracture minerals found at the CRL can be derived from a limited amount of REE data available for local calcites and silicates. It proved difficult to subsample fracture carbonates in a manner that they were not contaminated by small amounts of silicate host rock material but there were several samples that proved sufficient (Table 8). Where available these results provide an additional fingerprint to assess the historical origin of fluids that initially precipitated the carbonates (Munemoto et al., 2015). In three of these samples the REE measured in clean calcite was enriched relative to the adjacent host rock, but the patterns were virtually identical. This suggests that the fluid that precipitated the calcite in question had an opportunity to chemically equilibrate with the host rock or a chemically similar host rock nearby (Table 8, CRG-1-25.3m,

CRG-5-152.2m, CRG-6-182m). CRG-5-43.6m is a shallow vuggy calcite sample that shows a very different REE signature than the adjacent silicate host rock material (Figure 24). The calcite sampled at this location shows a significant negative Europium anomaly (0.5) relative to the host rock material (1.8) suggesting that the fluid from which it precipitated had derived a signature from another location and had not equilibrated with local rocks before crystallization. Only 100 m deeper in the same borehole at CRG-5-152.33m, both the calcite and adjacent host rock measured had very similar Europium anomalies (0.5 and 0.6 respectively) and distribution patterns with one another as well as CRG-5-43.61m. This finding shows movement of a fluid source prior to the fracture mineral precipitation event such as the hydrothermal mixing cells theorized to have been prevalent in similar sites historically (Carignan et al., 1997). If valid, this finding also demonstrates the geological variability effecting REE patterns with depth, as the silicates noted at 43.6 m and 152.3 m had very different δEu, positive and negative respectively (Figure 24). Such similarities support the existence of large-scale hydrothermal events that precipitated similar carbonate fracture mineralogy at numerous locations throughout the Chalk River Site.

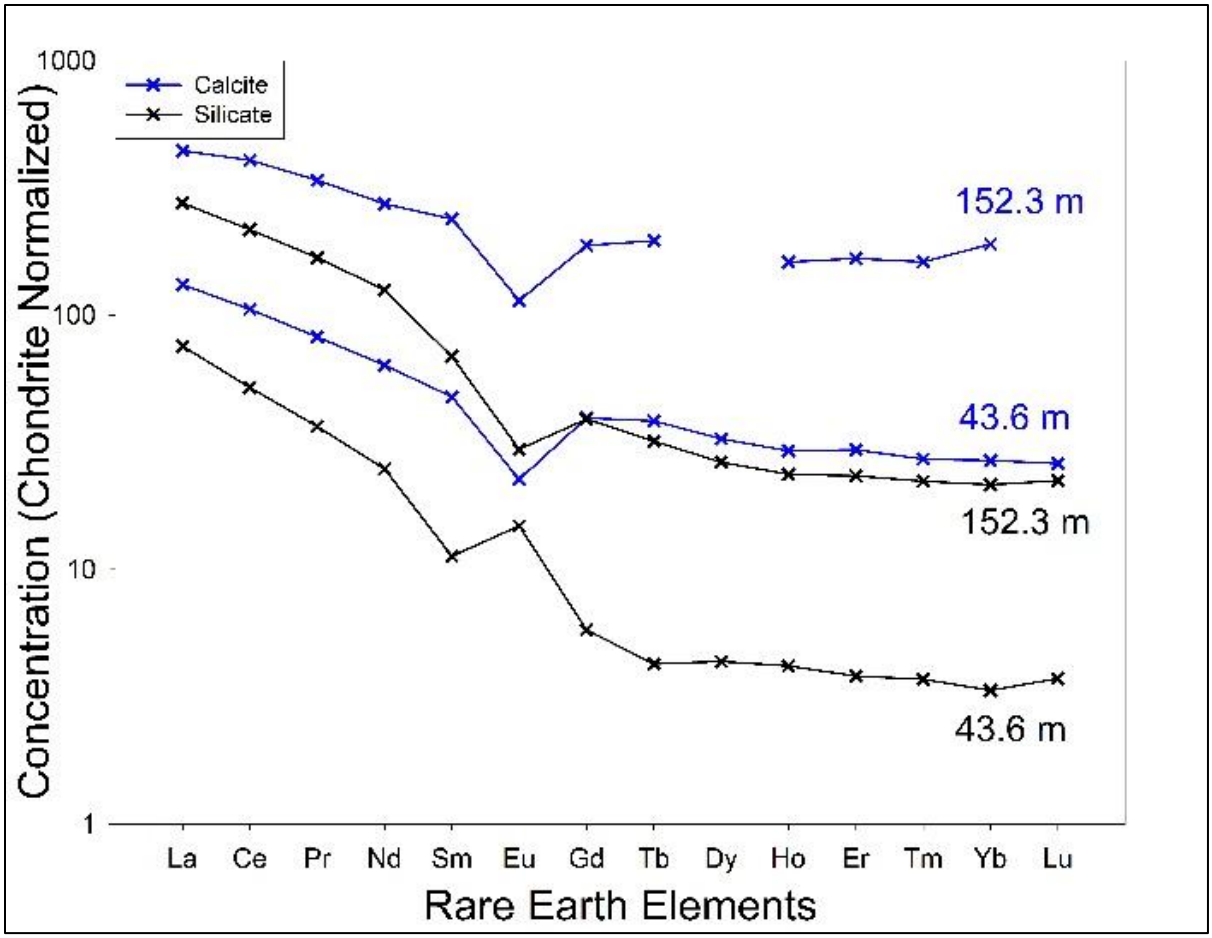

Figure 24. A comparison of REE patterns generated both from host rock silicates and fracture calcites for CRG-5-43.6m and CRG-5-152.3m.

4.5 Paleoseawater

One of the principal hypotheses to explain the high salinity groundwater zones noted most significantly in CR-9 (Figure 12) but also in CRG-1 (Figure 14) is the presence of a paleo-seawater component intruding and mixing with local groundwaters at depth (Bottomley et al., 1987). Seawater relative to other waters is high in sodium and chloride and plots as a Na-Cl type on a Piper Plot (Figure 21). The origins of the paleoseawater include but are not limited to several possibilities. Most recently the Champlain Sea, a temporary inlet of the Atlantic Ocean, covered the area south of the site from 13,000 to 10,000 years ago. Evidence of the Champlain Sea has been found at some locations in the region (Catto et al., 1982) and would have been

made up of partially diluted marine waters (Chapman and Putnam, 1984). Leachable marine sediments appear to have been deposited in the area over the complex history of the site (Catto et al. 1981). The evidence for potential seawater intrusion and mixing with resident groundwater lies in a relatively consistent geochemical and isotopic trend throughout the western boreholes of the CRL (Figure 14, Figure 15, Figure 16, Figure 17, Figure 18). There appear to be two distinct zones of influence, one with a comparatively minor effect on overall salinity and at shallower depths along the borehole (200-600 m) in a fracture zone in CR-13, CRG-3 and CRG-6 (Figure 16, Figure 17, Figure 18) and another with a more significant effect on salinity measurements and at deeper depths along the borehole (>700 m) in fracture zones in CR-9, CRG-1 and CRG-4A (Figure 14, Figure 15, Figure 17). The anomaly and possibility of the presence of Champlain seawater in the CR-13 borehole was reported by Bottomley et al. (1984) to explain a change in the Na/Cl for some borehole intervals (Bottomley et al., 1984). In this study, the Na-Cl type waters sampled from parts 8, 9, and 10 (341 m, 248 m, and 217 m respectively) of the CR-13 borehole were not thought to have evolved from the Na-HCO_3 type waters. Instead, it is suggested that a small amount of marine water with a comparatively depleted $\delta^{18}O$ value (i.e. colder climate) was mixed in the fractures and impacted the geochemical ratios and $\delta^{18}O$ values (Bottomley et al., 1984) (Figure 18). The appearance of marine clays and silts in the lower quaternary age sediments at Chalk River area (50-75 m depth) connected to the Champlain Sea is documented although it is suggested that ice cover over the site may have prevented earlier and more extensive infiltration and that exposure of the site was limited to the later phase of the Champlain Sea (11,300-11,100 a) (Catto et al., 1981). The possibility of intrusion of diluted glacially influenced seawater is relevant to the stability of the fracture filling minerals and permeability at the CRL as these high concentration fluids can significantly alter the chemistry of

comparatively dilute meteoric groundwaters and impact the solubility of carbonate mineral phases. However, based on current evidence and the results of this study, the presence of Champlain Sea water or another paleoseawater remains inconclusive (King-Sharp et al., 2016).

4.6 Glacial Meltwater

A significant consideration when it comes to predicting future site stability and groundwater connectivity in a fractured crystalline environment is the evolution and influence of modern and theoretical future waters on mineral solubility. In crystalline bedrock, most of bulk porosity and groundwater flow occurs due to fractures formed over the course of a site-specific tectonic history (Figure 1) (Smellie and Frape, 1997). These fractures are often sealed after opening due to the precipitation of minerals from waters advecting through available conduits (Tullborg, 1989b). The precipitated minerals do an effective job of sealing interconnected fracture systems, evident by the lack of open fractures found in the available boreholes; however, the stability of each mineral depends on specific fluid chemistry and temperature ranges. For this reason, it is important to consider modern and theoretical future groundwater chemical makeups and the effect these waters could have on calcite and other mineral solubilities.

One of the most important groundwater sources to consider when assessing possible fracture mineral dissolution at the CRL is the role of highly oxic glacial meltwaters. Four times over the past million years, continent-scale ice sheets covered the majority of the CRL region with up to a kilometer of ice (Catto et al., 1989). Glacial meltwaters due to the nature of their formation (from compressed snow) tend to be relatively fresh compared to other sources. This fact combined with relatively short warm up times (~10,000 years for the most recent retreat) and the resulting potential large-scale inundation of water poses a potential mechanism for fracture mineral dissolution and stability. Several surficial deposits and drainage patterns local to

the CRL are a result of glacial sedimentary deposits as well as glaciofluvial deposits and moraines showing evidence of the potential important aqueous sedimentary processes from past glaciations on the local geology and topography (Karrow and Calkin, 1985). This information combined with other potential indicators of the presence of glacial fluid creates an opportunity to assess the theoretical impact of glacial meltwaters on local calcite stability. Several fractionation factors act on the isotopes of water during evaporation and precipitation including the fact that ^{16}O will preferentially evaporate from a water source rather than ^{18}O with its magnitude of isotopic fractionation inversely proportional to temperature (Clark and Fritz, 1997). This phenomenon as well as the fact that initial coastal rains will preferentially rain out ^{18}O rather than ^{16}O (Clark and Fritz, 1997) mean that glacial inland precipitation sources tend to be significantly depleted in both $\delta^{18}O$ and $\delta^{2}H$ compared to modern waters along the Global Meteoric Waterline (Figure 13). A glacial meltwater mixed with local groundwaters will typically display $\delta^{18}O$ and $\delta^{2}H$ values more depleted than modern day meteoric waters, with models of the post-glacial Lake Agassi predicting a $\delta^{18}O$ value of approximately -25‰ VSMOW (Remenda et al., 1994). It has been theorized that several waters that are isotopically depleted in both $\delta^{18}O$ and $\delta^{2}H$ at depths of 200-400 m along the borehole in CR-9, CR-13, CRG-1 and CRG-6 may be the result of such an intrusion/mixing event (Figure 12, Figure 14, Figure 16, Figure 18) (Bottomley et al., 1984; Peterman et al., 2016; King-Sharp et al., 2016). PHREEQCI is a versatile computer model from the United States Geological Survey (USGS) that can input the physical and chemical parameters of a given aqueous system and calculate mineral solubility, in this case saturation indices. A saturation index is a useful statistical equation that is calculated by comparing the ion activity product (IAP) of the dissolved ions in the current system with their empirically derived equilibrium solubility product (K_{sp}) using equation (14):

$$SI = log\left(\frac{IAP}{K_{sp}}\right) \quad (14)$$

A comparison of the $\delta^{18}O$ profile of CRG-1 with depth and saturation index with depth does not show evidence of potential calcite dissolution and instability due to the presence of these waters other than a zone at a depth of 250 m along the borehole, although this interval is also associated with faulting (Figure 25).

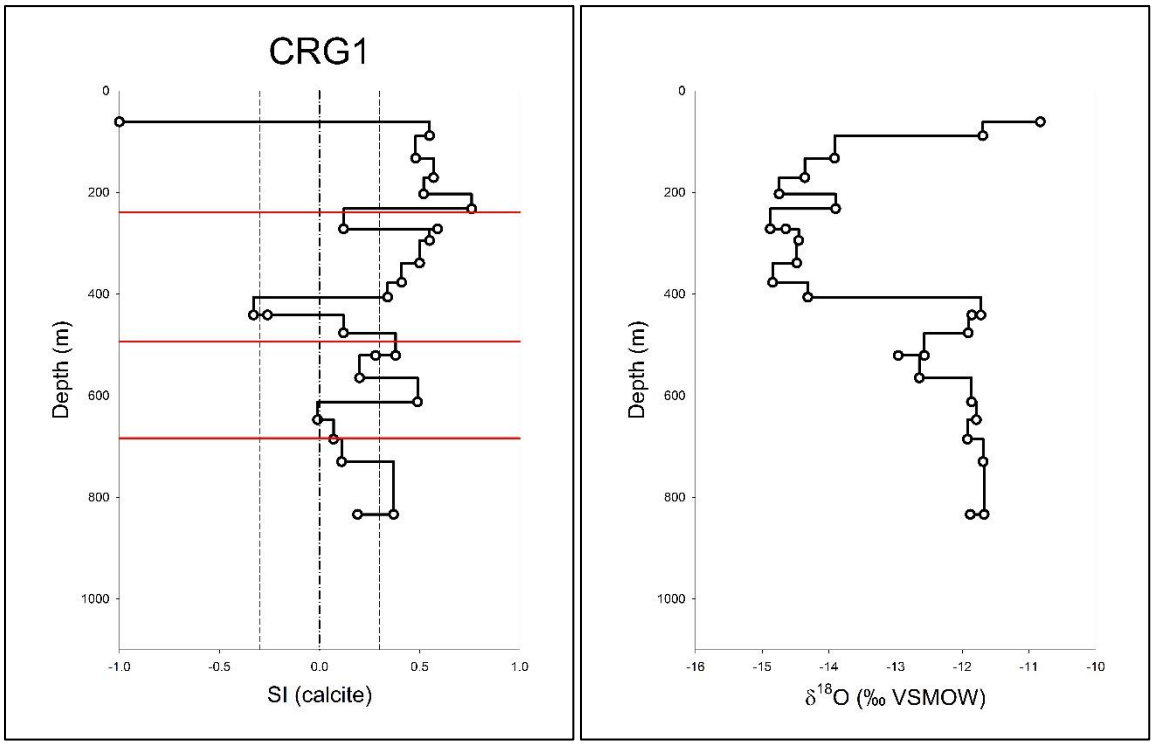

Figure 25. (A) a comparison of the saturation index of calcite computed with PHREEQCI versus depth along the borehole and (B) a comparison of the $\delta^{18}O$ sampled from groundwater in the CRG-1 borehole with depth along the borehole.

Additional modelling work was completed utilizing both geochemical and isotopic constraints in what is referred to as Multivariate Mixing and Mass-balance (M3) calculations using both geochemical and microbial sample data from the CRL (Laaksoharju et al., 1999; Gómez, 2006; Laaksoharju et al., 2008). The results of this model are displayed in Figure 26 (King-Sharp et al., 2016). The findings of this model were consistent with other findings at the

site and suggested that, historically, infiltrating meteoric waters make up the largest proportion of current groundwaters. Depending on the borehole studied, the theoretical component contributed from glacial meltwaters ranges from 10% (CRG-4A) to 40% (CRG-1) with meteoric water making up the remainder. The M3 model classified the higher salinity waters at depth in CR-9 as originating from the Champlain Sea (up to 70%), the only samples in the dataset that were thought to have been significantly influenced by paleoseawater (King-Sharp et al., 2016).

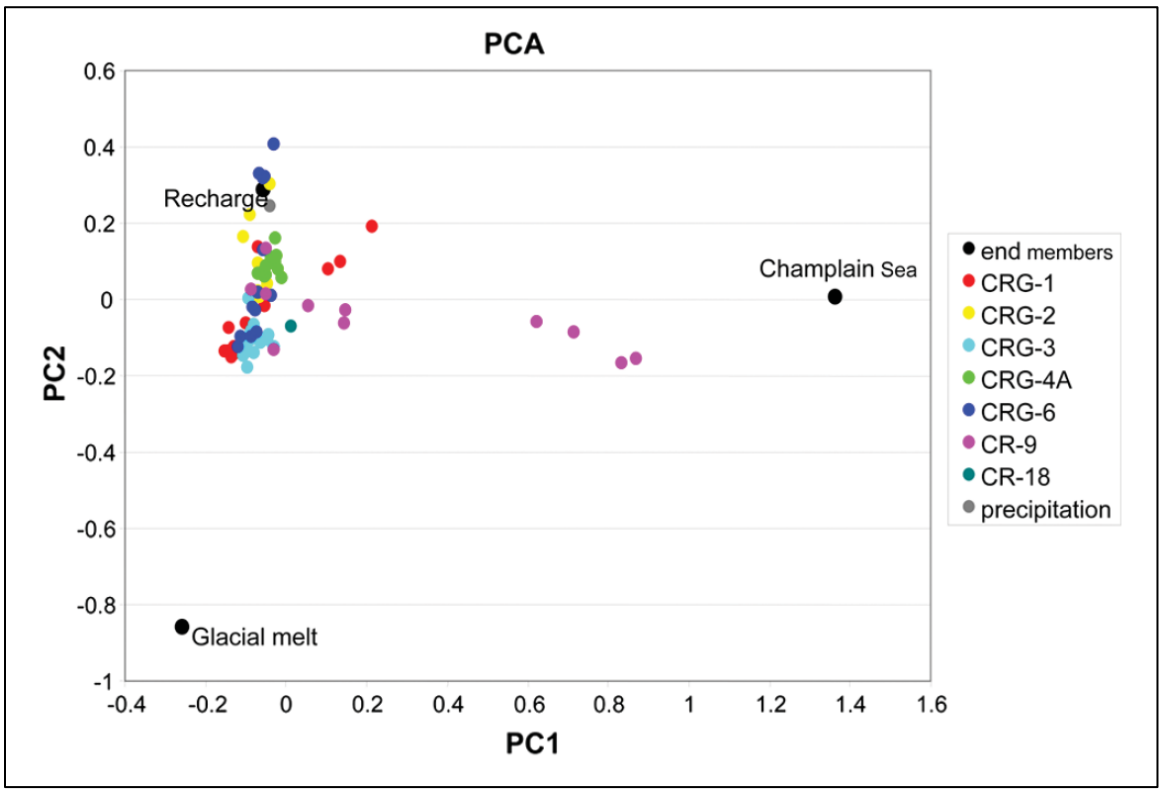

Figure 26. Principal Component "M3" Analysis (PCA) of CRL groundwater samples compared to theorized recharge endmembers (from King-Sharp et al., 2016).

5. Summary and Conclusions

With a coherent understanding of the geochemical and tectonic evolution of a potential crystalline waste repository site, it is important to refocus perspective and apply this knowledge to predict theoretical site suitability based on fracture mineral stability and possible future groundwater evolution. The objective of this investigation was to synthesize new groundwater

and porewater geochemical and isotopic data with existing research and datasets that focused on fracture minerals and geology in order to gain a more comprehensive understanding of the historical site stability and hydrogeological evolution. The intention is to help assess analogous crystalline bedrock sites for long term site stability pertaining to long term nuclear waste storage.

It has been discussed that the fractured crystalline bedrock of the CRL site as well as numerous analogues in the Canadian and Fennoscandian Shields are dominated by flow through available fracture network conduits (Clauer et al., 1989; Blyth et al., 2009, Drake et al., 2009). As these fractures are typically closed by minerals precipitated from the past fluids propagating through them, fracture mineral stability is an extremely important consideration when it comes to future hydrological stability. Building on the findings of Tian (2016) who assessed and revealed the importance of fracture mineral stable isotopes ($\delta^{13}C$ and $\delta^{18}O$) as well as petrographic techniques such as mineral petrography (for mineral identification) and fluid inclusion analyses, this study instead focused on geochemical and isotopic characterization of groundwaters available from packered intervals in the boreholes at the CRL. Groundwater was studied from samples obtained utilizing the Westbay packer system intervals in boreholes CR-9, CR-18, CRG-1, CRG-3, CRG-4A and CRG-6 (Figure 2). Several parameters including dissolved ion geochemistry, stable isotopes ($\delta^{18}O$, $\delta^{2}H$, $\delta^{13}C$, $\delta^{37}Cl$) and radioactive isotopes (^{3}H, ^{14}C, $^{87}Sr/^{86}Sr$) were incorporated into profiles which are illustrated for each borehole where available (Figure 12, Figure 14, Figure 15, Figure 16, Figure 17, Figure 18, Figure 19). This visual representation helps to illustrate patterns and anomalies as well as assist with comparisons between groundwaters from different boreholes. A Piper Plot was also utilized to visually represent the proportional breakdown of available major ion geochemistry for groundwaters from packer intervals. Figure 21 helps separate unique geochemical signatures and helps to

understand groundwater evolution as well as classify groundwaters into different groups based on the dominant ionic species (shallow Group I Ca-HCO_3 type, intermediate Group II Na-HCO_3 type, deeper Group III Na-HCO_3-Cl type and Group IV NaCl type waters). Overlaps do occur between different environments making a Piper Plot most valuable when combined with other parameters to help differentiate water types at the site (Figure 21).

Relative to similar sites in the Canadian and Fennoscandian shield (Larson and Tullborg, 1984; Gascoyne and Schwarcz, 1985; Fritz et al., 1989; Clauer et al., 1989; Peterman and Wallin, 1999; Blyth et al., 1998; Tullborg, 1989a; Blyth et al., 2000; Bukata, 2000; Blyth et al., 2004; Blyth et al., 2009; Drake et al., 2008; Tullborg et al., 2008; Drake and Tullborg, 2009), the CRL bedrock was found to be stable both geologically (available fractures sealed with calcite long-term at depth) stable for at least 250 ka (Neymark et al., 2013) and possibly as long as 200 Ma (Tian, 2016), both in excess of the 100 ka time period initially targeted. The additional data collected during this study cannot comment directly on the age of calcite emplacement and instead related to the stability of the calcite as it currently exists as effected by geochemical groundwater changes. Hydrologically, the CRL site was found to be geochemically stable when surveying groundwaters sampled under current conditions with no evidence of any significant impacts on stability from paleoseawater, glaciation or highly saline deep waters often associated with crystalline rock sites (Gascoyne et al., 1995). Looking forward, the most significant concern when it comes to hydrologic conditions relating to the transportation of hazardous radioactive substances in a fractured crystalline rock site is calcite stability, specifically the capacity for a theoretical groundwater fluid to dissolve calcite. An opportunity to assess the influence of a dilute source of recharge was to investigate the effect of recent glacial meltwaters on the CRL. There was not found to be a correlation between the areas identified as likely influenced by

glacial waters and calcite instability. Evidence exists of water-rock interaction influencing and evolving groundwater geochemically over long residence times (6-10 ka) (King-Sharp et al., 2016), impacting groundwater chemistry and evolving the shallow meteoric waters from Group I Ca-HCO_3 type waters (influenced by shallow mineral dissolution) to Group II Na-HCO_3 type waters (Ca to Na exchange), to Group III Na-HCO_3-Cl as proportionally more chloride is introduced at depth (Figure 21) (Kaija et al., 2000). Utilizing the available tools, several areas of relative stability were noted (i.e. CRG-3), however precise location and hosting of a geological waste management facility was not the focus of this investigation. The recommendation of this investigation would be to understand and effectively synthesize available groundwater and fracture mineral data for similar future investigations. The study of current groundwater conditions in available fracture networks in conjunction with comprehensively understanding the depositional history of fracture sealing minerals is an effective multi-faceted approach to project site stability as well as the potential influence current and theoretical future fluids could have on the stability of these minerals.

References

Activation Laboratories Ltd., (2016). 4Litho - Lithium Metaborate/Tetraborate Fusion - ICP and ICP/MS. (n.d.). Retrieved from http://www.actlabs.com/page.aspx?page=516&app=226&cat1=549&tp=12&lk

Alley, W., Alley, R., (2013). Too Hot to Touch: The Problem of High-level Nuclear Waste. Cambridge University Press, p. 383.

Ayuso, R., Foley, N. and Brown, C., (1987). Source of lead and mineralizing brines for Rossie-type Pb-Zn veins in the Frontenac Axis area, New York. *Economic Geology*, 82, 489-496.

Bau, M., and Möller, P. (1992). Rare earth element fractionation in metamorphogenic hydrothermal calcite, magnesite and siderite. *Mineralogy and Petrology*,45(3-4), 231-246.

Baumgartner, P., Chan, T., King-Sharp, K., Kitson, C., Kozak, E., Stroes-Gascoyne, S., and Thivierge, R., (2012). The suitability of the Chalk River Laboratories Site to host a proposed Geologic Waste Management Facility for low and intermediate-level radioactive waste: Supplementary Report, CRL Geologic Waste Management Facility, 361101-10260-REPT-003, Rev D1.

Blyth, A., Frape, S.K., Blomqvist, R., Nissinen, P., McNutt, R., (1998). An isotopic and fluid inclusion study of fracture calcite from borehole OL-KR1 at the Olkiluoto site, Finland. *Posiva Oy*. Report 98-04.

Blyth, A., Frape, S.K., Blomqvist, R., Nissinen, P., (2000). Assessing the past thermal and chemical history of fluids in crystalline rock by combining fluid inclusion and isotopic investigations of fracture calcite. Applied Geochemistry 14, 1417–1437.

Blyth, A., Frape, S.K., Ruskeenemi, T., Blomqvist, R., (2004). Origins, closed system formation and preservation of calcites in glaciated crystalline bedrock: evidence from the Palmottu natural analogue site, Finland. *Applied Geochemistry*. 19, 675–686.

Blyth, A.R., Frape, S.K., Tullborg, E.-L., (2009). A review and comparison of fracture mineral investigations and their application to radioactive waste disposal. Appl. Geochem. 24, 821–835.

Bottinga, Y., (1968). Calculation of fractionation factors for carbon and oxygen isotopic exchange in the system calcite-carbon dioxide-water. J. Phys. Chem. 72, 800–808.

Bottomley, J.D. Ross, and B.W. Graham. (1984). A Borehole Methodology for Hydrochemical Investigations in Fractured Rock. *Water Resources Research*, 20(9), pp. 1277–1300.

Bottomley, D.J., (1987). The isotope geochemistry of fracture calcites from the chalk river area, Ontario, Canada. *Applied Geochemistry*. 2, 81–91.

Bottomley, D.J., Veizer, J., (1992). The nature of groundwater in fractured rock: evidence from the isotopic and chemical evolution of recrystallized fracture calcites from the Canadian Precambrian Shield. *Geochimica et Cosmochimica Acta* 56, 369–388.

Bukata, A., 2000. Recrystallization of fracture-infilling calcite: evidence from d18O, d13C, U/Th Ages and Fluid Inclusions. Unpublished MSc Thesis, Trent University, Peterborough, Canada.

Capo, R. C., Stewart, B. W., & Chadwick, O. A., (1998). Strontium isotopes as tracers of ecosystem processes: theory and methods. *Geoderma* 82(1-3), 197-225.

Carignan, J., Garirpy, C., and Hillaire-Marcel, C., (1997). Hydrothermal fluids during Mesozoic reactivation of the St. Lawrence rift system, Canada: C, O, Sr and Pb isotopic characterization. *Chemical Geology* 147, 1-21.

Catto, N. R., Patterson, R. J., & Gorman, W. A. (1981). Late Quaternary marine sediments at Chalk River, Ontario. *Canadian Journal of Earth Sciences*, 18(8), 1261-1267.

Catto N. R., Patterson R., and Gorman W., (1982). The Late Quaternary geology of the Chalk River Region, Ontario and Quebec. *Canadian Journal of Earth Sciences* 19, 1218-1231.

Catto, N., Gorman, W., and Patterson, R., (1989). Quaternary Sedimentology and Stratigraphy of the Chalk River Region, Ontario and Quebec. Proceedings of a Workshop on Geophysical and Related Geoscientific Research at Chalk River, Ontario, Ottawa, ON, 14–15 December 1983, Edited by M.D. Thomas and D. Dixon.

Clark, I., & Fritz, P. (1997). Environmental isotopes in hydrogeology. Boca Raton: Lewis.

Clauer, N., Frape, S.K., Fritz, B., (1989). Calcite veins of the Stripa granite (Sweden) as records of the origin of the groundwaters and their interactions with the granitic body. *Geochimica et Cosmochimica* Acta 53, 1777–1781.

Deines, P., Langmuir, D., & Harmon, R. S. (1974). Stable carbon isotope ratios and the existence of a gas phase in the evolution of carbonate ground waters. *Geochimica Et Cosmochimica Acta*, 38(7), 1147-1164.

Downs, A. J., & Adams, C. J. (1975). The chemistry of chlorine, bromine, iodine and astatine. Oxford: Pergamon Press.

Drake, H., Tullborg, E.-L., Annersten, H., (2008). Red-staining of the wall rock and its influence on the reducing capacity around water conducting fractures. *Applied Geochemistry* 23, 1898–1920.

Drake, H., Tullborg, E.-L., Mackenzie, A., (2009). Detecting the near-surface redox front in crystalline bedrock using fracture mineral distribution, geochemistry and U-series disequilibrium. *Applied Geochemistry* 24, 1023–1039.

Drake, H., Tullborg, E.-L., (2009). Paleohydrogeological events recorded by stable isotopes, fluid inclusions and trace elements in fracture minerals in crystalline rock, Simpevarp area, SE Sweden. *Applied Geochemistry* 24, 715–732.

Drake, H., Heim, C., Roberts, N. M., Zack, T., Tillberg, M., Broman, C., Åström, M. E., (2017). Isotopic evidence for microbial production and consumption of methane in the upper continental crust throughout the Phanerozoic eon. *Earth and Planetary Science Letters* 470, 108-118.

Easton, R.M., (1986). Geochronology of the Grenville Province. *Geological Association of Canada Special Papers* 31, 127-173.

Eggenkamp, H., & Coleman, M. (2000). Rediscovery of classical methods and their application to the measurement of stable bromine isotopes in natural samples. *Chemical Geology*, 167(3-4), 393-402.

Eby G. N., (1975). Abundance and distribution of rare earth elements and yttrium in the rocks and minerals of the Oka carbonatite complex Quebec. *Geochimica et Cosmochimica Acta* 39, 597-620.

Environment Canada. (2018). Almanac Averages and Extremes for February 22. Retrieved from http://climate.weather.gc.ca/climate_data/almanac_e.html?StationID=47527

Epstein, S., Mayeda, T.K., (1953). Variation of the 18O content of waters from natural sources. *Geochimica et Cosmochimica Acta* 4, 213–224.

Franklyn M. T., McNutt R. H., Kamineni D. C., Gascoyne M., And Frape S. K., (1991). Groundwater $^{87}Sr/^{86}Sr$ values in the Eye-Dashwa Lakes pluton, Canada: Evidence for plagioclase-water reaction. *Chemical Geology* 86, 111-122.

Frape, S.K., Fritz, P., (1981). The chemistry and isotopic composition of saline groundwaters from the Sudbury Basin, Ontario. *Canadian Journal of Earth Science* 19, 645-661.

Frape, S.K., Fritz, P., McNutt, R.H., (1984). Water-rock interaction and chemistry of groundwaters from the Canadian Shield. *Geochimica et Cosmochimica Acta* 48, 1617-1627.

Frape, S.K., Fritz, P., Kamineni, D.C., Gibson, I.L., (1992). Hydrogeochemical Investigations in Boreholes at the Stripa Mine: the Hydrochemical Advisory Group and their Associates. Swedish Nuclear Fuel and Waste Management Company (SKB) Report 92(19), 30–63

Frape, S., Blyth, A., Stotler, R. Ruskeeniemi, T. Blomqvist, H., McNutt, R., & Gascoyne, M., (2014). Deep Fluids in the Continents. *Treatise on Geochemistry (Second Edition)* 7(15), 518-554.

Fritz, P., Frape, S.K., (1987). Saline Water and Gases in Crystalline Rocks. *Geological Association of Canada Special Papers* 33, 259.

Fritz, P., Fontes, J.-Ch., Frape, S.K., Louvat, D., Michelot, J.-L., Balderer, W., (1989). The isotope geochemistry of carbon in groundwater at Stripa. *Geochimica et Cosmochimica Acta* 53, 1765–1775.

Gascoyne, M., Schwarcz, H.P., (1986). Radionuclide migration over recent geologic time in a granitic pluton. *Chemical Geology*. 59, 75–86.

Gascoyne, M., Davison, C.C., Ross, J.D., Pearson, R., (1987). Saline groundwaters and brines in plutons in the Canadian Shield. In: Fritz, P., Frape, S.K. (Eds.), Saline Water and Gases in Crystalline Rocks, *Geological Association of Canada Special Papers*. 33, pp. 18e38.

Gascoyne M., Stroes-Gascoyne S., and Sargent F. P. (1995) Geochemical influences on the design, construction and operation of a nuclear water vault. *Applied Geochemistry*. 10, 657–671.

Gadd, N., (1958). Geological aspects of radioactive waste disposal, Chalk River, Ontario. Geological Survey of Canada, Preliminary report and map, 25.

Goldstein, R.H., Reynolds, T.J., (1994). Fluid inclusion microthermometry. In: Goldstein, R.H. (Ed.), Systematics of fluid inclusions in diagenetic minerals. SEPM Short Course, vol. 31. SEPM (Society for Sedimentary Geology), Tulsa, Oklahoma, pp. 87–121.

Goldstein, R., Samson, I., Anderson, A., & Marshall, D., (2003). Petrographic Analysis of Fluid Inclusions. Fluid inclusions: analysis and interpretation. *Mineralogical Association of Canada*, 9-54.

Gómez J B, Laaksoharju M, Skårman E, Gurban I (2006), M3 version 3.0: Concepts, methods and mathematical formulation. *SKB Technical Report* TR 06-27, Stockholm, Sweden

Habermann, D., Neuser, R. D., and Richter, D. K., (1996). REE-activated cathodoluminescence of calcite and dolomite: high-resolution spectrometric analysis of CL emission (HRS-CL). Sedimentary Geology 101(1), 1-7.

Henderson T., (1985). Geochemistry of ground water in two sandstone aquifer systems in the Northern Great Plains in parts of Montana, Wyoming, North Dakota, and South Dakota. *U.S. Geological Survey Professional Paper* 1402-C.

Hoefs, J. (2015). Stable Isotope Geochemistry (7th ed.). Cham, Switzerland.

International Atomic Energy Agency., (1983). Isotope techniques in the hydrogeological assessment of potential sites for the disposal of high-level radioactive wastes. (1983). Vienna: International Atomic Energy Agency.

International Atomic Energy Agency., (2013). Nuclear Safety Review. IAEA Annual Report, 57, 1-62.

Kaija, J., Blomqvist, R., Suksi, J., & Rasilanainen, K. (2000). The Palmottu Natural Analogue Project Summary Report 1996-1999. *Geological Survey of Finland Nuclear Waste Disposal Research*, YST-102.

Kamo, S. L., Krogh, T. E., & Kumarapeli, P. S. (1995). Age of the Grenville dyke swarm, Ontario–Quebec: Implications for the timing of lapetan rifting. *Canadian Journal of Earth Sciences*, 32(3), 273-280.

Karrow, P., and Calkin, P., (1985), Quaternary Evolution of the Great Lakes, *Geological Association of Canada Special Paper* 30.

King-Sharp, K., Frape, S., Peterman, Z., Gwynne, R., Tian, L. and Gurban, I., (2016). Synthesis of Geochemical and Fracture Mineral Studies Relevant to A Deep Geological Repository for Nonfuel Wastes at Chalk River. *CNL Nuclear Review*, pp.1-14.

Ketchum, J.W.F., Davidson, A., (2000). Crustal architecture and tectonic assembly of the Central Gneiss Belt, Grenville Province, Canada: a new interpretation. *Canadian Journal of Earth Science* 37, 217–234.

Kumarapeli, P.S., (1985). Vestiges of Iapetan rifting in the west of the northern Appalachians. *Geoscience Canada* 12, 54-59.

Laaksoharju M, Skårman C, and Skårman E, (1999). Multivariate Mixing and Mass-balance (M3) calculations, a new tool for decoding hydrogeochemical information. *Applied Geochemistry* 14(7), 861-871.

Laaksoharju M, Andersson, C, Gurban I, Gascoyne M. (2001) Demonstration of M3 modelling of the Canadian whiteshell research area (WRA) hydrogeochemical data. OPG/SKB M3 modelling project. *SKB Technical Report SKB TR-01-37*, Stockholm, Sweden.

Larson, S., and Tullborg, E., (1984). Stable isotopes of fracture-filling calcite from Finns. *Lithosphere* 17, 117-125.

McNutt, R., Frape, S., Fritz, P., Jones, M., and MacDonald, I., (1990). The $^{87}Sr/^{86}Sr$ values of Canadian Shield brines and fracture minerals with applications to groundwater mixing, fracture history and geochronology. *Geochimica et Cosmochimica Acta*, 54, 205-215.

McNutt, R.H., (2000). Strontium isotopes. In: Cook, Peter G., Herczeg, Andrew L. (Eds.), Environmental Tracers in Subsurface Hydrology. Kluwer Academic Publishers, Boston, pp. 232-260.

Mook, W.G., Bommerson, J.C., Staverman, W.H., (1974). Carbon isotopic fractionation between dissolved bicarbonate and gaseous carbon dioxide. *Earth and Planetary Science Letters* 22, 169– 176.

Munemoto, T., Ohmori, K., & Iwatsuki, T., (2015). Rare earth elements (REE) in deep groundwater from granite and fracture-filling calcite in the Tono area, central Japan: Prediction of REE fractionation in paleo- to present-day groundwater. *Chemical Geology* 417, 58-67.

Neymark, L. A., Peterman, Z. E., Moscati, R. J., and Thivierge R. H., (2013). U-Pb Rb-Sr, and U-series isotope geochemistry of rocks and fracture minerals from the Chalk River Laboratories site Grenville Province, Ontario, Canada. *Applied Geochemistry* 26 (2013) 10-33.

Nordstrom, D. K., Ball, J. W., Donahoe, R. J., & Whittemore, D. (1989). Groundwater chemistry and water-rock interactions at Stripa. *Geochimica Et Cosmochimica Acta*, 53(8), 1727-1740.

Nuclear Waste Management Organization, (2017). Implementing Adaptive Phased Management 2017 to 2021. NWMO, 1-68.

O'Neil, J. R., & Taylor, H. P. (1969). Oxygen isotope equilibrium between muscovite and water. *Journal of Geophysical Research*, 74(25), 6012-6022.

Ongaro, N. C. (2018). Laser Ablation ICP-MS of Fracture Fill Calcite from Chalk River, Ontario (Unpublished BSc thesis). University of Waterloo.

Peterman, Z.E., Wallin, B., (1999). Synopsis of strontium isotope variations in groundwater at Aspo, southern Sweden. *Applied Geochemistry* 14, 939-951.

Peterman, Z.E., Neymark, L., King-Sharp, K., and Gascoyne, M., (2016). Isotope Hydrology of the Chalk River Laboratories Site, Ontario, Canada. *Applied Geochemistry* 66, 149–161.

Peters, T., (1986). Structurally incorporated and water extractable chlorine in the Boettstein granite (N. Switzerland). *Contributions to Mineralogy and Petrology* 94, 272-273.

Prudêncio, M. I., Gouveia, M.A., Sequeira Braga, M.A., and Figueiredo, M.O. (1994). REE Distribution as an Indicator of the Origin of Carbonates and Silicates in Basaltic Rocks. *Mineralogical Magazine*, 58A(2), 744-745.

Quade, J. (2014). The Carbon, Oxygen, and Clumped Isotopic Composition of Soil Carbonate in Archeology. Treatise on Geochemistry, 129-143.

Remenda, V. H., Cherry, J. A., & Edwards, T. W. (1994). Isotopic Composition of Old Ground Water from Lake Agassiz: Implications for Late Pleistocene. *Climate. Science*, 266(5193), 1975-1978.

Rimando, R. E., & Benn, K., (2005). Evolution of faulting and paleo-stress field within the Ottawa graben, Canada. *Journal of Geodynamics* 39(4), 337-360.

Roedder, E., (1984). Fluid inclusions: an introduction to studies of all types of fluid inclusions, gas, liquid, or melt, trapped in materials from earth and space, and their application to the understanding of geologic processes. Washington, D.C. Mineralogical Society of America.

Sandström, B., & Tullborg, E. L., (2009). Episodic fluid migration in the Fennoscandian Shield recorded by stable isotopes, rare earth elements and fluid inclusions in fracture minerals at Forsmark, Sweden. *Chemical Geology* 266(3), 126-142.

Shouakar-Stash, O., Frape, S. K., & Drimmie, R. J. (2005). Determination of Bromine Stable Isotopes Using Continuous-Flow Isotope Ratio Mass Spectrometry. *Analytical Chemistry*, 77(13), 4027-4033

Shouakar-Stash, O., Drimmie, R. J., & Frape, S. K. (2005). Determination of inorganic chlorine stable isotopes by continuous flow isotope ratio mass spectrometry. *Rapid Communications in Mass Spectrometry*, 19(2), 121-127.

Smellie, J., Frape, S., (1997). Hydrogeochemical aspects of glaciation. In: King-Clayton et al. (eds): Glaciation and Hydrogeology, Workshop on the impact of climate change & glaciations on rock stresses, groundwater flow and hydrochemistry – past, present and future. SKI Report 97:13, 45–51.

Stotler, R. L., Frape, S. K., & Shouakar-Stash, O. (2010). An isotopic survey of δ81Br and δ37Cl of dissolved halides in the Canadian and Fennoscandian Shields. *Chemical Geology*, 274(1-2), 38-55.

Sykes, J.F., Normani, S.D., Jensen, M.R., Sudicky, E.A., 2009. Regional-scale groundwater flow in a Canadian Shield setting. *Canadian Geotechnical Journal*. 46, 813-827.

ThermoFinnigan. (2002). Triton Hardware Manual (12/2002 ed., Vol. 0). Bremen, Germany: Thermo Finnigan MAT.

Tian, L. (2016). Geochemical Evolution of Fracture Filling Minerals from the Chalk River Laboratory Site, Ontario, Canada (Unpublished MSc thesis). University of Waterloo.

Tullborg, E.L., (1989a). The influence of recharge water on fissure-filling minerals – a study from Klipperås, southern Sweden. *Chemical Geology* 76, 309–320.

Tullborg, E.L., (1989b). $\delta^{18}O$ and $\delta^{13}C$ in fracture calcite used for interpretation of recent meteoric water circulation. In: Miles, D.L. (Ed.), Proc. 6th International Symposium. (Water–Rock Interaction (WRI-6). A.A). Balkema, Rotterdam, pp. 95–698.

Tullborg, E.-L., Drake, H., Sandström, B., (2008). Palaeohydrogeology: a methodology based on fracture mineral studies. Applied Geochemistry 23, 1881–1897.

Tweed, S., Weaver, T., Cartwright, I., & Schaefer, B., (2006). Behavior of rare earth elements in groundwater during flow and mixing in fractured rock aquifers: An example from the Dandenong Ranges, southeast Australia. Chemical Geology 234(3-4), 291-307.

Veizer, J., (1989). Strontium Isotopes in Seawater Through Time. Annual Review of Earth and Planetary Sciences 17(1), 141-167.

Vogel, J. C., Grootes, P. M., & Mook, W. G. (1970). Isotopic fractionation between gaseous and dissolved carbon dioxide. Zeitschrift Für Physik A Hadrons and Nuclei, 230(3), 225-238.

Waber, H., & Smellie, J. (2008). Characterisation of pore water in crystalline rocks. Applied Geochemistry, 23(7), 1834-1861.

Wallin, B., Peterman, Z., (1999). Calcite fracture fillings as indicators of paleohydrology at Laxemar at the Äspö Hard Rock Laboratory, southern Sweden. Applied Geochemistry 14(7), 953-962.

Wallin, B., Peterman, Z.E., (2014). Compilation and review of $^{87}Sr/^{86}Sr$ and stable isotopes from groundwater, calcite fracture fillings, mineral and whole rock sampling at Aspo, Sweden. Applied Geochemistry 14(1999), 953-962.

Worrall, F., & Pearson, D. (2001). Water-rock interaction in an acidic mine discharge as indicated by rare earth element patterns. Geochimica Et Cosmochimica Acta, 65(18), 3027-3040.

Appendix: Tables

Table 1. Available $\delta^{13}C$, $\delta^{18}O$, fluid inclusion homogenization (T_h), and melting (T_m) temperatures and $^{87}Sr/^{86}Sr$ analyses for fracture minerals at the CRL (from Tian, 2016)

Borehole	Depth	Unit	$\delta^{13}C$	$\delta^{18}O$	$\delta^{18}O$	T_h	T_m	Salinity	$^{87}Sr/^{86}Sr$	Type
	(m)		‰ VPDB	‰ VPDB	‰ VSMOW	°C	°C	wt% NaCl		
CR18	28.14	B	-5.05	-13.24	17.27	106.1	-4.8	7.6		Crystalline
CR18	28.14	B	-5.05	-13.24	17.27	95.7	-3.7	6.0		Crystalline
CR18	28.14	B	-5.05	-13.24	17.27	90.1	-2.3	3.9		Crystalline
CR18	28.14	B	-5.05	-13.24	17.27	85.8	-3.7	6.0		Crystalline
CR18	28.14	B	-5.05	-13.24	17.27	83.7	-2.2	3.7		Crystalline
CR18	28.14	B	-5.05	-13.24	17.27	81	-33	26.4		Crystalline (S)
CR18	28.14	B	-5.05	-13.24	17.27	79	-32	26.0		Crystalline (S)
CR18	29.47	B	-5.04	-12.68	17.85					Crystalline
CR18	29.47	B	-5.14	-15.40	15.05					Crystalline
CR18	29.47	B	-4.97	-12.80	17.72					Crystalline
CR18	29.47	B	-9.34	-10.50	20.10					Fibrous
CR18	29.47	B	-7.14	-9.99	20.62					Fibrous
CR18	29.47	B	-9.23	-11.23	19.35					Fibrous
CR9	159.20	B	-4.46	-11.46	19.10					Crystalline
CR9	159.20	B	-8.23	-15.04	15.41					Fibrous
CR9	173.40	B	-6.72	-12.60	17.93					Fibrous
CR9	191.90	B	-3.85	-12.15	18.40					Fibrous
CR9	191.90	B	-5.92	-16.04	14.39					Fibrous
CR9	203.75	B	-6.11	-13.10	17.42				0.70853	Crystalline
CR9	203.75	B	-9.16	-14.66	15.81					Fibrous
CR9	238.20	B	-6.57	-12.60	17.93					Crystalline
CR9	238.20	B	-6.45	-10.03	20.58					Crystalline

Borehole	Depth	Unit	$\delta^{13}C$	$\delta^{18}O$	$\delta^{18}O$	T_h	T_m	Salinity	$^{87}Sr/^{86}Sr$	Type
	(m)		‰ VPDB	‰ VPDB	‰ VSMOW	°C	°C	wt% NaCl		
CR9	254.83	B	-6.91	-12.22	18.33					Crystalline
CR9	259.25	B	-5.95	-13.13	17.39					Crystalline
CR9	259.25	B	-8.64	-12.19	18.36					Fibrous
CR9	270.18	B	-4.18	-10.70	19.89					Fibrous
CR9	344.42	B	-4.98	-15.65	14.78					Crystalline
CR9	352.77	B	-3.26	-10.55	20.05					Fibrous
CR9	353.76	B	-7.22	-11.42	19.14					Fibrous
CR9	382.80	B	-5.57	-12.47	18.07					Crystalline
CR9	442.00	B	-5.83	-16.28	14.14					Fibrous
CR9	446.69	B	-7.75	-15.22	15.23					Crystalline
CR9	490.51	B	-5.13	-15.62	14.82	104	-4	6.0		Crystalline
CR9	491.85	B	-4.86	-16.11	14.31					Crystalline
CR9	491.85	B	-3.73	-12.60	17.93					Crystalline
CR9	498.30	B	-5.24	-16.13	14.29					Crystalline
CR9	499.50	B	-3.54	-14.80	15.67					Fibrous
CR9	500.30	B	-4.55	-17.31	13.08					Crystalline
CR9	521.21	B	-7.25	-13.41	17.09					Crystalline
CR9	545.40	B	-6.07	-10.91	19.67					Crystalline
CR9	545.40	B	-6.60	-11.26	19.31					Fibrous
CR9	553.70	B	-8.59	-14.66	15.81	90	-19	20.4		Metasomatic
CR9	553.70	B	-8.59	-14.66	15.81	90	-20	20.9		Metasomatic
CR9	553.70	B	-8.59	-14.66	15.81	90	-19	20.4		Metasomatic
CR9	553.70	B	-5.12	-11.98	18.57	73	-20	20.9		Metasomatic
CR9	560.86	B	-6.84	-13.52	16.98					Crystalline
CR9	562.00	B	-10.39	-11.28	19.29					Crystalline
CR9	577.06	B	-5.09	-12.37	18.17					Crystalline
CR9	635.27	B	-6.60	-12.77	17.75					Fibrous

Borehole	Depth	Unit	$\delta^{13}C$	$\delta^{18}O$	$\delta^{18}O$	T_h	T_m	Salinity	$^{87}Sr/^{86}Sr$	Type
	(m)		‰ VPDB	‰ VPDB	‰ VSMOW	°C	°C	wt% NaCl		
CR9	700.76	B	-4.51	-17.03	13.36	112.3	-8.3	12.1	0.70927	Crystalline
CR9	700.76	B	-4.51	-17.03	13.36	107.2	-5.1	8.0		Crystalline
CRG1	9.02	A	-7.37	-11.28	19.29				0.71056	Fibrous
CRG1	25.26	A	-7.13	-14.14	16.35	79	-6	9.2	0.71029	Crystalline
CRG1	25.26	A	-6.51	-9.72	20.90	72	-17	19.3		Crystalline (S)
CRG1	110.18	A	-8.38	-11.07	19.50				0.71614	Fibrous
CRG1	110.18	A	-9.27	-12.66	17.87					Fibrous
CRG1	230.90	B	-6.09	-14.37	16.10				0.70915	Crystalline
CRG1	230.90	B	-8.88	-11.70	18.86					Crystalline
CRG1	238.62	B	-7.38	-10.78	19.80				0.72057	Crystalline
CRG1	238.62	B	-6.99	-11.65	18.91					Vuggy
CRG1	246.28	B	-6.40	-13.58	16.92					Crystalline
CRG1	246.28	B	-8.18	-9.62	21.01					Fibrous
CRG1	308.73	B	-7.53	-9.44	21.19				0.70911	Crystalline
CRG1	361.04	B	-5.61	-16.04	14.38	113	-2	3.4		Crystalline
CRG1	361.04	B	-5.61	-16.04	14.38	113	-2	3.4	0.70905	Crystalline
CRG1	361.04	B	-5.61	-16.04	14.38	108	0	0.0		Crystalline
CRG1	361.04	B	-5.61	-16.04	14.38	106	0	0.0		Crystalline
CRG1	361.04	B	-5.82	-14.72	15.74					Crystalline
CRG1	448.57	B	-5.62	-14.90	15.56				0.70978	Crystalline
CRG1	448.57	B	-5.61	-13.49	17.02				0.70956	Crystalline
CRG1	448.57	B	-6.74	-12.76	17.77					Crystalline
CRG1	452.29	B	-6.55	-12.27	18.27				0.71006	Crystalline
CRG1	452.29	B	-6.32	-11.91	18.64					Fibrous
CRG1	493.66	B	-5.59	-15.40	15.04	197	-1	1.6	0.70870	Crystalline (HT)
CRG1	493.66	B	-5.71	-15.23	15.22	192	-2	2.7		Crystalline (HT)
CRG1	493.66	B	-5.68	-16.17	14.25	180	-1	1.2		Crystalline (HT)

Borehole	Depth	Unit	$\delta^{13}C$	$\delta^{18}O$	$\delta^{18}O$	T_h	T_m	Salinity	$^{87}Sr/^{86}Sr$	Type
	(m)		‰ VPDB	‰ VPDB	‰ VSMOW	°C	°C	wt% NaCl		
CRG1	493.66	B	-5.84	-15.26	15.19	95	-1	1.4		Crystalline
CRG1	493.66	B	-5.84	-15.20	15.25	86	-1	2.1	0.70963	Crystalline
CRG1	493.66	B	-5.72	-15.36	15.09	84	-2	3.9		Crystalline
CRG1	615.15	B	-7.64	-15.82	14.61	90	-6	8.5		Fibrous
CRG1	615.15	B	-7.71	-15.31	15.14	80	-4	6.1	0.70952	Fibrous
CRG1	615.15	B	-7.88	-17.34	13.05				0.71278	Fibrous
CRG1	615.15	B	-8.24	-14.53	15.94					Fibrous
CRG1	615.15	B	-8.42	-20.61	9.68				0.70981	Fibrous
CRG1	615.15	B	-8.15	-20.44	9.85				0.70887	Fibrous
CRG1	615.15	B	-8.14	-10.95	19.63					Fibrous
CRG1	615.15	B	-7.81	-10.95	19.63					Fibrous
CRG1	683.66	B	-6.22	-14.38	16.10	105	-8	11.5		Crystalline
CRG1	683.66	B	-6.80	-12.60	17.93	104	-24	22.9	0.70981	Crystalline (S)
CRG1	683.66	B	-6.22	-14.38	16.10					Crystalline
CRG1	739.30	B	-6.91	-16.66	13.74				0.70887	Crystalline
CRG1	739.30	B	-6.46	-16.94	13.46				0.71060	Crystalline
CRG3	24.70	A	-5.76	-11.52	19.05	73	-31	25.7		Dolomite
CRG3	24.70	A	-9.13	-10.55	20.05	73	-35	27.0		Dolomite
CRG3	96.33	A	-6.56	-14.31	16.17					Crystalline
CRG3	96.63	A	-5.75	-16.13	14.29					Crystalline
CRG3	127.64	B	-5.26	-10.84	19.74					Crystalline
CRG3	133.52	B	-5.72	-11.81	18.75	81	-4	6.0		Crystalline
CRG3	307.90	B	-4.94	-14.05	16.43	91	-7	10.5		Crystalline
CRG3	307.90	B	-4.94	-14.05	16.43	83	-7	10.5		Crystalline
CRG3	307.90	B	-4.94	-14.05	16.43	82	-3	4.9		Crystalline
CRG3	307.90	B	-4.94	-14.05	16.43	77	-7	10.5		Crystalline
CRG3	307.90	B	-8.15	-10.27	20.34	75	-3	4.9		Crystalline

Borehole	Depth	Unit	$\delta^{13}C$	$\delta^{18}O$	$\delta^{18}O$	T_h	T_m	Salinity	$^{87}Sr/^{86}Sr$	Type
	(m)		‰ VPDB	‰ VPDB	‰ VSMOW	°C	°C	wt% NaCl		
CRG3	307.90	B	-4.94	-14.05	16.43	70	-6	9.2		Crystalline
CRG3	307.90	B	-6.37	-14.73	15.73	67	-4	6.4		Crystalline
CRG3	389.38	B	-8.35	-10.31	20.29	92	-8	11.7		Crystalline
CRG3	389.38	B	-7.98	-10.76	19.83	89	-6	9.2		Crystalline
CRG3	389.38	B	-7.98	-10.76	19.83	88	-5	7.9		Crystalline
CRG3	389.38	B	-7.98	-10.76	19.83	86	-8	11.7		Crystalline
CRG3	389.38	B	-7.98	-10.76	19.83					Crystalline
CRG3	389.38	B	-7.98	-10.76	19.83					Crystalline
CRG3	389.38	B	-9.77	-8.43	22.23					Vuggy
CRG3	463.79	B	-4.82	-11.85	18.71					Crystalline
CRG3	548.40	B	-9.34	-10.50	20.10	90	-1	1.6		Crystalline
CRG3	627.31	B	-7.47	-10.59	20.00					Crystalline
CRG3	627.31	B	-6.48	-17.57	12.81					Fibrous
CRG3	630.29	B	-8.11	-10.22	20.38	102	-4	5.8		Crystalline
CRG3	630.29	B	-6.10	-15.52	14.92	92	-3	4.5		Crystalline
CRG3	630.29	B	-6.97	-12.72	17.81	90	0	0.5		Crystalline
CRG3	637.72	B	-8.35	-10.60	19.99	102	-6	9.6	0.70937	Crystalline
CRG3	637.72	B	-6.42	-15.04	15.42	92	-37	27.5	0.70925	Crystalline (S)
CRG3	672.71	B	-8.60	-9.32	21.31	89	-8	11.7		Vuggy
CRG3	672.71	B	-8.60	-9.32	21.31	89	-38	27.9		Vuggy
CRG3	861.45	B	-6.44	-12.93	17.59					Crystalline
CRG3	862.06	B	-5.83	-14.60	15.87	108	-1	1.4		Crystalline
CRG3	862.06	B	-5.83	-13.63	16.87	92	-3	5.1		Crystalline
CRG3	862.06	B	-5.89	-14.40	16.08	87	-8	11.7		Crystalline
CRG3	1171.77	C	-4.91	-15.32	15.12				0.70910	Fibrous
CRG3	1171.77	C	-5.27	-16.05	14.37					Fibrous
CRG4A	56.61	A	-6.32	-11.84	18.71					Crystalline

Borehole	Depth	Unit	$\delta^{13}C$	$\delta^{18}O$	$\delta^{18}O$	T_h	T_m	Salinity	$^{87}Sr/^{86}Sr$	Type
	(m)		‰ VPDB	‰ VPDB	‰ VSMOW	°C	°C	wt% NaCl		
CRG4A	115.75	A	-6.56	-12.79	17.74					Crystalline
CRG4A	115.75	A	-6.18	-13.66	16.84					Crystalline
CRG4A	115.75	A	-6.30	-13.09	17.42					Crystalline
CRG4A	124.20	A	-6.56	-13.87	16.62					Crystalline
CRG4A	124.20	A	-6.31	-13.43	17.08					Vuggy
CRG4A	206.53	A	-6.19	-14.45	16.02					Vuggy
CRG4A	382.14	A	-6.70	-9.81	20.80					Crystalline
CRG4A	425.35	A	-6.61	-14.43	16.04				0.70868	Crystalline
CRG4A	425.35	A	-6.65	-14.37	16.11					Crystalline
CRG4A	425.95	A	-6.16	-14.70	15.76					Crystalline
CRG4A	613.79	B	-7.74	-10.30	20.30	197	-5	7.4		Crystalline (HT)
CRG4A	613.79	B	-8.06	-12.48	18.05	181	-2	2.9		Crystalline (HT)
CRG5	12.68	C	-9.04	-7.73	22.95	87	-31	25.7		Vuggy
CRG5	12.68	C	-9.04	-7.73	22.95	85	-38	27.9		Vuggy
CRG5	16.27	C	-7.26	-11.63	18.93	124	0	0.0	0.70942	Fibrous
CRG5	16.27	C	-7.65	-10.66	19.93	78	-2	3.4		Fibrous
CRG5	16.27	C	-7.67	-9.36	21.27	78	-14	17.9		Fibrous
CRG5	16.27	C	-7.51	-11.35	19.22					Fibrous
CRG5	43.61	C	-12.71	-8.90	21.74				0.70939	Vuggy
CRG5	43.61	C	-12.89	-9.22	21.41					Vuggy
CRG5	43.61	C	-10.47	-10.81	19.78				0.70987	Vuggy
CRG5	147.70	C	-7.96	-12.40	18.14					Crystalline
CRG5	147.70	C	-5.73	-15.83	14.61					Crystalline
CRG5	147.70	C	-7.03	-12.93	17.59					Crystalline
CRG5	152.33	C	-6.61	-13.70	16.80					Crystalline
CRG5	152.33	C	-6.47	-13.95	16.54					Crystalline
CRG5	152.33	C	-6.15	-13.34	17.16					Crystalline

Borehole	Depth	Unit	$\delta^{13}C$	$\delta^{18}O$	$\delta^{18}O$	T_h	T_m	Salinity	$^{87}Sr/^{86}Sr$	Type
	(m)		‰ VPDB	‰ VPDB	‰ VSMOW	°C	°C	wt% NaCl		
CRG5	438.12	C	-13.60	-10.78	19.80				0.71211	Vuggy
CRG5	438.12	C	-12.99	-11.10	19.47					Vuggy
CRG5	438.12	C	-13.47	-10.74	19.85					Vuggy
CRG6	48.08	B	-10.46	-14.83	15.63				0.71227	Vuggy
CRG6	111.20	B	-7.10	-12.71	17.82	90	-21	23.6		Crystalline (S)
CRG6	111.20	B	-7.33	-12.80	17.73	86	-31	30.1	0.70889	Crystalline (S)
CRG6	116.93	B	-7.30	-12.78	17.74					Vuggy
CRG6	116.93	B	-6.73	-13.98	16.51					Crystalline
CRG6	123.26	B	-6.51	-13.84	16.66					Crystalline
CRG6	149.84	B	-6.95	-12.64	17.89					Crystalline
CRG6	149.84	B	-7.69	-10.89	19.69					Vuggy
CRG6	159.55	B	-7.27	-13.55	16.95	90	-4	6.0		Crystalline
CRG6	159.55	B	-7.69	-11.47	19.09	90	-5	7.2		Crystalline
CRG6	159.55	B	-6.62	-12.34	18.20	86	-29	24.9		Crystalline (S)
CRG6	159.55	B	-6.14	-12.36	18.18	81	-9	13.0		Crystalline
CRG6	159.55	B	-7.54	-11.75	18.80	76	-6	9.6		Crystalline
CRG6	169.12	B	-7.20	-12.18	18.36	100	-15	18.4		Crystalline (S)
CRG6	169.12	B	-6.24	-14.36	16.12	94	0	0.2		Crystalline
CRG6	170.79	B	-8.15	-10.90	19.69	88	-8	11.7		Crystalline
CRG6	170.79	B	-6.48	-14.47	16.00	87	-8	11.7		Crystalline
CRG6	170.79	B	-10.42	-8.35	22.32	72	-11	15.0		Crystalline
CRG6	170.79	B	-10.05	-8.71	21.95					Crystalline
CRG6	182.04	B	-7.16	-12.77	17.76	84	-6	9.2	0.70899	Crystalline
CRG6	182.04	B	-7.16	-12.77	17.76	84	-6	9.2	0.70899	Crystalline
CRG6	182.04	B	-7.16	-12.77	17.76	84	-2	3.4	0.70899	Crystalline
CRG6	182.04	B	-7.16	-12.77	17.76	84	-9	12.9	0.70899	Crystalline
CRG6	182.04	B	-13.34	-11.21	19.36	84	-2	3.4	0.70904	Vuggy

Borehole	Depth	Unit	$\delta^{13}C$	$\delta^{18}O$	$\delta^{18}O$	T_h	T_m	Salinity	$^{87}Sr/^{86}Sr$	Type
	(m)		‰ VPDB	‰ VPDB	‰ VSMOW	°C	°C	wt% NaCl		
CRG6	182.04	B	-7.16	-12.77	17.76	83	-6	9.2	0.70899	Crystalline
CRG6	182.04	B	-7.16	-12.77	17.76	82	-7	10.5	0.70899	Crystalline
CRG6	217.15	B	-8.47	-11.16	19.41					Vuggy
CRG6	217.15	B	-6.40	-15.49	14.95					Crystalline
CRG6	219.33	B	-5.17	-14.73	15.74					Crystalline
CRG6	219.33	B	-4.58	-14.22	16.26					Crystalline
CRG6	346.00	B	-5.05	-13.10	17.41	85	-31	25.7		Vuggy
CRG6	346.00	B	-4.53	-14.25	16.23					Vuggy
CRG6	346.00	B	-4.65	-12.98	17.54					Vuggy
CRG6	348.09	B	-7.72	-13.85	16.64					Crystalline
CRG6	348.09	B	-7.12	-12.41	18.12					Fibrous
CRG6	359.62	B	-9.41	-10.53	20.06				0.70900	Fibrous
CRG6	395.79	B	-6.99	-10.89	19.70					Crystalline
CRG6	410.20	B	-6.38	-13.23	17.28	91	-19	20.1		Metasomatic
CRG6	410.20	B	-6.38	-13.23	17.28	80	-9	13.3		Crystalline
CRG6	691.19	B	-4.98	-14.19	16.29					Crystalline
CRG6	691.19	B	-4.96	-13.08	17.43					Crystalline
CRG6	724.72	B	-4.64	-14.98	15.48	80	-39	28.1		Crystalline (S)
CRG6	724.72	B	-5.03	-15.08	15.37	77	-37	27.7	0.70849	Crystalline (S)
CRG6	724.72	B	-5.03	-15.08	15.37	77	-37	27.7	0.70849	Crystalline (S)
CRG6	724.72	B	-4.64	-14.98	15.48	76	-39	28.3		Crystalline (S)
CRG6	724.72	B	-5.03	-15.08	15.37	75	-10	14.4	0.70849	Crystalline (S)
CRG6	724.72	B	-4.64	-14.98	15.48	74	-36	27.4		Crystalline (S)
CRG6	724.72	B	-4.64	-14.98	15.48	73	-29	25.0		Crystalline (S)
CRG6	724.72	B	-5.03	-15.08	15.37	72	-38	27.8	0.70849	Crystalline (S)
CRG6	724.72	B		-15.08	15.37	62	-22	21.6	0.70849	Crystalline (S)

Table 2. Major ion geochemistry for CR-9 and CR-13 (from Bottomley et al., 1984)

Sample ID	Depth	pH	Cl	Br	SO4	HCO_3+CO_3	Ca	K	Mg	Na
	m		mg/L	mg/L	mg/L	mg/L	mg/L	mg/L	mg/L	mg/L
CR-9 2014 Interval 1	67	8.0	20	0.17	7.2	107	21	1.3	2.5	23
CR-9 2014 Interval 2	104	8.9	16	0.13	4.7	113	9	0.8	0.8	44
CR-9 2014 Interval 3	139	8.9	16	0.12	4.7	113	9	0.8	0.8	45
CR-9 2014 Interval 4	198	9.5	67	0.52	11.3	28	5	0.2	0.2	63
CR-9 2014 Interval 5	285	9.4	21	0.17	7.2	74	5	0.4	0.2	56
CR-9 2014 Interval 6	363	8.9	154	1.60	21.4	64	32	0.9	1.3	110
CR-9 2014 Interval 7	433	8.6	297	2.74	38.9	47	39	1.2	1.9	140
CR-9 2014 Interval 8	503	8.7	206	1.98	56.0	39	27	0.8	1.2	120
CR-9 2014 Interval 9	534	8.3	1251	11.27	67.8	34	190	2.0	7.1	380
CR-9 2014 Interval 10	569	8.3	1490	13.45	78.6	22	200	2.2	7.9	420
CR-9 2014 Interval 11	621	8.4	1854	16.88	87.1	14	280	1.9	8.3	480
CR-9 2014 Interval 12	650	8.2	1836	16.62	88.3	15	260	2.0	7.6	450
Cr-13 1984 Interval 1	86	8.5	1	0.20	8.0	158	17	0.4	2.8	36
Cr-13 1984 Interval 2	217	8.5	98	0.60	19.0	93	14	1.0	1.8	92
Cr-13 1984 Interval 3	248	8.3	121	1.90	23.6	91	16	0.8	1.7	97
Cr-13 1984 Interval 4	341	7.9	325	3.00	53.0	50	35	1.1	2.4	209
Cr-13 1984 Interval 5	423	7.3	37	0.30	21.9	155	15	2.6	2.8	70
Cr-13 1984 Interval 6	486	8.3	48	0.50	8.2	171	8	5.8	1.5	92
Cr-13 1984 Interval 7	576	8.1	29	0.10	8.8	159	19	2.8	2.8	53

Table 3. Major ion geochemistry for the CRG series boreholes

Sample ID	Depth	pH	Cl	Br	SO4	HCO_3+CO_3	Ca	K	Mg	Na
	m		mg/L	mg/L	mg/L	mg/L	mg/L	mg/L	mg/L	mg/L
CRG-1 2011 Interval 1	61	5.9	226	0.03	27.0	59	51	2.1	18.3	67
CRG-1 2011 Interval 2	88	7.8	56	0.01	3.1	182	37	1.2	6.2	33
CRG-1 2011 Interval 3	133	8.5	5	0.01	1.3	153	11	0.7	1.5	40
CRG-1 2011 Interval 4	171	8.5	27	0.01	1.3	136	20	0.8	2.8	31
CRG-1 2011 Interval 5	203	8.4	3	0.01	0.2	148	19	0.7	2.7	24
CRG-1 2011 Interval 6	232	8.5	31	0.01	0.5	138	23	1.7	4.1	31
CRG-1 2016 Interval 7	272	8.3	19	0.05	0.1	133	17	1.0	0.0	31
CRG-1 2011 Interval 8	295	8.6	6	0.01	0.1	137	11	0.9	1.3	36
CRG-1 2011 Interval 9	339	8.9	17	0.01	0.6	120	8	0.6	0.8	46
CRG-1 2011 Interval 10	377	8.9	20	0.10	0.6	118	5	0.6	0.7	48
CRG-1 2011 Interval 11	406	8.9	30	0.12	0.9	111	5	0.6	0.6	52
CRG-1 2016 Interval 12	441	7.8	642	0.05	0.1	138	101	4.1	14.5	178
CRG-1 2016 Interval 13	476	7.8	551	0.09	0.1	104	80	5.1	12.6	158
CRG-1 2016 Interval 14	521	9.4	34	0.12	2.9	78	3	0.8	0.2	50
CRG-1 2016 Interval 15	565	8.6	209	0.35	2.8	71	19	2.0	1.7	106
CRG-1 2016 Interval 16	612	8.6	264	0.09	0.2	91	30	3.2	3.2	115
CRG-1 2016 Interval 17	647	8.0	463	0.12	0.1	72	45	4.1	4.8	168
CRG-1 2016 Interval 18	686	8.8	499	0.40	0.1	71	38	5.7	2.6	200
CRG-1 2016 Interval 19	730	8.0	639	1.67	0.1	67	69	4.9	5.4	210
CRG-1 2016 Interval 20	834	8.3	275	0.33	2.9	52	48	3.0	6.1	109

Sample ID	Depth	pH	Cl	Br	SO4	HCO_3+CO_3	Ca	K	Mg	Na
	m		mg/L	mg/L	mg/L	mg/L	mg/L	mg/L	mg/L	mg/L
CRG-2 2011 Interval 1	47	7.8	1.8	0.01	19.0	156	40	1.4	7.0	7.6
CRG-2 2011 Interval 2	72	8.6	0.5	0.01	11.4	125	11	0.6	1.2	39
CRG-2 2011 Interval 3	98	8.5	0.5	0.01	11.6	127	7	0.7	0.6	45
CRG-2 2011 Interval 4	127	9.4	1.0	0.01	10.8	100	3	0.6	0.2	43
CRG-2 2011 Interval 5	166	9.4	2.0	0.01	12.4	99	3	0.6	0.2	44
CRG-2 2011 Interval 6	208	9.0	2.3	0.01	10.5	125	5	0.7	0.3	48
CRG-2 2011 Interval 7	255	8.9	2.7	0.01	5.4	124	7	0.7	0.5	42
CRG-2 2011 Interval 8	284	9.4	16.0	0.15	12.4	82	6	0.8	0.6	42
CRG-3 2013 Interval 1	69	8.2	4	0.04	6.7	151	12	3.1	2.4	40
CRG-3 2013 Interval 2	123	8.7	9	0.09	9.0	122	12	3.0	2.4	40
CRG-3 2013 Interval 3	185	9.1	10	0.10	31.2	87	8	1.4	1.3	42
CRG-3 2013 Interval 4	223	9.6	7	0.06	16.0	90	3	0.7	0.2	54
CRG-3 2013 Interval 5	255	9.1	16	0.11	20.0	95	3	2.7	0.2	53
CRG-3 2013 Interval 6	324	9.2	13	0.10	16.0	113	4	1.0	0.2	56
CRG-3 2013 Interval 7	396	9.0	44	0.33	8.3	102	4	1.4	0.3	54
CRG-3 2013 Interval 8	471	9.5	69	0.47	11.3	80	4	1.0	0.3	60
CRG-3 2013 Interval 9	527	9.2	27	0.19	9.8	110	4	0.8	0.2	67
CRG-3 2013 Interval 10	593	9.4	27	0.17	11.6	97	3	0.8	0.2	56
CRG-3 2016 Interval 11	667	9.5	23	0.20	21.9	76	3	1.3	0.1	60
CRG-3 2016 Interval 12	757	9.4	28	0.23	7.6	94	2	0.8	0.1	58
CRG-3 2016 Interval 13	832	9.2	35	0.26	8.2	95	3	0.8	0.1	59
CRG-3 2016 Interval 14	904	9.5	24	0.20	2.8	72	2	1.0	0.1	52
CRG-3 2016 Interval 15	953	9.5	25	0.19	0.9	62	2	0.4	0.1	51
CRG-3 2016 Interval 16	1024	9.1	101	0.90	9.2	94	9	1.8	0.3	86
CRG-3 2013 Interval 17	1081	9.2	38	0.29	5.5	62	2	0.3	0.0	51

Sample ID	Depth	pH	Cl	Br	SO4	HCO_3+CO_3	Ca	K	Mg	Na
	m		mg/L	mg/L	mg/L	mg/L	mg/L	mg/L	mg/L	mg/L
CRG-4A 2011 Interval 1	66	8.6	1	0.06	12.4	276	18	2.4	5.0	24
CRG-4A 2011 Interval 2	120	8.6	1	0.06	19.5	138	21	1.7	5.9	17
CRG-4A 2011 Interval 3	167	8.6	2	0.06	13.5	173	16	2.7	4.0	32
CRG-4A 2011 Interval 4	214	8.5	2	0.06	13.6	172	16	3.4	4.1	33
CRG-4A 2011 Interval 5	268	8.4	5	0.06	5.4	169	13	1.9	2.8	31
CRG-4A 2011 Interval 6	345	8.4	5	0.06	7.0	155	10	1.7	1.8	35
CRG-4A 2011 Interval 7	432	8.8	5	0.06	5.2	147	11	2.0	2.0	30
CRG-4A 2011 Interval 8	519	9.1	13	0.11	3.3	120	7	1.6	1.0	41
CRG-4A 2011 Interval 9	612	9.1	14	0.14	0.2	145	13	2.3	1.2	53
CRG-4A 2011 Interval 10	666	8.4	15	0.11	1.1	204	10	1.9	0.9	54
CRG-4A 2011 Interval 11	744	7.7	19	0.12	2.2	172	10	1.6	0.8	53
CRG-4A 2011 Interval 12	843	7.9	84	0.67	0.1	298	9	1.9	0.6	83
CRG-6 2013 Interval 1	60	7.2	34	0.12	7.5	301	54	2.6	10.6	13
CRG-6 2013 Interval 2	89	8.9	9	0.12	3.5	168	5	0.6	0.3	52
CRG-6 2013 Interval 3	124	8.4	6	0.05	3.6	214	7	0.8	0.9	44
CRG-6 2013 Interval 4	168	9.1	15	0.10	5.5	184	5	1.7	0.6	47
CRG-6 2013 Interval 5	237	9.0	21	0.12	4.7	133	3	1.4	0.4	50
CRG-6 2013 Interval 6	297	7.9	43	0.24	20.8	156	10	1.2	1.5	60
CRG-6 2013 Interval 7	364	8.6	27	0.16	15.0	156	5	0.9	0.7	58
CRG-6 2013 Interval 8	414	7.8	33	0.12	7.4	11	21	1.8	3.7	57
CRG-6 2013 Interval 9	458	7.6	34	0.12	5.0	263	19	1.9	3.4	62
CRG-6 2013 Interval 10	503	7.4	33	0.12	7.1	252	25	1.8	4.4	53
CRG-6 2013 Interval 11	559	8.0	32	0.13	10.4	179	11	1.4	1.6	54
CRG-6 2013 Interval 12	622	8.6	29	0.16	9.0	165	6	1.0	0.9	56
CRG-6 2013 Interval 14	723	8.7	27	0.15	10.6	171	6	0.9	0.8	57

Table 4. Available isotope geochemistry for CR-9 and CR-13 (from Bottomley et al., 1984)

Sample ID	Depth	pH	Cl	Sr	$\delta^{18}O$	$\delta^{2}H$	$\delta^{13}C_{DIC}$	$\delta^{37}Cl$	$^{87}Sr/^{86}Sr$
	m		mg/L	mg/L	‰ SMOW	‰ SMOW	‰ VPDB	‰ SMOC	
CR-9 2014 Interval 1	67	8.0	20	0.8	-11.3	-81.2	N/A	0.04	0.70905
CR-9 2014 Interval 2	104	8.9	16	0.3	-12.5	-87.6	N/A	-0.04	0.70917
CR-9 2014 Interval 3	139	8.9	16	0.3	-12.5	-87.4	-19.0	-0.05	0.70915
CR-9 2014 Interval 4	198	9.5	67	0.1	-13.9	-97.1	N/A	0.04	0.70932
CR-9 2014 Interval 5	285	9.4	21	0.2	-12.3	-84.4	-19.5	-0.10	0.70966
CR-9 2014 Interval 6	363	8.9	154	1.0	-12.5	-85.9	N/A	0.09	0.70935
CR-9 2014 Interval 7	433	8.6	297	1.2	-12.4	-85.8	N/A	0.04	0.70927
CR-9 2014 Interval 8	503	8.7	206	0.8	-12.8	-87.9	-19.7	-0.09	0.70931
CR-9 2014 Interval 9	534	8.3	1251	6.0	-11.8	-80.0	-18.9	-0.04	0.70936
CR-9 2014 Interval 10	569	8.3	1490	6.7	-11.9	-80.2	-18.6	-0.07	0.70940
CR-9 2014 Interval 11	621	8.4	1854	9.0	-12.3	-84.8	-14.5	0.07	0.70980
CR-9 2014 Interval 12	650	8.2	1836	8.1	-12.7	-85.4	-14.8	-0.03	0.70980
Cr-13 1984 Interval 1	86	8.5	1	0.9	N/A	N/A	N/A	N/A	N/A
Cr-13 1984 Interval 2	217	8.5	98	0.7	N/A	N/A	N/A	N/A	N/A
Cr-13 1984 Interval 3	248	8.3	121	0.5	N/A	N/A	N/A	N/A	N/A
Cr-13 1984 Interval 4	341	7.9	325	1.7	N/A	N/A	N/A	N/A	N/A
Cr-13 1984 Interval 5	423	7.3	37	0.5	N/A	N/A	N/A	N/A	N/A
Cr-13 1984 Interval 6	486	8.3	48	0.3	N/A	N/A	N/A	N/A	N/A
Cr-13 1984 Interval 7	576	8.1	29	0.6	N/A	N/A	N/A	N/A	N/A

Table 5. Available isotope geochemistry for the CRG series boreholes.

Sample ID	Depth	pH	Cl	Sr	$\delta^{18}O$	$\delta^{2}H$	$\delta^{13}C_{DIC}$	$\delta^{37}Cl$	$^{87}Sr/^{86}Sr$
	m		mg/L	mg/L	‰ SMOW	‰ SMOW	‰ VPDB	‰ SMOC	
CRG-1 2011 Interval 1	61	5.9	226	0.4	-10.8	-77.3	N/A	0.20	0.71148
CRG-1 2011 Interval 2	88	7.8	56	1.5	-11.7	-79.0	-18.9	0.41	0.70919
CRG-1 2011 Interval 3	133	8.5	5	0.4	-13.9	-98.6	-16.2	-0.01	0.70938
CRG-1 2011 Interval 4	171	8.5	27	0.9	-14.4	-104.6	N/A	N/A	0.70970
CRG-1 2011 Interval 5	203	8.4	3	0.8	-14.7	-105.6	-15.2	-0.30	0.70969
CRG-1 2011 Interval 6	232	8.5	31	1.0	-13.9	-96.2	-16.1	0.14	0.70987
CRG-1 2016 Interval 7	272	8.3	19	0.7	-14.6	-104.6	-13.8	-0.20	0.70989
CRG-1 2011 Interval 8	295	8.6	6	0.4	-14.5	-105.3	-15.9	-0.54	0.71003
CRG-1 2011 Interval 9	339	8.9	17	0.3	-14.5	-102.9	N/A	N/A	0.71002
CRG-1 2011 Interval 10	377	8.9	20	0.2	-14.8	-101.9	-17.1	-0.14	0.71016
CRG-1 2011 Interval 11	406	8.9	30	0.1	-14.3	-101.5	N/A	N/A	0.71026
CRG-1 2016 Interval 12	441	7.8	642	2.8	-11.9	-83.1	-16.3	0.39	0.71035
CRG-1 2016 Interval 13	476	7.8	551	2.1	-11.9	-83.9	N/A	N/A	0.71066
CRG-1 2016 Interval 14	521	9.4	34	0.1	-13.0	-91.4	-15.4	-0.20	0.71073
CRG-1 2016 Interval 15	565	8.6	209	0.5	-12.6	-89.1	N/A	N/A	0.71063
CRG-1 2016 Interval 16	612	8.6	264	0.8	-11.9	-84.6	-16.4	0.70	0.71060
CRG-1 2016 Interval 17	647	8.0	463	1.1	-11.8	-83.6	N/A	N/A	0.71049
CRG-1 2016 Interval 18	686	8.8	499	0.9	-11.7	-82.8	-14.4	0.29	0.71053
CRG-1 2016 Interval 19	730	8.0	639	1.5	-11.7	-82.5	N/A	N/A	0.71030
CRG-1 2016 Interval 20	834	8.3	275	1.2	-11.5	-85.1	-16.1	0.23	0.71126

Sample ID	Depth	pH	Cl	Sr	$\delta^{18}O$	$\delta^{2}H$	$\delta^{13}C_{DIC}$	$\delta^{37}Cl$	$^{87}Sr/^{86}Sr$
	m		mg/L	mg/L	‰ SMOW	‰ SMOW	‰ VPDB	‰ SMOC	
CRG-2 2011 Interval 1	47	7.8	1.8	1.5	-11.3	-79.3	N/A	N/A	N/A
CRG-2 2011 Interval 2	72	8.6	0.5	0.4	-11.4	-83.6	N/A	N/A	N/A
CRG-2 2011 Interval 3	98	8.5	0.5	0.2	-11.3	-83.8	N/A	N/A	N/A
CRG-2 2011 Interval 4	127	9.4	1.0	0.1	-12.1	-88.6	N/A	N/A	N/A
CRG-2 2011 Interval 5	166	9.4	2.0	0.1	-12.9	-89.5	N/A	N/A	N/A
CRG-2 2011 Interval 6	208	9.0	2.3	0.1	-12.0	-85.9	N/A	N/A	N/A
CRG-2 2011 Interval 7	255	8.9	2.7	0.2	-12.2	-88.7	N/A	N/A	N/A
CRG-2 2011 Interval 8	284	9.4	16.0	0.2	-12.2	-87.3	N/A	N/A	N/A
CRG-3 2013 Interval 1	69	8.2	4	0.2	-13.1	-92.3	N/A	N/A	0.71172
CRG-3 2013 Interval 2	123	8.7	9	0.2	-14.3	-100.0	-16.0	-0.24	0.70985
CRG-3 2013 Interval 3	185	9.1	10	0.3	-14.1	-99.0	N/A	N/A	0.70957
CRG-3 2013 Interval 4	223	9.6	7	0.1	-13.9	-97.8	-17.1	-0.17	0.70997
CRG-3 2013 Interval 5	255	9.1	16	0.1	-13.9	-98.0	N/A	N/A	0.70945
CRG-3 2013 Interval 6	324	9.2	13	0.1	-13.9	-98.4	-16.1	-0.34	0.70985
CRG-3 2013 Interval 7	396	9.0	44	0.1	-13.6	-95.3	N/A	N/A	0.70958
CRG-3 2013 Interval 8	471	9.5	69	0.1	-13.7	-94.7	-14.7	-0.29	0.70958
CRG-3 2013 Interval 9	527	9.2	27	0.1	-13.8	-96.0	N/A	N/A	0.70970
CRG-3 2013 Interval 10	593	9.4	27	0.1	-13.9	-97.2	N/A	N/A	0.70974
CRG-3 2016 Interval 11	667	9.5	23	0.1	-13.9	-97.1	-15.5	-0.23	0.70992
CRG-3 2016 Interval 12	757	9.4	28	0.1	-13.8	-96.7	N/A	N/A	0.71052
CRG-3 2016 Interval 13	832	9.2	35	0.1	-14.1	-98.3	N/A	N/A	0.71039
CRG-3 2016 Interval 14	904	9.5	24	0.0	-14.3	-101.5	-16.8	-0.29	0.71037
CRG-3 2016 Interval 15	953	9.5	25	0.0	-14.5	-101.1	N/A	N/A	0.71033
CRG-3 2016 Interval 16	1024	9.1	101	0.2	-13.8	-97.4	N/A	N/A	N/A
CRG-3 2013 Interval 17	1081	9.2	38	0.0	-14.3	-99.5	N/A	-0.35	0.71073

Sample ID	Depth	pH	Cl	Sr	$\delta^{18}O$	$\delta^{2}H$	$\delta^{13}C_{DIC}$	$\delta^{37}Cl$	$^{87}Sr/^{86}Sr$
	m		mg/L	mg/L	‰ SMOW	‰ SMOW	‰ VPDB	‰ SMOC	
CRG-4A 2011 Interval 1	66	8.6	1	0.5	-12.1	-80.5	N/A	N/A	N/A
CRG-4A 2011 Interval 2	120	8.6	1	1.0	-12.1	-80.4	N/A	N/A	N/A
CRG-4A 2011 Interval 3	167	8.6	2	0.8	-11.9	-79.8	-20.0	N/A	N/A
CRG-4A 2011 Interval 4	214	8.5	2	0.7	-11.9	-80.0	N/A	N/A	N/A
CRG-4A 2011 Interval 5	268	8.4	5	0.6	-12.3	-82.3	-18.0	N/A	N/A
CRG-4A 2011 Interval 6	345	8.4	5	0.3	-12.7	-86.4	N/A	N/A	N/A
CRG-4A 2011 Interval 7	432	8.8	5	0.4	-12.4	-83.7	-20.3	N/A	N/A
CRG-4A 2011 Interval 8	519	9.1	13	0.2	-12.0	-84.6	N/A	N/A	N/A
CRG-4A 2011 Interval 9	612	9.1	14	0.3	-12.0	-85.5	-14.2	N/A	N/A
CRG-4A 2011 Interval 10	666	8.4	15	0.2	-11.7	-84.3	N/A	N/A	N/A
CRG-4A 2011 Interval 11	744	7.7	19	0.2	-11.6	-84.1	N/A	N/A	N/A
CRG-4A 2011 Interval 12	843	7.9	84	0.2	-11.5	-83.2	-15.0	-0.68	0.71010
CRG-6 2013 Interval 1	60	7.2	34	0.9	-9.8	-74.5	N/A	N/A	0.71019
CRG-6 2013 Interval 2	89	8.9	9	0.1	-13.9	-100.1	-15.1	-0.08	0.70970
CRG-6 2013 Interval 3	124	8.4	6	0.3	-14.1	-103.3	-16.8	-0.72	0.70928
CRG-6 2013 Interval 4	168	9.1	15	0.2	-13.9	-97.9	N/A	N/A	0.70936
CRG-6 2013 Interval 5	237	9.0	21	0.1	-12.8	-93.5	-15.9	-0.12	0.70948
CRG-6 2013 Interval 6	297	7.9	43	0.3	-12.7	-91.6	N/A	N/A	0.70948
CRG-6 2013 Interval 7	364	8.6	27	0.2	-13.8	-96.8	-19.3	-0.44	0.70936
CRG-6 2013 Interval 8	414	7.8	33	0.7	-10.2	-77.0	-22.2	0.06	0.70941
CRG-6 2013 Interval 9	458	7.6	34	0.6	-10.2	-76.3	N/A	N/A	0.70944
CRG-6 2013 Interval 10	503	7.4	33	0.8	-10.4	-76.5	N/A	N/A	0.70942
CRG-6 2013 Interval 11	559	8.0	32	0.3	-11.6	-85.3	-18.8	-0.26	0.70954
CRG-6 2013 Interval 12	622	8.6	29	0.2	-12.6	-91.0	N/A	N/A	0.70953
CRG-6 2013 Interval 14	723	8.7	27	0.0	-13.1	-94.3	-17.3	-0.21	0.70969

Table 6. Average pH, major ion and Sr^{2+} concentrations as well as $\delta^{37}Cl$ and $^{87}Sr/^{86}Sr$ measured in groundwaters sampled from packered intervals from select CRL boreholes.

Borehole	pH	Cl^-	SO_4^{2+}	HCO_3^-	Ca^{2+}	K^+	Mg^{2+}	Na^+	Sr^{2-}	$\delta^{37}Cl$	$^{87}Sr/^{86}Sr$
		mg/L	mg/L	mg/L	mg/L	mg/L	mg/L	mg/L	mg/L	‰ SMOC	
CR-9	8.7	602	39	56	90	1.2	3.3	194	2.9	-0.01	0.7094
CRG-1	8.3	201	2	109	32	2.1	4.5	87	0.9	0.07	0.7103
CRG-3	9.1	21	11	123	3.8	1.3	0.4	55	0.1	-0.27	0.7101
CRG-6	8.2	26	8	168	14	1.4	2.3	51	0.3	-0.31	0.7096
CRG-4A	7.8	10	14	118	13	2.1	2.5	40	0.5		

Table 7. A selection of isotopic results from crush and leach experiments performed at the University of Waterloo

Borehole	Depth (m)	$^{87}Sr/^{86}Sr$	$\delta^{37}Cl$ (‰ SMOC)
CR-9	153.6	N/A	-0.35
CR-9	217.7	N/A	0.32
CR-9	305.8	0.71191	-0.31
CR-9	340.6	N/A	-0.23
CR-9	383.0	N/A	-0.04
CR-9	427.7	N/A	-0.52
CR-9	432.6	0.70979	-0.28
CR-9	457.5	N/A	0.09
CR-9	482.3	N/A	0.15
CR-9	508.7	0.70959	0.03
CR-9	528.5	N/A	0.40
CR-9	550.2	0.71043	-0.13
CR-9	570.1	N/A	-0.48
CR-9	606.9	0.71098	-0.72
CRG-1	432.2	0.71063	-0.42
CRG-1	592.0	0.71087	0.76
CRG-1	646.3	0.71706	-0.47
CRG-1	685.9	N/A	-0.40
CRG-1	700.6	N/A	-0.16
CRG-1	722.0	N/A	0.14
CRG-1	801.7	0.71310	-0.03
CRG-3	340.9	0.70942	-0.40
CRG-3	808.7	0.70994	-1.40
CRG-3	1023.5	0.71111	-0.42
CRG-4A	888.7	N/A	-0.57
CRG-4A	889.3	N/A	-0.11
CRG-4A	890.6	N/A	-0.39
CRG-6	44.7	0.71630	-0.39
CRG-6	91.3	0.71341	-0.44
CRG-6	180.4	0.71207	-0.49
CRG-6	323.1	0.71140	-0.13
CRG-6	396.0	0.70923	0.12
CRG-6	628.8	0.71217	-0.30
CRG-6	650.2	0.71171	-0.56

Table 8. A selection of chondrite normalized Rare Earth Element values from silicate and carbonate samples.

Borehole	Depth (m)	Sample Type	La	Ce	Pr	Nd	Sm	Eu	Gd	Tb	Dy	Ho	Er	Tm	Yb	Lu
CR-9	238.2	Calcite	374	293	186	149	64	38	40	26	14	9	9	7	8	7
CR-9	553.7	Calcite	835	601	403	333	187	181	139	137	102	93	86	86	76	75
CRG-1	25.26	Calcite	687	538	378	315	210	113	158	157	139	123	117	124	113	110
CRG-1	448.56	Calcite	308	295	230	203	166	127	124	121	91	75	62	53	42	36
CRG-1	493.66	Calcite	254	175	120	84	46	22	28	23	58	18	20	18	21	294
CRG-3	24.7	Calcite	432	400	290	232	162	39	111	115	88	72	65	70	60	54
CRG-3	307.9	Calcite	217	175	146	123	89	48	61	61	48	37	32	33	29	33
CRG-3	389.38	Calcite	95	77	71	67	78	49	76	74	68	57	54	43	33	28
CRG-3	1171.77	Calcite	1374	827	531	407	133	97	73	30	10	5	5	3	2	3
CRG-5	43.61	Calcite	132	105	82	64	48	23	39	38	33	29	30	27	27	26
CRG-5	43.61	Calcite	122	86	71	54	28	14	22	21	20	19	19	20	17	13
CRG-5	152.33	Calcite	442	406	339	273	238	114	188	196	407	162	167	162	190	1522
CRG-6	170.79	Calcite	161	129	109	92	89	68	67	57	158	38	35	27	24	742
CRG-6	182.04	Calcite	835	583	407	337	205	112	132	105	67	49	43	36	33	30

Borehole	Depth (m)	Sample Type	La	Ce	Pr	Nd	Sm	Eu	Gd	Tb	Dy	Ho	Er	Tm	Yb	Lu
CR-9	203.8	Silicate	109	86	74	65	42	43	25	23	20	17	18	19	21	20
CR-9	203.8	Silicate	143	116	98	78	43	24	26	21	17	17	16	14	14	15
CR-9	490.51	Silicate	55	37	29	24	16	14	10	9	9	8	9	9	10	9
CR-9	700.76	Silicate	58	39	31	24	14	13	10	9	8	8	8	8	8	9
CR-9	191.9	Silicate	34	28	26	26	19	38	14	13	11	10	10	10	11	11
CRG-1	493.66	Silicate	201	151	120	100	54	27	25	17	12	10	8	7	7	7
CRG-1	615.15	Silicate	36	28	28	29	23	24	13	9	7	6	4	4	3	2
CRG-1	739.29	Silicate	63	44	33	22	11	21	6	4	4	4	4	5	5	6
CRG-1	25.26	Silicate	116	92	76	62	37	24	23	19	18	17	17	17	17	18
CRG-1	110.18	Silicate	442	463	487	485	298	154	132	74	44	29	24	18	15	13
CRG-1	110.18	Silicate	432	467	492	457	280	154	134	70	43	29	23	17	15	13
CRG-3	206.3	Silicate	72	65	59	53	35	46	20	19	15	13	13	13	14	14
CRG-3	389.38	Silicate	70	55	47	38	28	28	22	19	18	17	15	14	13	14
CRG-3	861.45	Silicate	332	277	217	173	99	51	44	34	25	19	19	19	18	16
CRG-3	1171.77	Silicate	135	101	81	62	36	32	22	17	15	14	14	13	14	15
CRG-4A	613.79	Silicate	442	309	239	180	88	81	44	26	18	14	11	9	7	7
CRG-5	43.61	Silicate	85	64	53	44	28	29	20	17	15	14	14	13	15	15
CRG-5	43.61	Silicate	91	73	62	51	32	26	24	19	18	17	16	14	14	16
CRG-5	152.33	Silicate	103	78	64	50	31	35	22	19	17	17	17	16	18	20
CRG-6	48.08	Silicate	56	40	31	23	12	31	6	4	2	1	2	0	1	2
CRG-6	49.41	Silicate	73	51	35	25	12	15	6	4	4	4	4	4	4	4
CRG-6	101.44	Silicate	75	52	36	25	11	15	6	4	4	4	4	4	3	4
CRG-6	170.79	Silicate	157	119	89	67	34	16	18	13	11	10	10	10	10	10
CRG-6	200.78	Silicate	275	217	168	126	69	30	39	32	26	24	23	22	22	22
CRG-6	252.77	Silicate	201	184	161	128	79	30	50	40	36	32	30	28	27	27
CRG-6	360.03	Silicate	240	204	168	123	69	29	43	36	32	29	30	28	28	28
CRG-6	440.2	Silicate	187	136	101	71	35	23	21	17	16	14	15	15	14	16